CK

MMPHIL

FREE CONVECTION HEAT TRANSFER

IN FINNED HEAT EXCHANGERS

GARY MOOR BSc

A thesis in partial fulfilment of the requirements of

the Council for National Academic Awards for the degree of

Master of Philosophy

April 1992

Nottingham Polytechnic in collaboration with

Baxi Partnership Ltd.

Dedicated to my loving family

ACKNOWLEDGEMENTS

To my director of studies, Dr K. Jambunathan, I express my sincere gratitude for his continuous support, encouragement and invaluable advice throughout this project. I also express my gratitude to my second supervisor, from Lancashire Polytechnic, Dr J.D. Heys, for his invaluable support and for taking on the arduous task of proof reading this thesis. My sincere thanks also go to Mr J. Dutfield, Technical Director of Baxi Partnership Ltd, and Professor B.L. Button, Head of Department of Nottingham Polytechnic, without whose consent and funding would have made this project impossible.

I am also thankful to the librarian, Mr J. Corlett, who provided an excellent and comprehensive service throughout the period of this work. I thank Dr R. Edwards, my original second supervisor, for his interest and direction in the early stages of this work, and also to Mr A. Stewart, of Lancashire Polytechnic, for his advice on transputer technology. I would also like to thank Mr R. Potter, fluids laboratory technician at Nottingham Polytechnic, for his help with the liquid crystal application and thermal tunnel.

Lastly I give grateful thanks to my family, who have given me patience, support and hours of silence, when needed most.

② ABSTRACT

The steady state heat transfer, from a vertical, extended surface heat exchanger, under the influence of free convection has been investigated. The investigation used a liquid crystal approach, in conjunction with acrylic models. The models represented a cast iron heat exchanger, with base dimensions of 200 mm wide × 160 mm high, these dimensions being maintained throughout the investigation. The extended surfaces used were vertical fins of 3 mm width, their spatial separation being altered between 11 mm and 37 mm, and their length being altered between 15 mm and 30 mm.

The method used, in this investigation, was to pre-heat the heat exchange model, and allow it to cool in free convection, whilst recording the isotherms onto video tape. The timing data, deduced from the video recordings, were analysed using a one dimensional transient technique. The resultant local heat transfer coefficient values are plotted to give contour maps. The validity of the technique is verified, giving good agreement to previously published correlations for vertical flat surfaces in free convection, with the presented data giving a non-dimensional correlation of.

$$\mathbf{Nu_x = 0.805\ Pr^{1/4}\ Gr_x^{1/6}}$$

The investigation defines an optimal spatial separation, for the fins, of 14 mm, based upon volumetric optimisation. There is also a dependency shown, for the increase in heat transfer, above that of a vertical flat plate, to the total volume of the fins added to a flat plate. The equation given is with reference to an overall total fin

volume of $60 \times 10^{-6} < V_{f,TOT} < 165 \times 10^{-6}$, the equation being.

$$\mathbf{Q_{inc} = -25367\ (V_{f,TOT} \times 10^{3})^{2} + 9.313\ V_{f,TOT} \times 10^{6} - 300.293}$$

This equation is expanded to provide a correlation between the fin length and increase in heat transfer, above that of the vertical flat plate, giving

$$\mathbf{Q_{inc} = -228303\ H^{2}\ L^{2}\ N^{2} + 27939\ H\ L\ N - 300.293}$$

and the maximum number of fins given as an integer value, being related to the spatial separation and base width by.

$$\mathbf{N_{max} = \frac{Bw}{0.003 + S}}$$

CONTENTS

LIST OF FIGURES

CHAPTER 5

FIGURE

APPENDIX A

FIGURE

APPENDIX D

FIGURE

NOMENCLATURE

GENERAL NOMENCLATURE

a	= distance	(m)
A	= area	(m^2)
b	= distance	(m)
Bi	= Biot number ($h \Delta x / k$)	
Bw	= Base width	(m)
c	= distance	(m)
c	= concentration	
c_p	= specific heat	(J/kgK)
C	= constant	
d	= distance	(m)
D	= base depth or thickness	(m)
dH	= vertical distance	(m)
F	= shape factor	
Fo	= Fourier number ($k \Delta t / \rho c_p \Delta x^2$)	
g	= gravity	(m/s^2)
Gr	= Grashof number ($x^3\rho^2\beta g\Delta T/\mu^2$)	
h	= heat transfer coefficient	(W/m^2K)
h_m	= mass transfer coefficient	(m/s)
H	= internal heat generation	(W)
H	= fin height	(m)
k	= thermal conductivity	(W/mK)
L	= fin length	(m)

L^+	=	dimensionless fin length	
m	=	mass loss	(kg)
m	=	nodal location	
n	=	step in value	
n	=	nodal location	
N	=	number of fins	
Nu	=	Nusselt number (hL/k)	
P	=	argument variable	
Pr	=	Prandtl number ($\mu c_p/k_F$)	
q^*	=	dimensionless average radiative heat flux	
Q	=	heat transfer rate	(W)
r	=	residual	
R	=	resistance	(Ω)
R	=	radiation term (analogous to Bi) ($F \epsilon \sigma \Delta x$ / k)	($1/k^3$)
Ra	=	Rayleigh number (Gr Pr)	
Ra^*	=	modified Rayleigh number	
Re	=	Reynolds number	
S	=	inter fin spacing	(m)
S^+	=	dimensionless inter fin spacing	
t	=	time	(s)
tc	=	time constant	(s)
T	=	temperature	(°C)
V	=	volume	(m^3)
W	=	width	(m)

x	= coordinate in x direction	
y	= coordinate in y direction	
z	= coordinate in z direction	

GREEK NOMENCLATURE

α	= thermal diffusivity ($k/\rho c_p$)	(m^2/s)
β	= coefficient of volumetric expansion	(1/K)
ϵ	= emissivity	
Θ	= dimensionless temperature $[(T-T_b)/(T_w-T_b)]$	
μ	= Absolute viscosity	(kg/ms)
ν	= kinematic viscosity	(m^2/s)
ρ	= density	(kg/m^3)
σ	= Stefan-Boltzmann constant	(W/m^2K^4)

SUBSCRIPTS

b	= bulk fluid
B	= base
c	= centre fin
f	= fin
F	= fluid
g	= green coloured isotherm
H	= based on fin height

i = internal

in = input value

inc = increase in value above that of a vertical flat plate

I = initial

L = average value

m = mass

m = location in y coordinate

max = maximum value

n = number

n = location in x coordinate

o = outer fin

out = output value

S = based on fin spacing

sum = sum of sections

w = wall

TOT = total value

x = local value

PREFIX

Δ = increment in unit

∇^2 = Laplacian operator $[\partial^2/\partial x^2 + \partial^2/\partial y^2 + \partial^2/\partial z^2]$

∂ = partial derivative

CHAPTER 1

INTRODUCTION

1.1 Background

Convection heat exchangers aided by extended surfaces are used to transfer heat from one medium to another. Disciplines as diverse as electronic component cooling, to domestic dwelling heating use this type of configuration. Marketing requirements for these heat exchangers usually incorporat restraints upon the design, the most common of which are size or cost limitations.

In domestic heating extended surface heat exchangers are extensively used by the gas and oil boiler manufacturers. Forced or natural (free) convection is used to remove heat from a high temperature source, such as a flame and combustion products, and distribute it to the appropriate media. With a heating appliance, generally referred to as a boiler, the primary heat exchanger, inside the boiler, transfers the heat from the flame and combustion products to water that is being pumped around the heating system. The hot side of the heat exchanger uses either free or forced convection, the water side primarily using forced convection. On reaching the room the heated water now becomes the higher temperature source, and a secondary heat exchanger, known as a radiator, removes this heat by free convection of the dwellings ambient air.

A more direct approach, usually associated with the gas industry, is the wall convector heater. Unlike the name suggests the heat exchanger is not used to heat the wall (the name is derived from the unit being wall mounted), but is used to remove heat from the flame and combustion products, transferring it to the room. Both sides of the heat exchanger are under the influence of free convection. The heat exchanger can be of a fabricated or cast construction, the usual casting material, for this type of unit, being iron. A typical shape for the cast heat exchanger is a box section with vertical extended surfaces, known as fins. Figure (1-1) shows one such unit, the Baxi Brazilia Slimline 5.

Extended surfaces enhance the rate of heat transfer by increasing the area of the transfer surface and by restarting (tripping) the developing boundary layer, Figure (1-2). Theoretically, the more area on the transfer surface the greater the heat transfer. This is not always true as an over reduction in the spatial separation of adjacent extended surfaces can result in the free convection currents being inhibited. This generates a resultant loss in heat transfer. If a set base area for the design of a heat exchanger is imposed, then by using an increasing number of fins the heat transfer will increase, up to the aforementioned limitation. From this an optimal spatial separation, based on the maximum heat flow, will be obtained. If further restraints, such as cost or maximum allowable heat transfer, are imposed then an optimal spatial separation based on material volume will be required. The two optimal values will not necessarily be the same, hence the design engineer must have a complete design specification before designing the heat exchanger.

1.2 Purpose of investigation

Manufacturers of domestic heating appliances currently take a practical

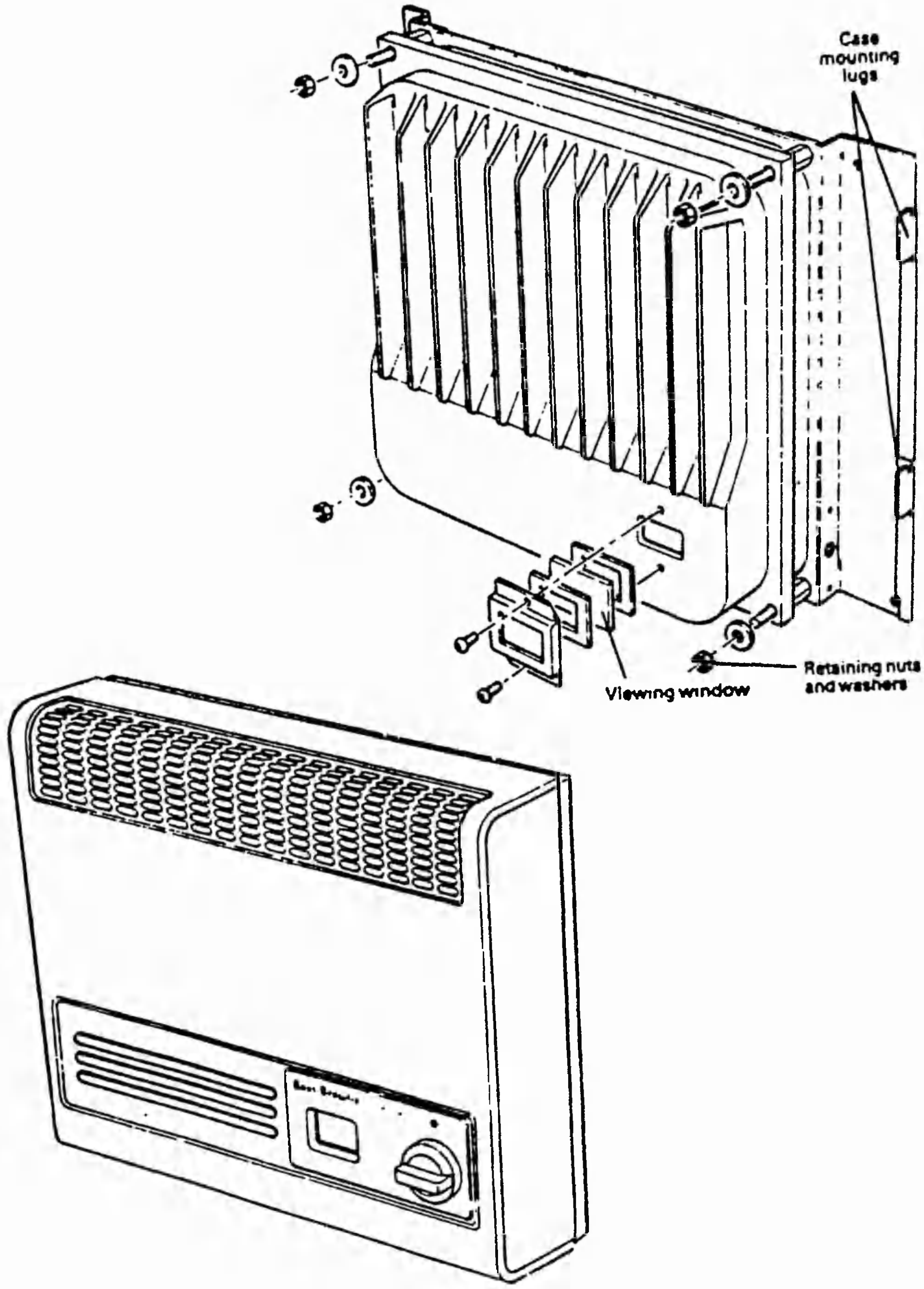

FIGURE 1-1 Baxi Brazilia Slimline 5

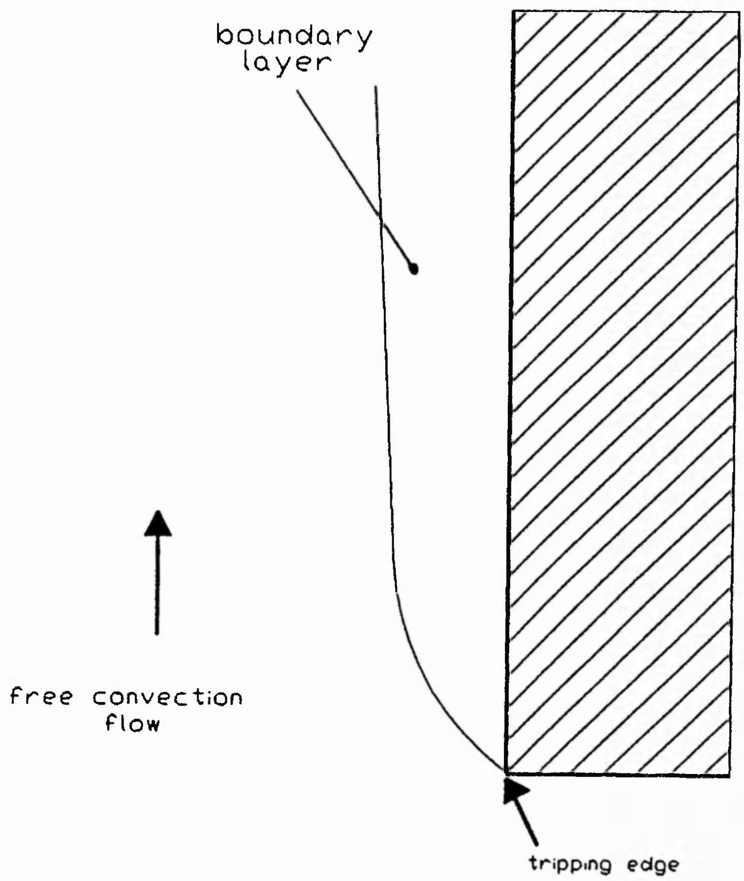

FIGURE 1-2 Boundary layer development from the tripping edge

approach to their designs. This approach involves building and testing heat exchangers, the configuration of which is based upon experience. This results in a heat exchanger that meets the marketing requirements, but is not always of an optimal design. The method is costly in both time and material, this being especially true for cast iron due to pattern making constraints. Intricate patterns are firstly made from wood and a cast alloy master pattern produced. It is hard to build much flexibility into this pattern, hence many of the design changes result in a new master being produced. Any method which can reduce the number of pattern changes is of a great advantage to both the pattern maker and the design engineer in terms of both material and labour costs.

The design engineer relies upon information from previous tests to make a calculation as to what the next design profile should be. The more extensive and accurate the information, the better the next iteration will be. By modelling the design ideas, in ways other than by the use of cast iron, localised information rather than the general performance of the unit, will be available. If the model is easier to produce and at a lower cost consideration, then more models may be produced in a shorter period of time, within the design budget. By using the localised information the engineer can examine the performance of each extended surface. The information will also allow optimisation, of the extended surfaces, with regards to both the maximum heat flow and volumetric considerations.

The investigation is to review literature, regarding extended surface optimisation, forward a method of modelling a cast type heat exchanger, at both lower cost and shorter time considerations, and perform volumetric optimisation on an existing finned cast iron heat exchanger.

1.3 Approach to the investigation

A domestic wall heater designed at BAXI PARTNERSHIP Ltd. has been investigated to determine its optimal fin geometry. The appliance chosen is the Baxi Brazilia Slimline 5, which is a balanced flued wall convector heater, Figure (1-1).

The unit works by the inner side of the heat exchanger removing heat from the flame and combustion products, created from the burnt gases. The combustion products exit the combustion chamber, and flue, under the influence of free convection. The heat is transferred through the heat exchanger by conduction. The hot outer finned surface of the heat exchanger then releases its heat, to the ambient air, again by free convection; Figure (1-3). The actual heat transfer out of the casting is determined by values of radiation and localised convection heat transfer coefficients.

The local heat transfer coefficients are determined by the heat exchange surface geometry. The appliance investigated uses vertical rectangular fins at an inter fin spacing of 20 mm and fin length of 25 mm. The fin shape and spacing was determined by the design engineers, based upon both experience and full casting tests, considering only the total heat output, and combustion requirements of the appliance.

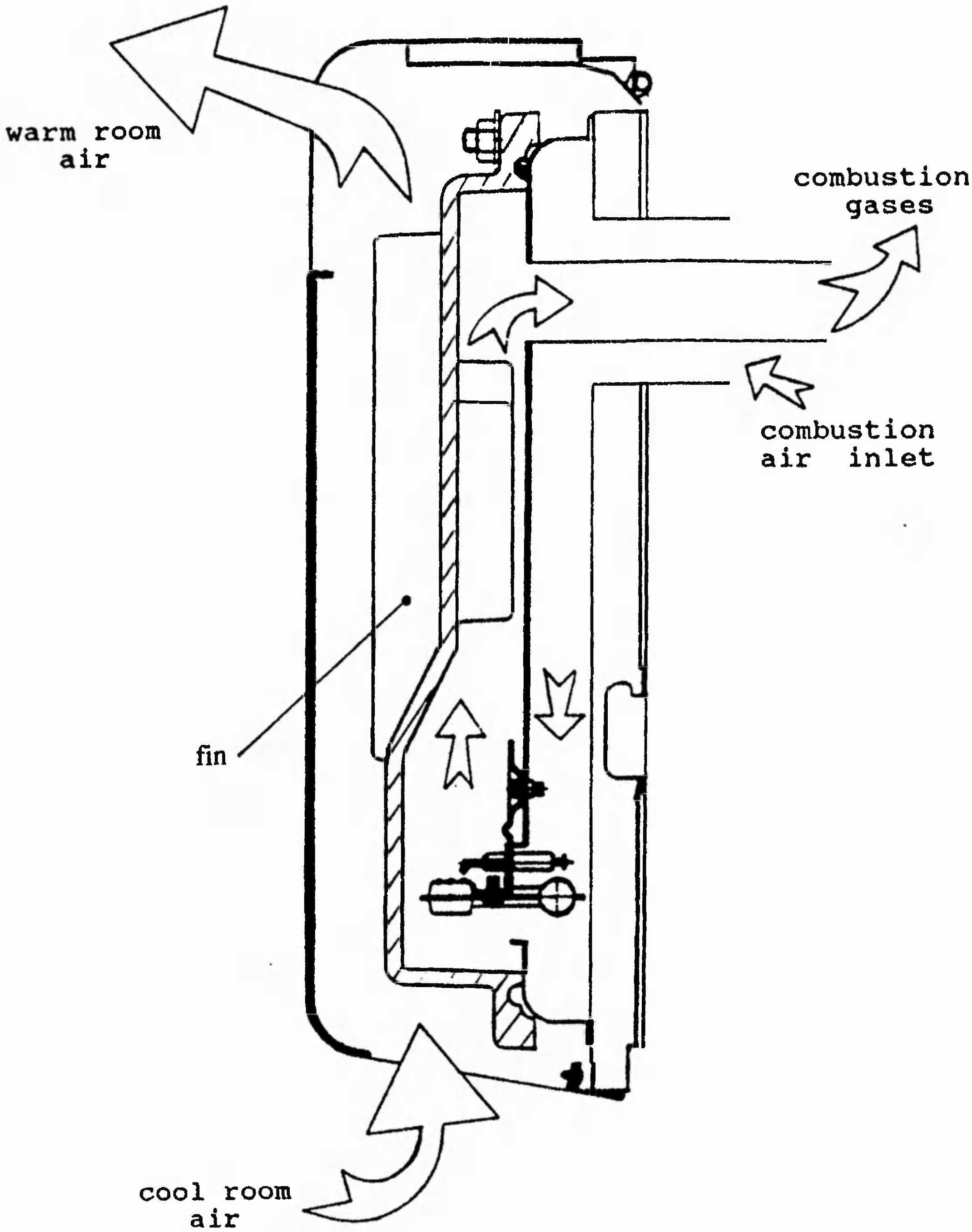

FIGURE 1-3 Heat flow through casting

No local heat transfer coefficients for this casting are known. The fin shape and dimensions are given in Figure (1-4).

A method of determining local heat transfer coefficients has been investigated, and this method used to optimize the fin geometry on the outer surface of the heat exchanger. The optimisation is in respect to volumetric considerations, keeping the heat transfer to the same value as the original Baxi Brazilia Slimline 5. The inner surface has fins which act not only for enhancing of heat transfer but as channels to guide the combustion products. Although the shape and size of these fins affect the flow of heat into the casting, their dimensions are critical to the combustion performance of the appliance, hence alteration of their dimensions is outside the scope of this investigation. As the heat exchanger and fin shapes are relatively complex a simplified heat exchange and fin shape will be used. The model configuration is given in Figure (1-5).

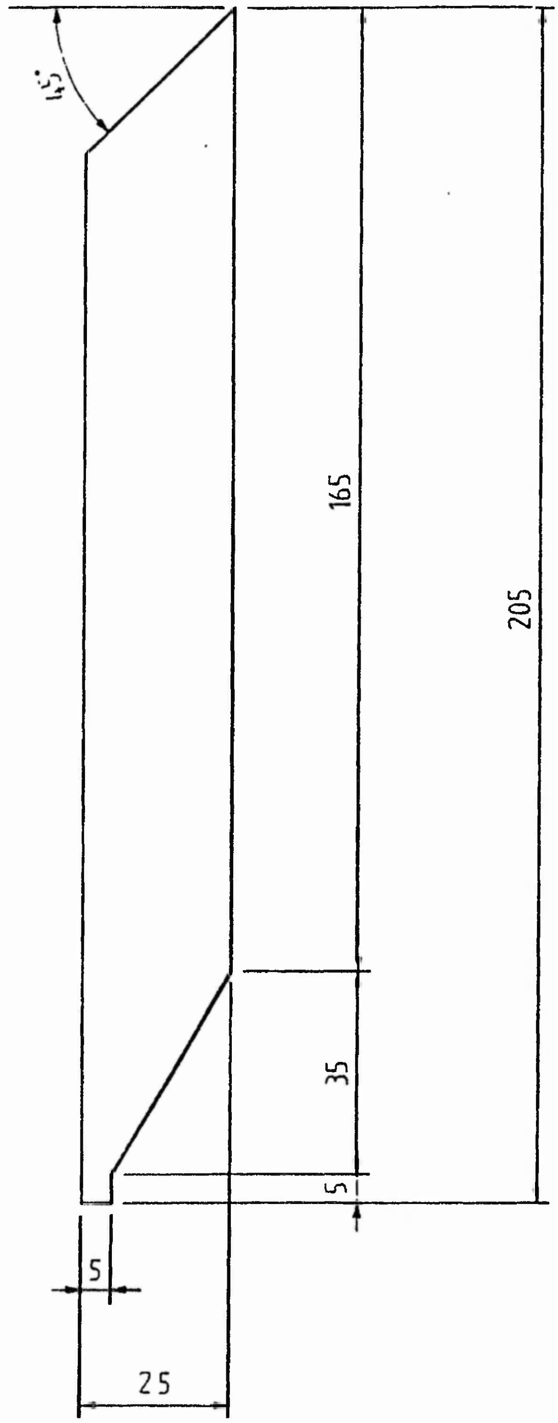

FIGURE 1-4 Actual fin shape

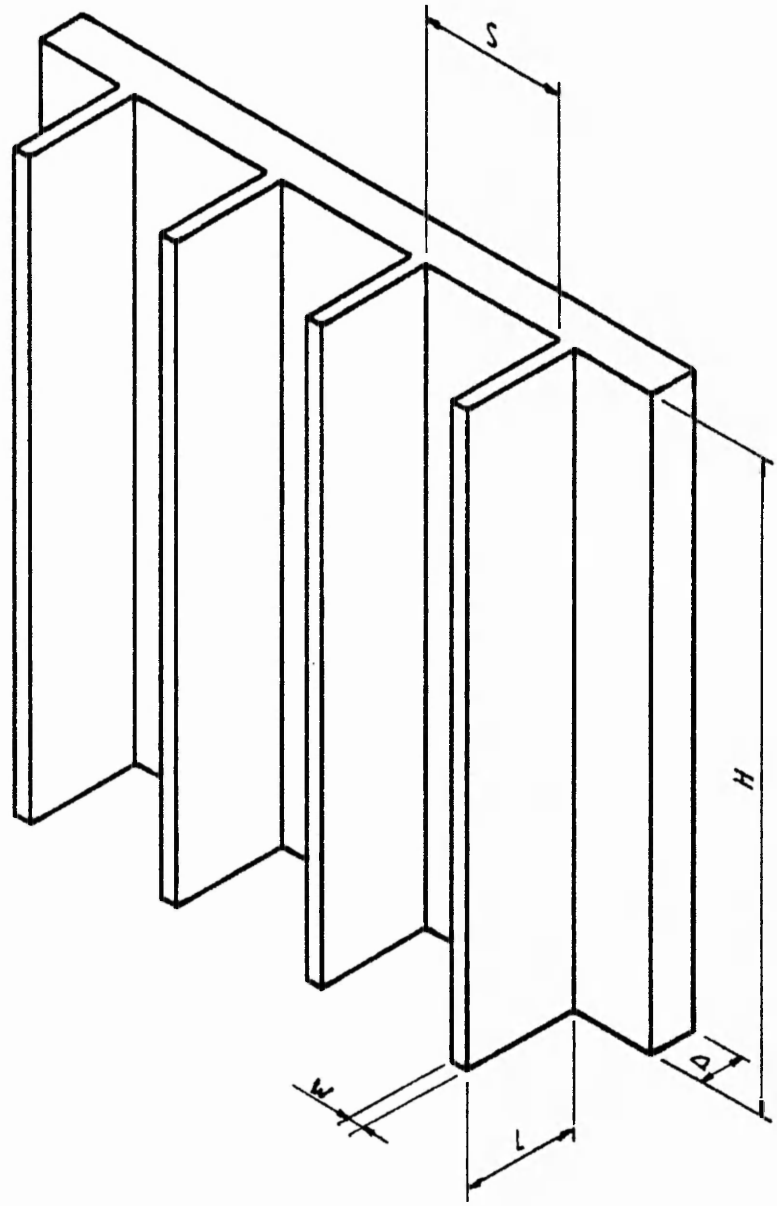

FIGURE 1-5 Model for heat transfer optimization

CHAPTER 2

LITERATURE REVIEW OF

EXTENDED SURFACE OPTIMISATION

2.1 Introduction

Papers dated as early as the 1960s give rise to discussions on extended surface heat transfer. The subject covers all types of geometries, including parallel fins, pin fins, annular fins and fins in ducts. Consideration has been given to papers on the determination of heat transfer through various types of heat exchangers. These range from flat surfaces to complex extended surface shapes, also to models of fluid flow inside ducts and pipes. The majority of these papers however fall outside the scope of this investigation and only the significant papers are reviewed.

The papers reviewed relate to heat transfer optimisation by the use of rectangular fins emanating from flat surfaces. There are basically two approaches to this problem, practical and theoretical. Both types of approach are reviewed and the papers categorised under the appropriate heading.

2.2 Practical approach

Naik et al [1] investigated vertical fin arrays from a horizontal base. It is shown in this case that the optimal fin spacing increases with forced convection and decreases with natural convection, as the protrusion of the fin increases. The heat exchanger is of an alloy construction, with an electrical heating element to give the steady state base temperature. Thermocouples are used to record the fin and base temperatures. One problem with this technique is the intrusive nature, of the thermocouples, to the flow. No generalised quantitive recommendation is forwarded.

A similar investigation was considered by Jambunathan et al [2] where again a fabricated alloy heat exchanger was used, with an electrical heating element providing the steady state base temperature. The investigation was conducted using an interferometric approach, measuring the temperature across the air gap. Thermocouples were used for deducing the local fin temperatures. An optimal fin spacing of 16 mm is proposed for the convection model, with reference to radiation reducing this value as the emissivity increases.

Leung et al [3] used a vertical base with vertical fins. The construction was of alloy, with an electrical heating source, for the investigation of the steady state heat loss. The fins had a thickness of 3 mm, and an optimal spacing of 10 ± 1 mm reported. This corresponds to a base temperature between 15°C and 100°C.

Work along similar lines, by Leung et al [4], looked at the investigation into increasing the height of fins from 250 mm to 375 mm. The fins had a constant depth of 60 mm. The optimal separation is reported at 10 ± 1 mm and 11 ± 1 mm respectively. Further investigation of rectangular fin arrays protruding from vertical bases, by Leung and Probert [5], found the optimal fin spacing to be 11.1 mm. This spacing was recorded with a fin depth of 30 mm. The methodology used thermocouples to measure the fin temperatures. The authors proposed that an increase in emissivity, of the transfer surface, increases the boundary layer, hence increases the optimal fin spatial separation.

The authors reported again, in 1989 [6], this paper considering fins of 150 mm in height, with depths of 10 mm and 17 mm. The optimal inter fin separations for these fins was found to be 9.0 ± 0.5 mm. Polished duralumin with an emissivity value of 0.1 was used to limit the effects of radiation. Also, the excess temperature of the heat exchanger, above ambient conditions, varied between 20 K to 40 K. This made the radiation component almost independent of conduction and convection. From this a maximum radiation heat dissipation of less than 5% was estimated.

2.3 Theoretical approach

Van de Pol and Tierney [7] used extruded aluminum heat sinks, used in the electronics industry, to build a mathematical model for analysing natural convection and radiation heat transfer from parallel finned sections. The iterative analysis technique developed, for the conjugate problem, allows for a non-uniform base temperature. The model is restricted to having a heat source diameter which is a fraction of the total heat transfer base area. If the heat source diameter becomes larger than the centre fin spacing, the model collapses.

Sukhatme [8] proposed separate convection and radiation models for high thermal conductivity heat exchangers. An imaginary rectangular domain, portioned from the heat exchanger, is used to negate edge effects. The convection correlation is established from the fin base and flat areas, the fin height being the characteristic dimension. The average Nusselt number is based on a Prandtl number of 0.7 and is expressed as.

$$\mathbf{Nu_{L\,H} = 0.929\ Gr_H^{0.217}\ (S^+)^{0.015}\ (L^+)^{0.139}} \qquad (2.3.1)$$

given.

$$\mathbf{Gr_H = g\ \beta\ \Delta T\ H^3\ /\ \nu^2} \qquad (2.3.2)$$

$$\mathbf{S^+ = S/H} \qquad (2.3.3)$$

$$\mathbf{L^+ = L/H} \qquad (2.3.4)$$

The average radiation heat flux is given in a dimensionless form, where the dimensionless temperature (Θ) lies between specified limits.

given $0 < \Theta < 1.25$;

$$\mathbf{q^* = [\ (0.33 - 3\epsilon - 2.14\epsilon^2) + (-0.38 + 2.99\epsilon + 2.67\epsilon^2)\ \Theta + (0.07 - 0.08\epsilon - 0.59\epsilon^2)\ \Theta^4\ ]\ (S^+)^{0.64}\ (L^+)^{0.3}} \qquad (2.3.5)$$

The correlations give an estimation of the heat transfer through the heat exchanger, however there is no estimation for the optimal fin spacing. On the heat exchanger examined the minimum inter fin spacing that can be analysed, with this correlation, is 16 mm.

Further investigation along the same lines, by Sukhatme and Saikhedkar [9], gives rise to two correlations for the determination of the average Nusselt number. The correlations are related to the inter fin spacing and are limited to set boundary values of the modified Rayleigh number. Given,

$$\mathbf{Ra_S^* = S^+ \, Gr_S \, Pr} \qquad (2.3.6)$$

$$\mathbf{Gr_H = g \, \beta \, \Delta T \, S^3 \, / \, \nu^2} \qquad (2.3.7)$$

For the range $0 < Ra_S^* < 250$

$$\mathbf{Nu_{L\,S} = 0.079 \, (S^+)^{0.579} \, (L^+)^{-0.261} \, (Gr_S \, Pr)^{0.509}} \qquad (2.3.8)$$

This correlation *(2.3.8)*, relating to the lower modified Rayleigh number range, fits the curve provided in the paper. The second correlation provided relates to the higher modified Rayleigh number range, this range being $250 < Ra_S^* < 3 \times 10^4$. The correlation however has a misprint, and does not calculate points which fit the provided curve. Due to this fact the second correlation, of this paper, has not been shown in this review.

In other work on optimal fin geometries, longitudinal fin arrays have been studied. Tanaka and Kunitomo [10] developed an algorithm to solve for minimum fin volume for a known heat flux. This study also considers longitudinal fins with a trapezoidal profile. Further work by Tanaka et al [11] involved the investigation into volume optimisation. An isothermal base plate was used to provide optimal configuration parameters as regards fin number, fin spacing, fin height and fin thickness. The numerical analysis performed is of an iterative procedure with the resultant values being verified against experiment. The optimisation of the fin parameters was possible by giving known values of base temperature, environmental fluid temperature, emissivity with height and width of the heat exchanger. It was found that to minimise the fin volume a larger and wider heat exchanger at a higher emissivity is an advantage. In the case of non-isothermal base temperatures large errors were observed. The actual iterative procedure used has not been presented.

Leung et al [12] studied convection and radiation for vertical fins on a vertical base, using a two dimensional model. The technique employed a finite difference matrix approach, making the assumption that the flow of the convection current lay inside two parallel plates. The convection and radiation components are independently estimated, then summated. The model produced, and compared to experimental observations, gives a first approximation solution for optimal separation.

Fins arrays, arranged in clusters, can exhibit a choking effect. The choking effect is where one fin does not permit sufficient heat transfer to a remote fin. The choking effect, and optimisation, has been the study of Kraus and Snider [13], with Kraus [14] continuing the investigation. The papers give guidelines for the selection of intricate fin shapes. These shapes would not be feasible in the production of a cast iron heat exchanger of the type investigated.

Combined analysis and optimisation of extended heat transfer surfaces has been the study for Hrymak et al [15]. This study is based upon a finite element approach to the solution, and gives the optimisation algorithm used. The results are for radiation only, and combined convection and radiation. Both solutions are compared to previous work.

2.4 Conclusion

From the significant papers reviewed values of optimal fin spacing are offered between 9.0 ± 0.5 mm and 11 ± 1 mm. These values are determined by a practical approach, and are offered by Leung et al, [3] and [4], and Leung and Probert [5]. The optimal values relate to the maximum heat transfer for a given heat exchanger. Consideration to both convection and radiation is given, the methodology using temperature sensors that are obtrusive to the free convection flow. The reference to the emissivity, from the authors, defines a reduction in the spatial separation with a reduction in emissivity. This appears to be in contradiction to the paper by Jambunathan et al [2], where a reduction in spatial separation is related to an increase in emissivity, however this investigation is for a horizontal base heat exchanger. The paper by Jambunathan et al offers an optimal separation of 16 mm.

The theoretical approach, to extended heat transfer, mainly deals with the estimation of the heat transfer rate. Of the papers that give optimisation, for finned heat exchangers, a discussion of the technique used is given, but not the actual algorithm used. No optimal value for the spatial separation is given.

CHAPTER 3

EXPERIMENTAL HEAT TRANSFER INVESTIGATION

3.1 Introduction

Designing extended surface heat exchangers using full size cast iron models, is both time consuming and expensive. The test results, from this type of approach, yield only average values of the heat transfer, by calculating the flue loss efficiency as specified in BS 5258 [16]. This approach does not produce any indication as to which part of the design needs to be concentrated on.

A practical approach, to extended surface optimisation, is required that is simplistic in its approach and detailed in localised information. The localised information required is the convective heat transfer coefficient. This gives the engineer knowledge of the performance of a small area of the design. By mapping the values for the whole geometry a profilometric description, with respect to convective heat transfer coefficient contours, is obtained. Techniques available, for profilometric mapping, can be broadly categorised into direct and indirect measurement methods. A discussion on both types of approach is given, along with an explanation of three direct and three indirect techniques.

3.2 Discussion of available methods

3.2.1 The direct approach

Direct measurement, of the local convective heat transfer coefficient, is preformed by allowing convection heat transfer to take place, and measuring the change in surface temperature, of the heat exchanger. The three techniques reviewed are Infra-red thermography, colour change paints and liquid crystals.

Infra-red thermography was used by Roberts [17] and Kreider and Sheahen [18]. The method is non-contact, hence non-obtrusive to the flow regime. It is highly dependent on the surface emissivity and geometry, this effectively limiting its usefulness. Infra-red thermography exhibits a high degree of uncertainty in the measured local convective heat transfer coefficient, due to the above limitations, and also requires high capital cost, compared with both colour change paints and liquid crystals.

Colour change paints can be used on complex surface geometrics, although application may cause some difficulties. The paints exhibit a colour change at differing temperatures thereby enabling contour mapping of the surface. As the paints are not truly reversible they can usually only be used once, and with the transient form of analysis. They are however non-obtrusive to the flow regime, and have been successfully used by Jambunathan et al [19]. The authors discuss the limitations of the technique, with regard to the rate of colour change, leading to errors in the calculated local convective heat transfer coefficient. Due to the limitations of the paints, they have been superseded by liquid crystals.

Liquid crystals, although used in this field as far back as the early 1970's, by Ouden and Hoogendoorn [20], have only recently been widely accepted as a powerful technique for the determination of local convective heat transfer coefficients. Early problems in application to the transfer surface have been overcome, and now micro encapsulated crystals may be applied by dipping the transfer surface into a liquid crystal solution, painting or spraying them onto the surface, or by applying the liquid crystals to the surface in sheet form. Isothermal contours can be measured by using either the steady state or transient forms of analysis. As the crystals are truly reversible the test piece can be reused. The liquid crystal technique is low-cost, compared to Infra-red thermography or full sized cast iron models, and the resultant mapping of the local convective heat transfer coefficient can be accurately undertaken due to the crystals exhibiting a low discrimination error.

3.2.2 The indirect approach

Determination of local convective heat transfer coefficients by an indirect approach uses the analogy between heat and mass transfer. Mass transfer is the process of transferring one constituent of a fluid from a region of higher concentration to a region of lower concentration. This is analogous to heat transfer in that they both transfer in a direction which reduces an existing concentration gradient. The similarity in the processes can be shown by comparison of the heat transfer and mass transfer equations.

$$\mathbf{Q = h\ A\ (T_w - T_b)} \qquad (3.2.1)$$

$$\mathbf{m = h_m\ A\ (c_w - c_b)} \qquad (3.2.2)$$

The local mass transfer coefficient is determined by measuring modification to an incident light path. The modification is created by surface deformation, the deformation being produced from either a subliming or recessing surface coating. The change in the incident light is measured by the mass transfer instrumentation, of which three methods are reviewed, these being Electronic speckle pattern interferometry, Moiré topography and Holographic interferometry.

Holographic interferometry is a process where photographic plates are used to record a fringe pattern. The transfer surface is firstly coated with a swollen polymer layer, and a laser beam used to illuminate the surface. The light scattered from the surface falls onto the photographic plate. The surface then undergoes mass transfer, where the surface coating recesses. The surface is again illuminated and recorded on the same photographic plate, where a series of fringes are observed. The fringe ordinal numbering, with this technique, has proven to be difficult, however it has been successfully employed in the study of jet impingement by Galaud [21]. An explanation of the principles of holography are given Gates [22].

Electronic speckle pattern interferometry has the capability of real time measurements. The technique has been used by Saluja et al [23], with reference being made to its large uncertainty in the measured mass transfer coefficient. The reported uncertainty is in the region of 26.5%. The technique is very susceptible to vibrations and elaborate damping, of the experimental rig, is necessary.

Moiré topography, the technique used by Pirodda [24], Flanagan et al [25] and Reid et al [26], can also be used for real time measurements. Reid et al [26] used a projection Moiré topography technique, allowing the use of fully automatic analysis. Flanagan et al [25] used the shadow approach to Moiré topography, where a grating, illuminated by a collimating beam, is placed near to the transfer surface for a shadow to be cast. Pirodda [24] describes both techniques in detail. Moiré topography is simple in its approach however, the quality in the observed fringes and size of the observed geometry is limited.

All of the three indirect measurement techniques possess uncertainty in the measured mass transfer coefficient. The heat transfer coefficient is generally deduced from the Chilton-Colburn analogy between heat and mass transfer, thus invariably transferring the uncertainties in the measured values of the mass transfer coefficient.

3.2.3 Types of analysis

Two types of analysis, for heat transfer determination, are used, these being steady state or transient. In steady state analysis an electrical heater is used to provide a known heat input. The current to the heater is increased until the desired pre-determined temperature is reached. The local convective heat transfer coefficient is then calculated from *(3.2.1)*. This technique was used by Simonich and Moffat [27]. Problems posed by this technique are its dependency upon a uniform temperature. With complex geometries, especially where changes in thickness occur, this may prove difficult.

Transient analysis, of a body cooling under the influence of free convection, requires the whole body to be heated to a uniform elevated temperature. The body is then subjected to ambient conditions for free convection to take place. The time it takes the surface to cool, from the elevated temperature, to a known temperature (between the elevated and ambient temperatures), gives the differential time variable required to solve the governing equation.

$$\nabla^2 T = \frac{1}{\alpha}\frac{\partial T}{\partial t} \qquad (3.2.3)$$

3.2.4 Concluding remarks

Due to the high capital costs and large uncertainty in the measured coefficient the three indirect measurement techniques were considered to be inappropriate. Of the three direct measurement methods, the liquid crystal method is deemed to be the most suitable based upon capital costs, flexibility of required analysis, capability of real time measurements, reusable test surfaces and ease of analysing complex geometries.

Further information on the techniques reviewed is offered by Law and Masliyah [28], Button and Mohamad [29] and Jambunathan et al [30]. This last paper reviews all six techniques in detail and offers liquid crystals as the most advantageous technique for the determination of local convective heat transfer coefficients.

Due to the steady state analysis limitation, requiring uniform surface heating, on a finned structure transient analysis is considered superior. The methodology is to obtain the temperature profile data, from the liquid crystal coated heat exchanger, under transient conditions, and use transient analysis to determine the local heat transfer coefficients. The transient analysis method is explained in chapter 4.

The determined local heat transfer coefficients are used in a steady state numerical model. Heat transfer rates, from differing geometries, are compared by basing the steady state model at a uniform internal temperature and a nominal bulk fluid temperature. The comparisons made are to the geometry representing the dimensions of the Brazilia Slimline 5.

3.3 Liquid crystals

3.3.1 Technique review

Early reports by Ouden and Hoogendoorn [20] suggested the use of liquid crystals for the determination of the local convective heat transfer coefficient for jet impingement. They cited problems of spraying liquid crystals directly onto a surface, and proposed the use of a polyacrylate resin solution to be used for application. This methodology involved a 24 hour soak period, to clear the solvent used for the mixing of the polyacrylate and liquid crystal solution.

Later papers show the use of liquid crystals for investigations into fluid convection. Fitzjarrald [31] used a working fluid of nematic liquid crystals to investigate the convection of a fluid exhibiting a phase change. Hodson et al. [32] looked at the thermal instabilities of nematic liquid crystals by placing a thin sample of the crystals between two horizontal flat plates, in the presence of a vertical temperature gradient.

Application of the crystals can be in many forms. Ireland and Jones [33] used a dispersal of liquid crystals, in a polymer matrix, in the form of a thin grease. The grease was applied to the outside surface of a Perspex model and protected from chemical contamination by a thin backing sheet of Mylar. The backing sheet was reported to improve the visibility of the liquid crystals. The body was subjected to heat from a thermal wind tunnel and then cooled, by drawing air over it, to obtain transient analysis. The same authors [34] also reported on liquid crystals applied to the transfer surface by screen printing.

Application by painting the crystals onto a test surface was undertaken by Simonich and Moffat [35], in the study of concavely curved turbulent boundary layers. They qualified the liquid crystal technique based on earlier work reported by the same authors [27]. In this study the liquid crystals were calibrated to ±0.25 °C for a given colour.

More recent studies yield liquid crystals, used for thermal monitoring, applied to the test surface by spraying. Jones and Hippensteele [36] used multiple layers of chiral nematic liquid crystals to obtain two colour changes at two differing temperatures, at the same point. This is referred to as the double crystal method. The double crystal method was used to firstly determine the initial wall temperature and then the local convective heat transfer coefficient. Edwards et al. [37] sprayed the liquid crystals onto the test surface, but used only one colour change. They determined the initial body temperature by the use of a thermometer. Four coats of the liquid crystals were used in this study, sprayed onto a black acrylic surface. The surface was prepared by rubbing with wire wool, to aid adhesion and reduce reflections. The black surface also gave a good background, for observing the isotherms, enhancing the clarity of the colour change.

Yianneskis [38] reviewed thermal monitoring by liquid crystals, looking at surface temperature measurements, convective heat transfer and flow visualisation. The review brought forward five main areas where care must be taken when using liquid crystals for surface measurements, this being with respect to:

a. Calibration of the crystals
b. Type of illumination used to avoid radiation effects
c. angle of viewing and calibration to be less than 30° to the normal
d. Use of narrow band filters to ease detection of the isotherm
e. reducing glare by the use of polarized light

3.3.2 Liquid crystal theory

Yianneskis [38] reported that there are about 20,000 materials that exhibit liquid crystal properties, the most common example being soap bubbles. In the field of thermal monitoring, and heat transfer coefficient determination, cholesteric crystal compounds where the first type of liquid crystals to be used. Later, after a breakthrough by BDH of Pool [39], chiral nematics became available, making both microencapsulation and surface application easier.

Cholesteric crystals are cholesteryl esters and other sterol related chemicals. They are photochemically (UV light) unstable and, as cholesterol is a natural product, varying in quality dependent upon the source, the mixture formulation varies from batch to batch. Microencapsulation of the crystals may also vary the colour play. Most of the cholesteryl esters are solids at room temperature. Cholesteryl esters, which show temperatures above 65 °C, are difficult to make and relatively high usage of material is required to give acceptable results.

Chiral nematic crystals (non-sterol based chemicals) are much more stable both chemically and photochemically. Being high purity chemicals, reproducible physical properties, and colour play, are possible from batch to batch. Microencapsulation of the crystals is easier to perform, with very or little change in the colour play properties. Mixtures which show colours up to 150 °C are possible without crystallisation at room temperatures. Mixtures can also be produced that will show temperatures as low as -30 °C. With this type of liquid crystal less volume is required to show colour changes, hence thinner film applications on the transfer surface can be used.

The liquid crystals used in this investigation are made by Hallcrest of Illinois [40]. They are microencapsulated chiral nematics, which means they have twisted molecular structures. They are classified as thermotropic crystals which are thermally activated mesophases (between crystalline solid and isotropic liquid). The optical properties are formed by melting of the mesogenic (liquid crystal forming) solids to a temperature above which the crystalline lattice is no longer stable. Chiral nematic crystals are optically active in that they rotate the plane of linearly polarized light. Within the temperature range of the chiral nematic mesophase the structure is responsive to temperature variations. As the temperature increases there is further thermal motion, resulting in an increase in the molecular volume. This results in a displacement in the angle between adjacent molecules. Only a 7 minute of arc change in displacement is required to cause a scan of the whole visible spectrum. The mixtures display temperatures by turning from colourless to red, through the visible spectrum, to blue/violet and back to colourless again, under the influence of a positive temperature gradient. This is depicted in Figure (3-1).

Microencapsulation is used to stabilise the liquid crystal mixture and give it a protective barrier. The process is to encapsulate tiny droplets of liquid crystals in a continuous polymer coating. The microcapsule diameters are generally between a few microns and a few millimetres.

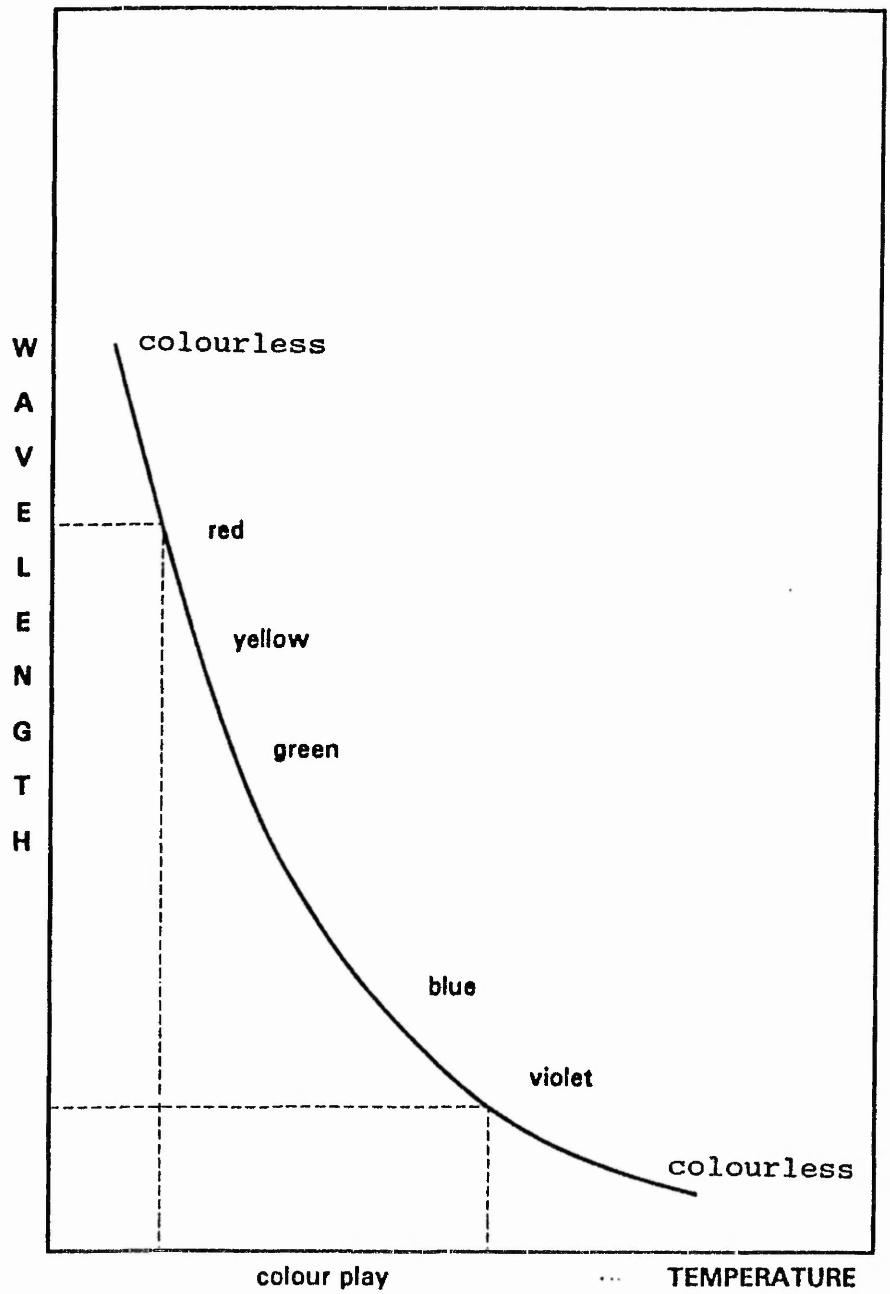

FIGURE 3-1 WAVELENGTH RESPONSE TO TEMPERATURE

The crystals, used in the experiments, have a manufactures colour change specification of red at 35 °C, with a blue start temperature of 36 °C. This information is deemed insufficient for the accuracy required and, as suggested by Yianneskis [38] a calibration plate was made. The plate is a flat surface with a platinum resistance thermometer placed level with the top. This is as described by Edwards [41]. A dimensional drawing of the calibration plate is given in Appendix A (A-1). The platinum resistance thermometer (type F232 - 100 Ω at 0 °C) was firstly calibrated, in a thermal bath, to give a curve over the range of 20 °C to 40 °C. The curve obtained is shown in Figure (3-2). The equation for this curve, found by linear regression (Appendix B (B.1)), is

$$\mathbf{T = 2.99\,R - 301.74} \quad (°C) \qquad (3.3.1)$$

The crystals were applied after spraying the calibration plate with a water based black paint, from Hallcrest. The paint is designed for use with liquid crystals, and has no effect upon them. Three coats of the liquid crystals was then applied, over the paint. A time interval of 30 minutes was allowed, between coats, for drying. The calibration plate was placed in a thermal tunnel and the platinum resistance thermometer output recorded, when the <u>green</u> isotherm passed over it. This was repeated eight times, with the thermal tunnel both rising and falling in temperature, to allow for any hysteresis of the colour play. The resultant resistance readings, of the platinum resistance thermometer, were taken with a calibrated Keithley digital multi meter. The results are shown in Table (3-A).

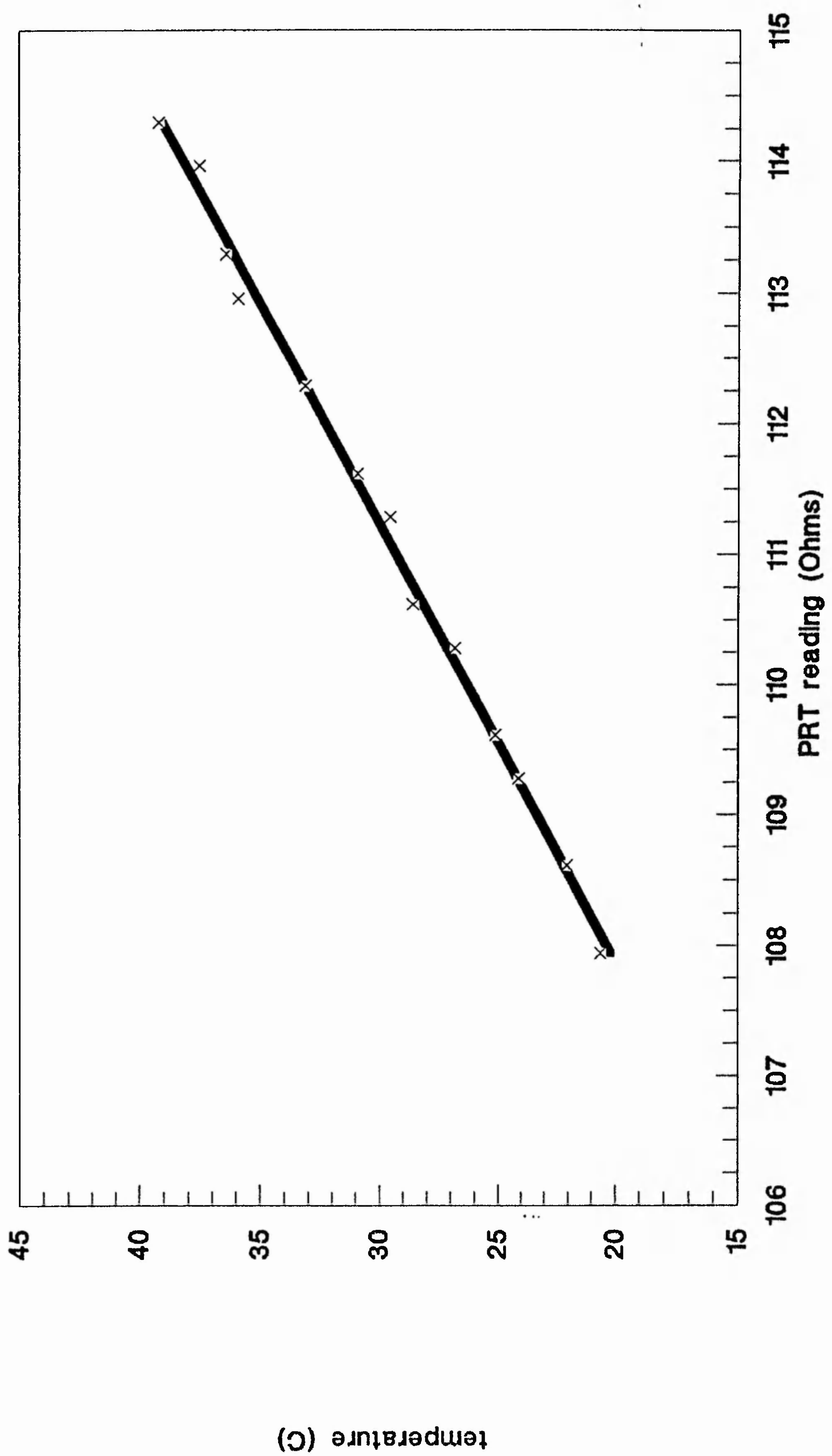

FIGURE 3-2 Platinum resistance thermometer calibration

resistance reading (Ω)	calculated temperature (°C)
113.08	36.369
113.1	36.429
113.07	36.339
113.09	36.399
113.1	36.429
113.09	36.399
113.1	36.429
113.1	36.429

TABLE 3-A RESISTANCE READINGS

The corresponding average temperature, of the green colour change, with an estimated error, as outlined in Appendix B (B.2), is thus

$$T_g = 36.40 \pm 0.01 \ °C \qquad (3.3.2)$$

3.4 Methodology

3.4.1 Thermal tunnel and model

The heat transfer surfaces tested are heated to a uniform temperature in a thermal wind tunnel. The tunnel provides a uniform temperature to a tolerance of ±0.4 °C over a measured 5 minute time period. The tunnel is the same design as used for transient analysis by Edwards [41]. A dimensional drawing is given in

Appendix A (A-2). The tunnel draws air into a centrifugal fan via a 24.5 kW heater. The heated air is then fed through a series of diffusers, flow straighteners and turbulence eliminating screens, finally being reduced by an 8.5:1 ratio and exhausted over the transfer surface. The transfer surface is held on two ledges, and suspended in the centre of the flow. The flow temperature is recorded, by a calibrated thermometer, to an accuracy of ± 0.1 °C. A schematic of the tunnel is given in Figure (3-3).

Once the model has been uniformly heated in the tunnel, it is quickly removed and placed on a stand, where the results are instantaneously recorded. Appendix A (A-3) and (A-4) give dimensional drawings of the base and stand respectively. The model dimensions given are base dimensions to which extended surfaces are adhered. Both the base and extended surfaces are made from acrylic, with a thermal conductivity value of 0.1884 W/mK. Adhesion of the extended surfaces to the base is by chloroform. Chloroform allows the two pieces to be welded together, yet also allows removal and subsequent adhesion of differing configurations.

The handle attached to the base is designed to hold the transfer surface in the correct orientation, for the convection process to take place. The back of the handle fits onto the top of the stand. It is designed to minimise conduction, from the base to the handle, by minimising the contact area between the handle and base. The details of the handle are on the base drawing given in Appendix A (A-3).

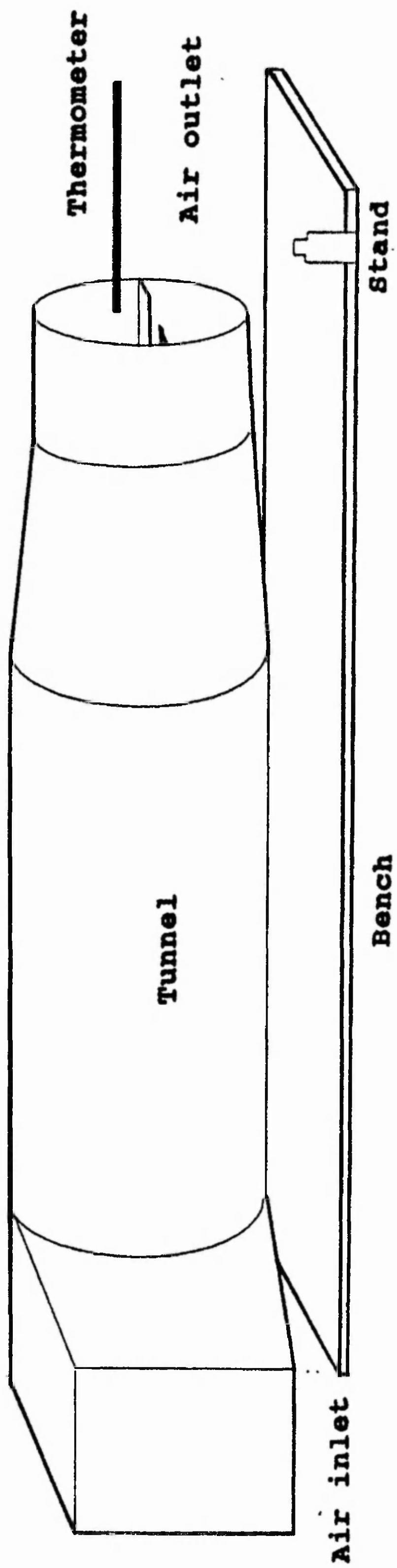

FIGURE 3-3 TUNNEL SCHEMATIC

3.4.2 Experimental procedure

Preparation, of the heat transfer surface, is by firstly washing and then scouring the surface, to remove any grease deposits that may remain from handling, and then drying. The application of the black paint and liquid crystals is undertaken as outlined in section 3.3.2. The black paint aids both adhesion of the crystals and viewing of the isotherms.

The thermal tunnel is prepared by turning on the fan, followed by the heating element. This sequence reduces the possibility of over heating the tunnels electrical heating elements. The tunnel is left to stabilise for a period of 2 hours, this being deduced from Figure (3-4). The heat transfer model is then introduced into the flow field for heating.

The model is left to stabilise for a period of 1 hour, shown in Figure (3-5). This period is found by placing a thermocouple at the centre of a flat plate, measuring the centre temperature and tunnel temperature simultaneously. The temperature of the model stabilises 3 °C below the thermometer reading at the centre of the tunnel. This discrepancy is allowed for in the calculation of the local heat transfer coefficient.

After uniformly heating the model, for the 1 hour period, the initial temperature of the body is found by reading the thermometer in the exit flow field of the tunnel. The body is quickly removed and placed on the stand, for free convection to take place. Recording of the temperature contours is by the use of a Sony

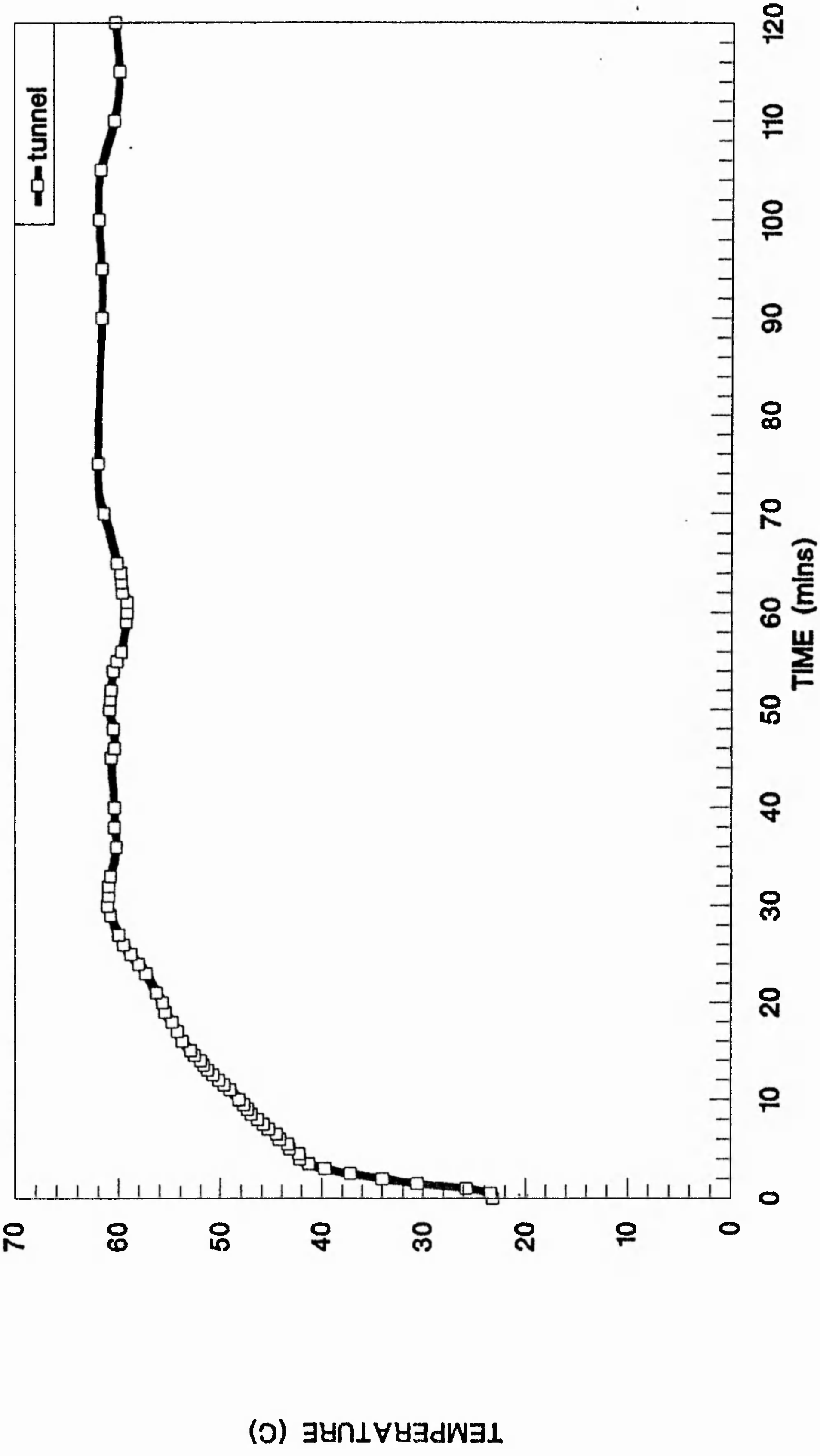

FIGURE 3-4 Tunnel stabilisation time

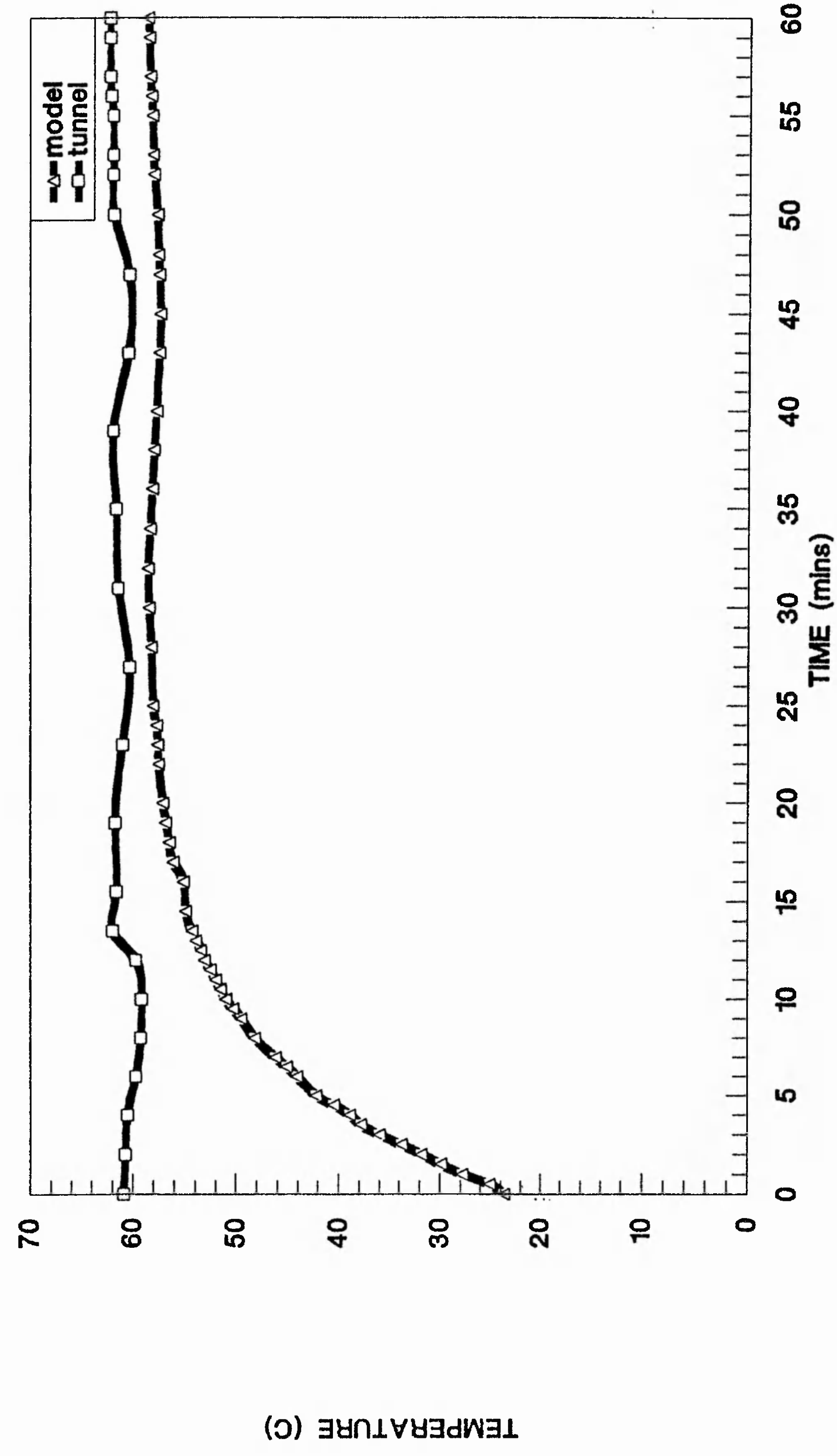

FIGURE 3-5 Model stabilisation time

CCD-F380E video 8 camera recorder onto 8 mm metal video tapes. The camera is held steady by a tripod stand, and the model lit by a halogen spot light. To further enhance the viewing a black background is used behind the stand holding the model. The spot light is placed so that the light is reflected onto the model, and not directly aimed at it. This reduces the effects of U-V light degradation of the crystals, and also thermal radiation effects. Once the entire surface temperature has dropped below the liquid crystals green melt temperature, the video is stopped. Throughout the recording the ambient temperature is monitored, and the average value calculated.

Play back of the recording is via the recorder onto a colour monitor. The time of the green isotherm to reach a pre-determined point is recorded. Only half of the centre, and outer fin faces are recorded, as the heat transfer coefficients are assumed to be symmetrical about the centre lines. The areas of symmetry are shown in Figure (3-6).

The height of the fin is portioned into ten sections, the top and bottom being half the height of the centre sections. Node points are marked on the sections and numbered 1 to 10. There are eight node points per section, prefixed A though H, these being equally spaced along the fins length and base inter fin spacing. The locations are shown in Figure (3-7).

The localised heat transfer coefficients are computed for the eighty node points by one dimensional transient analysis. This information is then used in a steady state

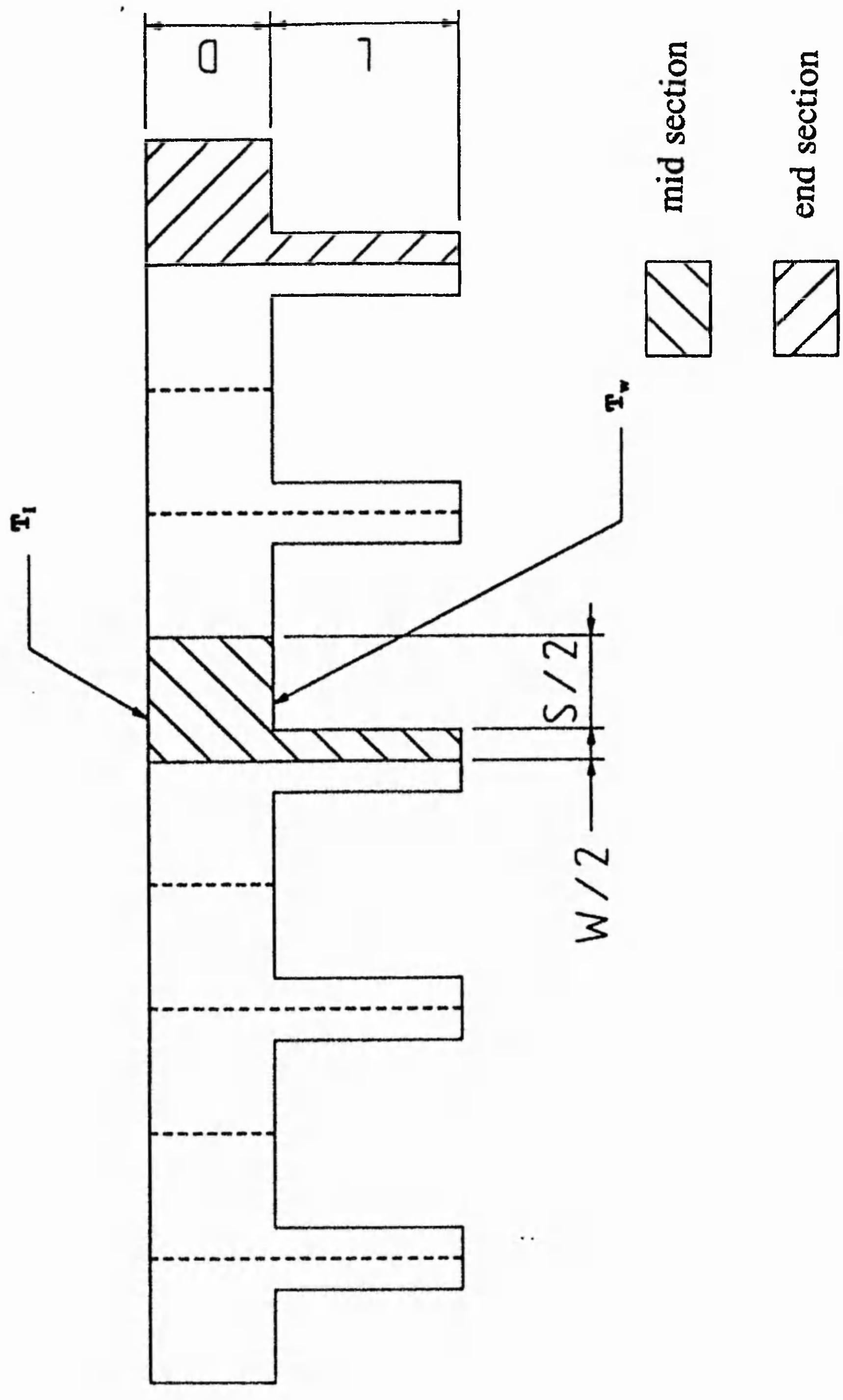

FIGURE (3-6) Areas of symmetry

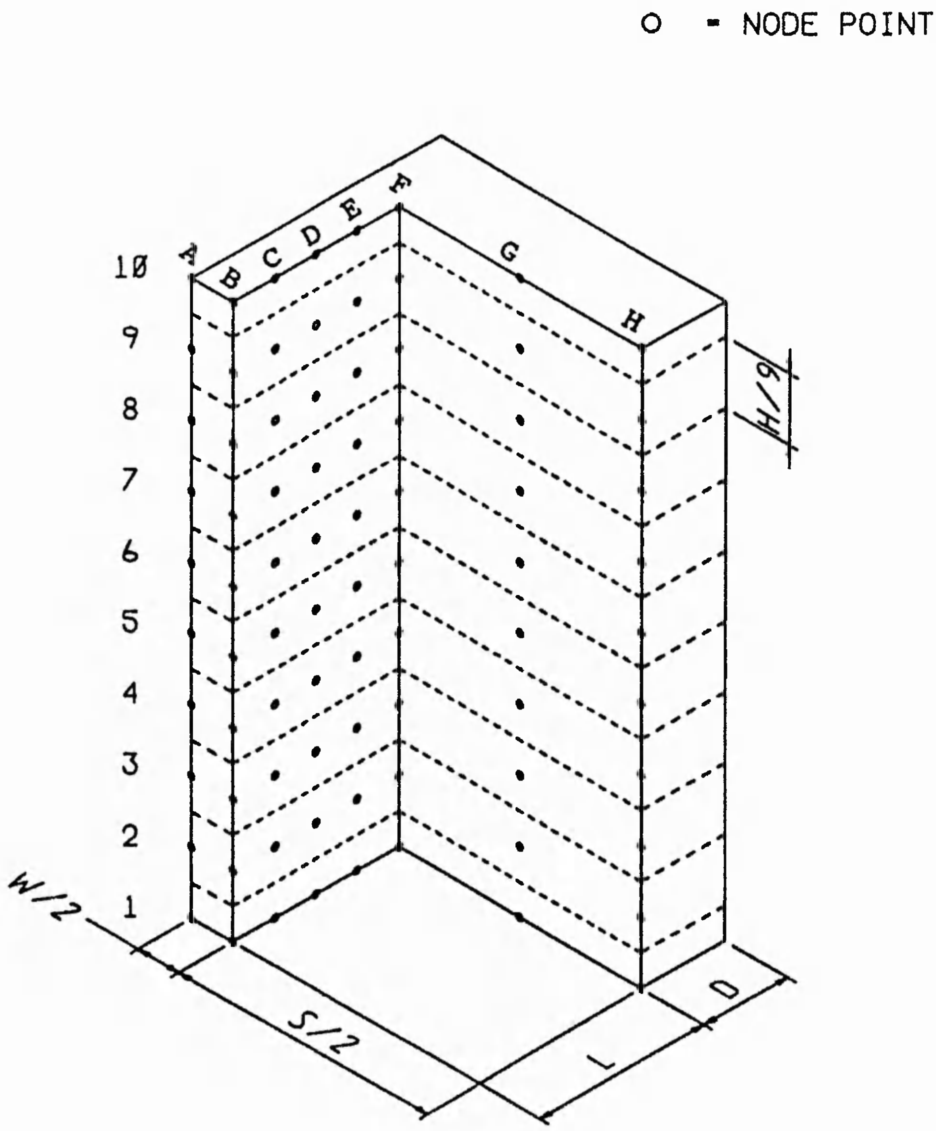

FIGURE (3-7) nodal distribution

iterative process to assess the heat transfer through each section (Q_n). The heat transfer through the area of symmetry is found by the summation of the heat transfer through the sections,

$$\mathbf{Q_{sum} = \Sigma_{\,n=1,10}\; Q_n} \qquad (3.4.1)$$

and the total heat transfer for the transfer model

$$\mathbf{Q_{TOT} = 2(n\text{-}1)\; Q_{sum,c} \;+\; 2\; Q_{sum,o}} \qquad (3.4.2)$$

To offset the calculated and size errors in the model, all the tests are based upon the reference model with the same fin length (L) and spatial separation (S) as the Brazilia Slimline 5. The uniform internal wall temperature is obtained from Figure (3-8), at a reference point of 60 mm down from the top of the fin. The ambient temperature (T_b) is taken as the recognised comfort level within the domestic heating industry, and the thermal conductivity (k) for cast iron given by Perry and Chilton [44]. These values are

$$\underline{\mathbf{L = 0.025\ m}} \qquad (3.4.3)$$

$$\underline{\mathbf{S = 0.020\ m}} \qquad (3.4.4)$$

$$\underline{\mathbf{T_w = 300\ \ ^\circ C}} \qquad (3.4.5)$$

$$\underline{\mathbf{T_b = 20\ \ ^\circ C}} \qquad (3.4.6)$$

$$\underline{\mathbf{k = 44.7\ \ W/mK}} \qquad (3.4.7)$$

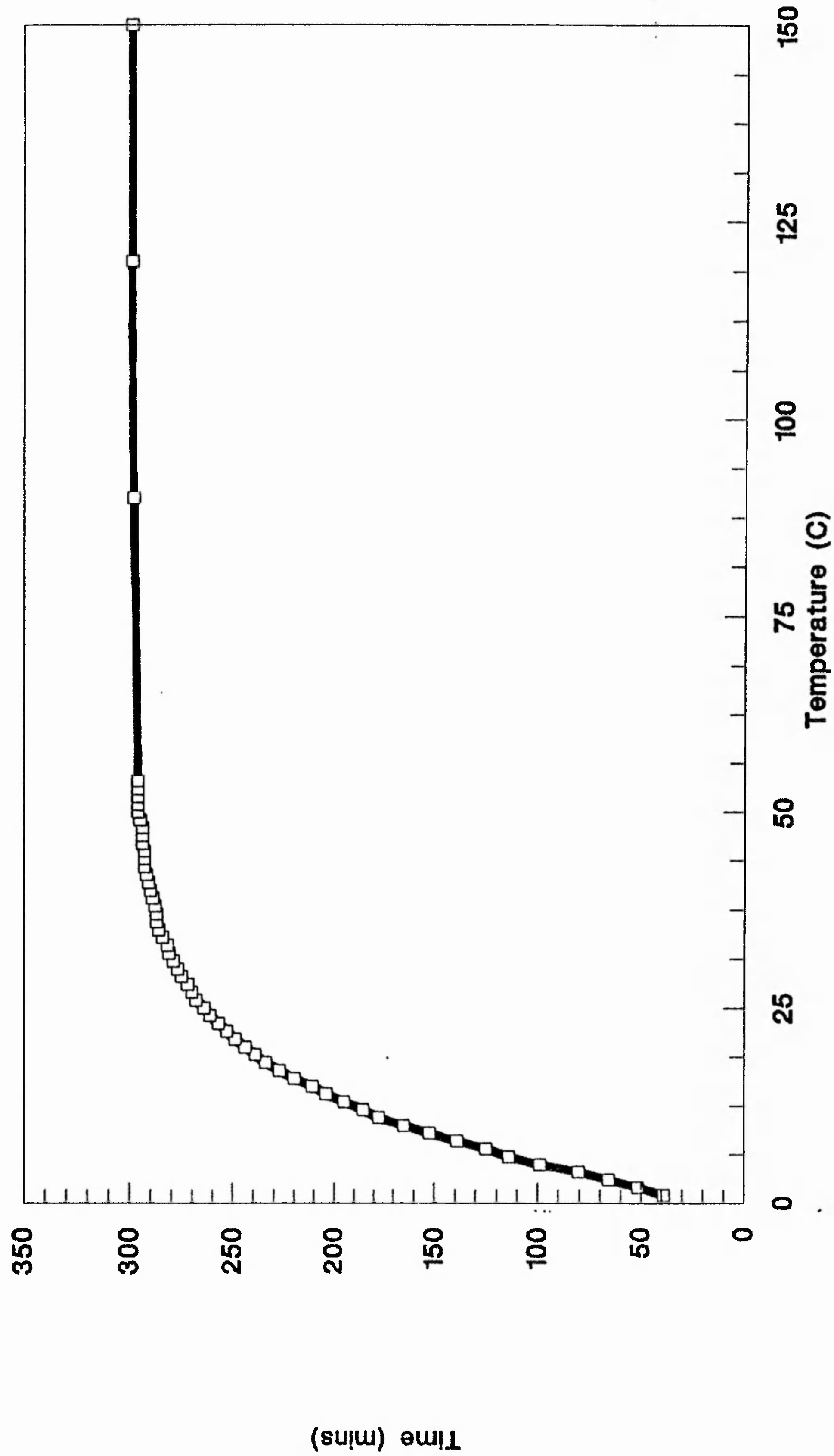

FIGURE 3-8 Brazilia Slimline 5 internal wall temperature

CHAPTER 4

NUMERICAL DETERMINATION

4.1 Introduction

For the purpose of this investigation, one dimensional (1-D) transient analysis has been used for the determination of the local heat transfer coefficients, and two dimensional (2-D) steady state analysis to estimate the heat transfer through the heat exchanger. The grid discretisation, for the 1-D analysis, is found by apportioning the sectional width into 18 parts, along the x directional axis, Figure (4-2). This gives an incremental distance between each node of,

$$\Delta x = \frac{W}{18} \tag{4.1.1}$$

The 2-D steady state mode of analysis uses the coefficients determined from the 1-D analysis, and performs a linear interpolation between adjacent values, to increase the number of nodes by three. The increase in nodal points also reduces the grid size, and increases the iteration accuracy. The grid type is of cartesian ordered rectangular elements, the size of which are determined by the fin spatial separation and length.

Both transient and steady state analysis computational programs are written in Fortran 77. Flow charts of the programs are given, along with a detailed explanation of the derivations involved.

4.2 Transient analysis

4.2.1 1-D finite difference

For the determination of the local heat transfer coefficient, from liquid crystal data, the governing equation *(3.2.3)* must be solved. For 1-D transient analysis the equation is reduced to the 1-D cartesian form of,

$$\frac{\partial T}{\partial t} = \alpha \frac{\partial^2 T}{\partial x^2} \tag{4.2.1}$$

The partial differential terms are replaced by finite difference approximations. Referring to Figure (4-1), Schmidt's method, the conduction through the material for points n=2 → 9 are related by,

$$T_{n-1} + T_{n+1} = 2\,T_n + \left(\frac{\partial^2 T}{\partial x^2}\right) \Delta x^2 \tag{4.2.2}$$

given a forward time step of,

$$\frac{\partial T}{\partial t} = \frac{T'_n - T_n}{\Delta t} \tag{4.2.3}$$

where T'_n is the new temperature, thus

$$\frac{T'_n - T_n}{\Delta t} = \alpha \left(\frac{T_{n-1} + T_{n+1} - 2\,T_n}{\Delta x^2}\right) \tag{4.2.4}$$

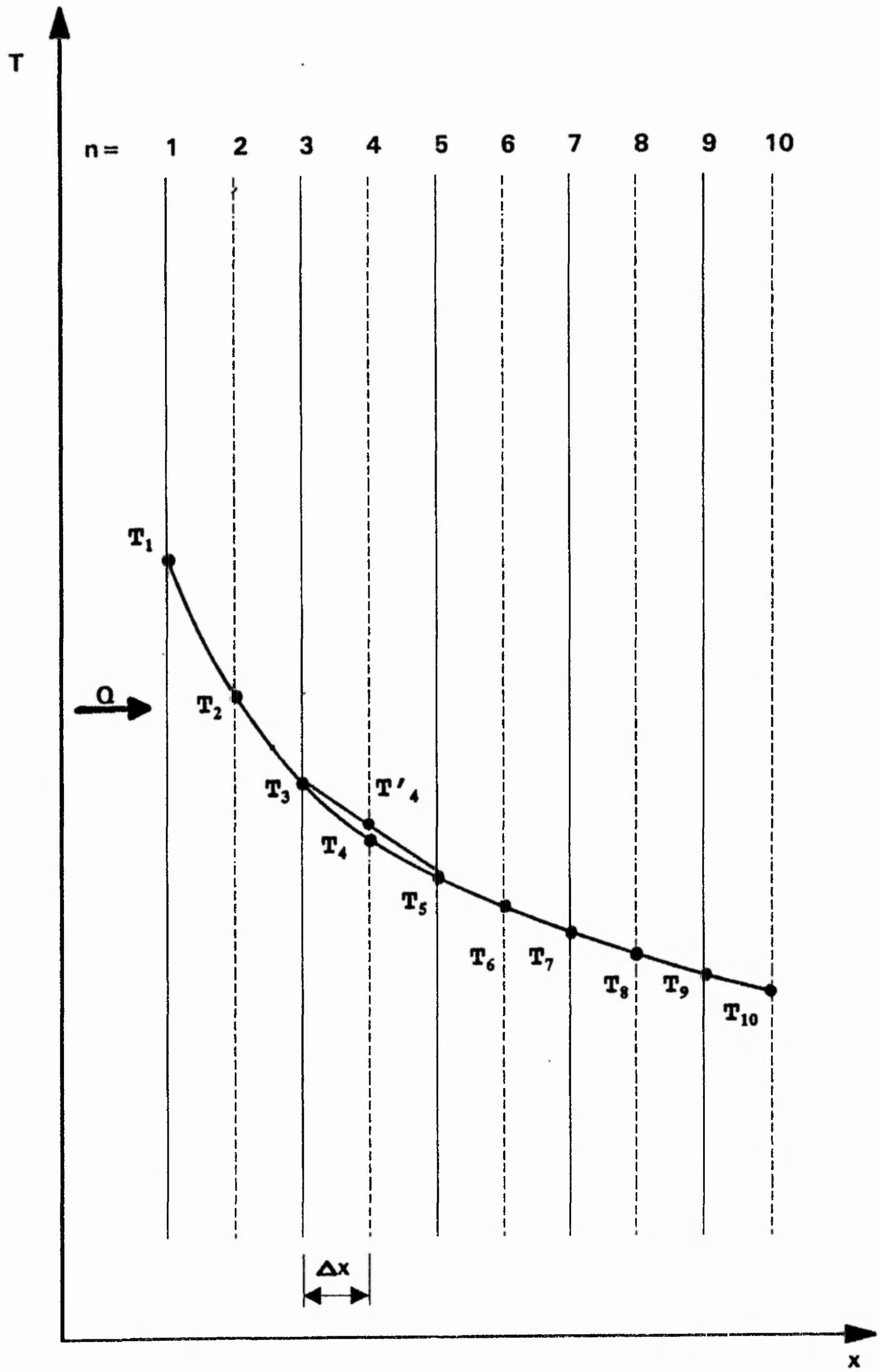

FIGURE 4-1 TEMPERATURE PROFILE THROUGH MATERIAL

The ratio of conducted heat rate to storage of heat rate is given by the Fourier number, hence the explicit finite difference conduction equation becomes,

$$T'_n = Fo \left[T_{n-1} + T_{n+1} + T_n \left(\frac{1}{Fo} - 2 \right) \right] \tag{4.2.5}$$

Values of Δt and Δx are chosen so that the new temperature (T'_n) remains positive. For this to occur the coefficient of T_n must be ≥ 0, hence for stability of the solution.

$$Fo \leq 0.5 \tag{4.2.6}$$

Figure (4-2) gives a view of a section of the heat exchanger where 1-D transient analysis is to be performed. Equation *(4.2.5)* is for conduction only and where the surface node occurs (n=1), convection and radiation will occur. This gives an energy balance equation, from Croft and Stone [45], of

$$\rho c_p \frac{\Delta x}{2} \frac{T'_1 - T_1}{\Delta t} = \frac{k}{\Delta x} (T_2 - T_1) + h (T_b - T_1) + F\epsilon\sigma (T_b^4 - T_1^4) \tag{4.2.7}$$

Given that the ratio of surface conductance to thermal conductivity is the Biot number and R is the analogous radiation term, the new surface temperature for the combined heat transfer modes is given by,

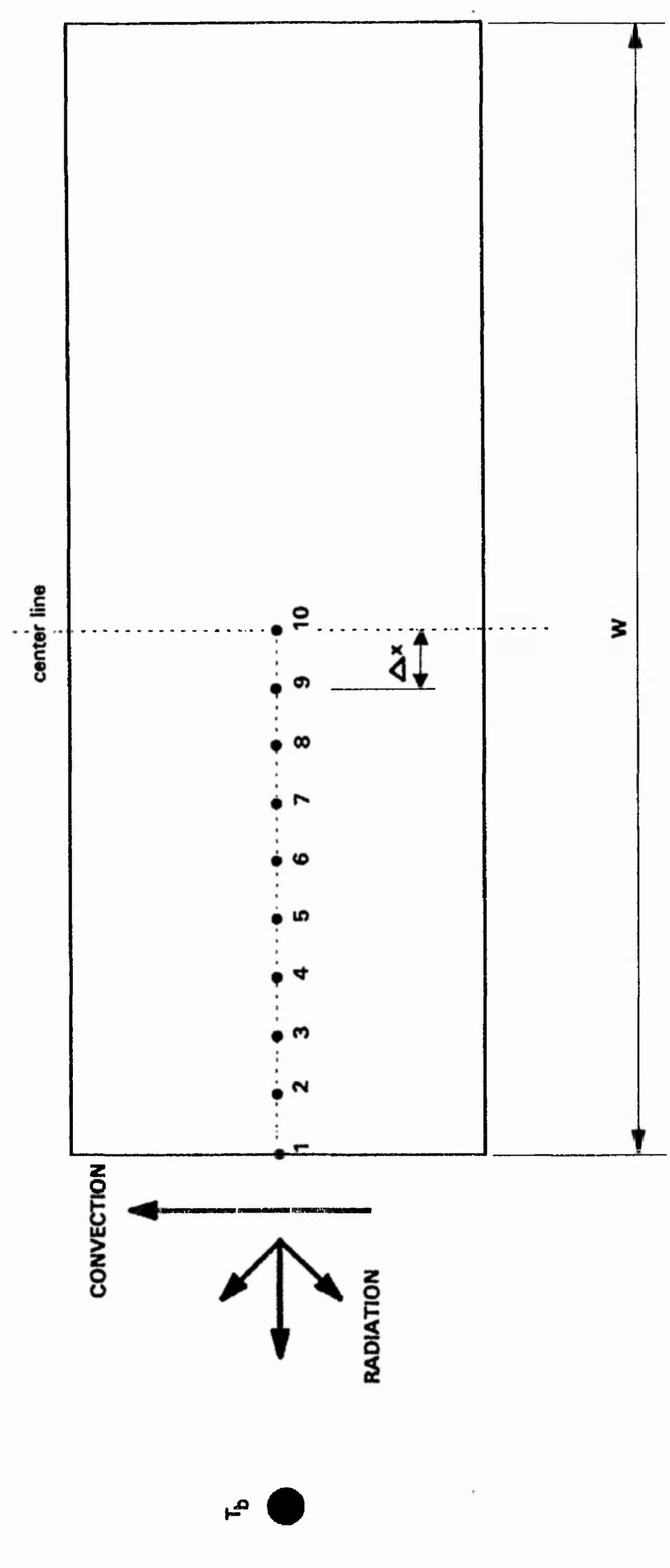

FIGURE 4-2 1-D node points to centre line of material

$$T'_1 = 2Fo\left[T_2 + Bi\,T_b + R\,T_b^4 + T_1 \left(\frac{1}{2Fo} - Bi - 1 - R\,T_1^3\right)\right] \qquad (4.2.8)$$

The stability criterion for the combined heat transfer modes will similarly lead to

$$Fo \leq \frac{1}{2(\,Bi + 1 + R\,T_1^3\,)} \qquad (4.2.9)$$

The centre node (n=10) is determined by introducing a fictitious node, which is a mirror image of node 9. The nodal temperature is hence a summation of the two T_9 temperatures and product of the centre temperature and argument. This results in the new centre temperature being,

$$T'_{10} = Fo\left[2\,T_9 + T_{10}\left(\frac{1}{Fo} - 2\right)\right] \qquad (4.2.10)$$

From Figure (4-2) the node at the centre of the material has an initial temperature T_I. This will decay with increasing time. At the start of the test the outer surface wall temperature (T_w) is also at the initial temperature. Considering the cooling of the wall to have the same cooling mode as that of a lumped capacity system, Simonson [46], then a logarithmic decay of the outer wall temperature between T_I and T_g in a time interval of Δt will be related by a time constant of tc. This relationship is given in *(4.2.11)*.

$$\ln \frac{T'_w}{T_w} = -\frac{\Delta t}{tc} \qquad (4.2.11)$$

Hence, for a given time step Δt, the estimated wall temperature, ascertained from *(4.2.11)*, is used to calculate the new centre temperature (T_{10}), by using the explicit finite difference equations *(4.2.5)* and *(4.2.10)*. The calculated curves for the wall and centre temperatures, of a 10 mm acrylic section, cooling from an initial surface temperature of 65 °C down to a temperature of 35 °C, at a bulk fluid temperature of 20 °C are given in Figure (4-3). The plots represent two different locations along the vertical axis, with cooling time periods of 800 s and 300 s.

4.2.2 1-D Transient program development

Data obtained for the node points, given in Figure (3-7), from the test model are the initial temperature (T_I), green isotherm temperature (T_g) and time (t). The time is for the surface to cool from T_I to T_g at each surface node. Other variables used are the wall thickness (W) (or D dependent upon nodal location) and shape factor (F). All the models used have set values of thermal conductivity (k), thermal diffusivity (α) and emissivity (ϵ). To use 1-D transient analysis, an estimation of the local heat transfer coefficient must be made. This is required to set the values of the Biot number (Bi) and time increment (Δt), for given values of the Fourier number (Fo) and nodal spacing (Δx). Stability is resolved by considering both criteria in equations *(4.2.6)* and *(4.2.9)*.

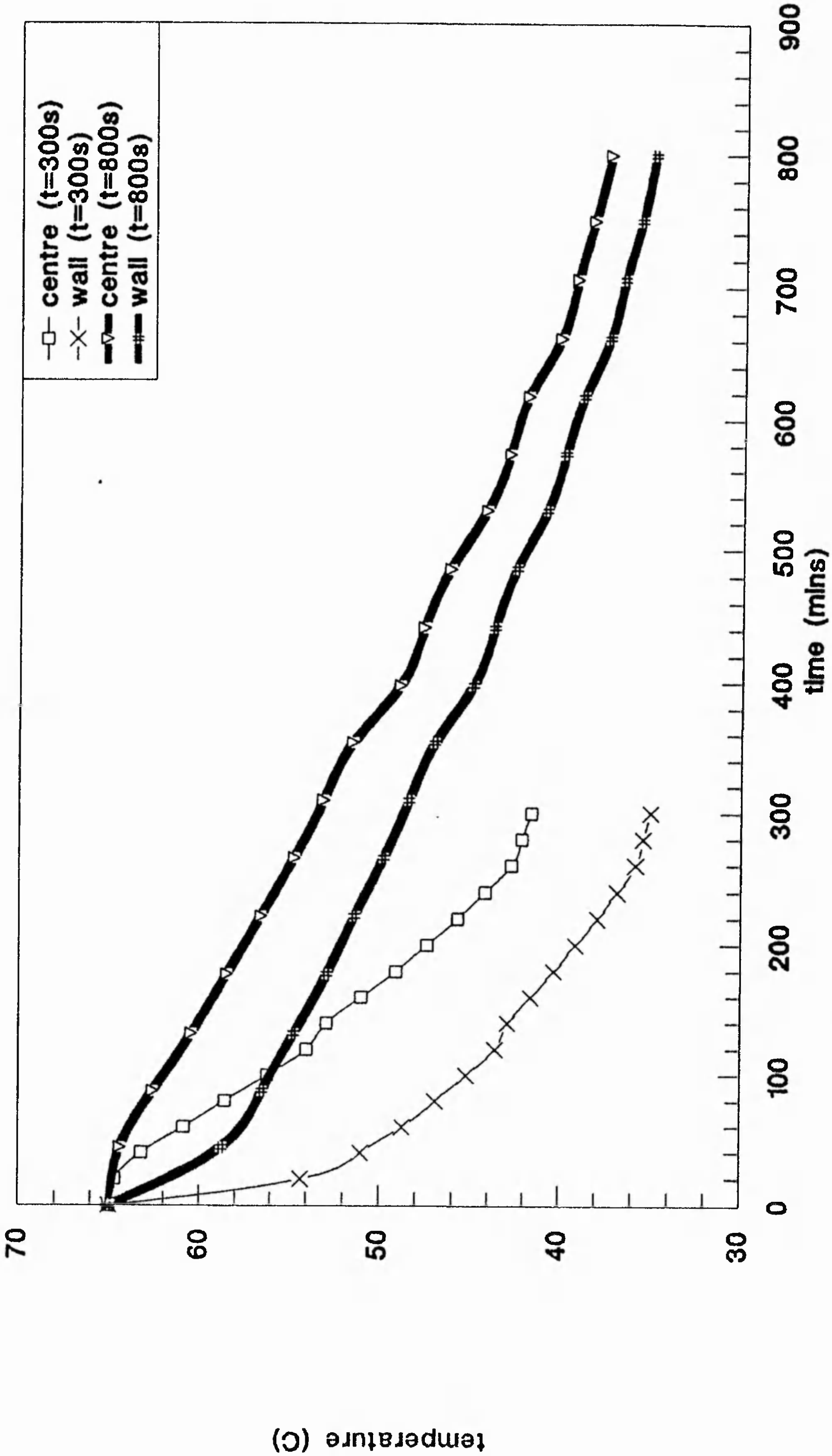

FIGURE 4-3 Predicted centre and wall temperature decays

The time step sets the number of iterations (n), of the explicit technique, to be performed. On completion of the iterations the resultant wall temperature is determined. The resultant temperature is compared to the known actual wall temperature (T_g). If the temperature is within an estimated residual tolerance, found by increasing the residual tolerance for a number of known coefficient values until the computed value starts to rise or fall, then the correct value for the heat transfer coefficient has been determined. If the comparison is outside the residual tolerance, then a new estimation is made and the process repeated. The format for the comparison is given in equation *(4.2.12)*.

$$|T_w - T_g| = \pm 0.05 \quad {}^\circ C \tag{4.2.12}$$

At each iteration a modified centre temperature is computed, to allow for the decay at this point. This is ascertained from equations *(4.2.5)*, *(4.2.10)* and *(4.2.11)*. To ensure stability, in the estimations of the local heat transfer coefficient, a successive approximation technique is used. The technique works by allowing the estimated value, for the heat transfer coefficient, to become larger than the true value. This is determined from the resultant temperature being lower than T_g-0.05 °C. The next value is estimated to be half way between the higher value and the previous lower value. This new estimation is returned, into the 1-D transient analysis program, and further resultant temperature determined. The process is repeated, successively reducing the error between the estimated value and true value, by taking the half way points between the latest high and low values.

The initial estimation of the local heat transfer coefficient is made by considering the input parameters, for the 1-D transient analysis program. An equation is used which gives a close approximation to the actual value, this being based upon correlations produced for reference conditions of,

$$\mathbf{T_I = 62\ °C} \tag{4.2.13}$$

$$\mathbf{T_g = 34\ °C} \tag{4.2.14}$$

$$\mathbf{T_b = 16\ °C} \tag{4.2.15}$$

$$\mathbf{W = 3\ mm} \tag{4.2.16}$$

The reference values are incremented in differing steps to a maximum value where,

$$\mathbf{T_I = T_I + n \qquad (n=0\ to\ 7\ ,1)} \tag{4.2.17}$$

$$\mathbf{T_g = T_g + n \qquad (n=0\ to\ 1.2\ ,0.2)} \tag{4.2.18}$$

$$\mathbf{T_b = T_b + n \qquad (n=0\ to\ 7\ ,1)} \tag{4.2.19}$$

$$\mathbf{W = W + n \qquad (n=0\ to\ 7\ ,1)} \tag{4.2.20}$$

Each local heat transfer coefficient is calculated for time steps of 50 to 600 seconds in 50 second increments. The resultant values are plotted in Figures (4-4) to (4-7), showing a series of curves with a near rectangular hyperbola conformity, under the influence of a parallel shift. The rectangular hyperbola equation form is,

$$\mathbf{h\ t = C} \tag{4.2.21}$$

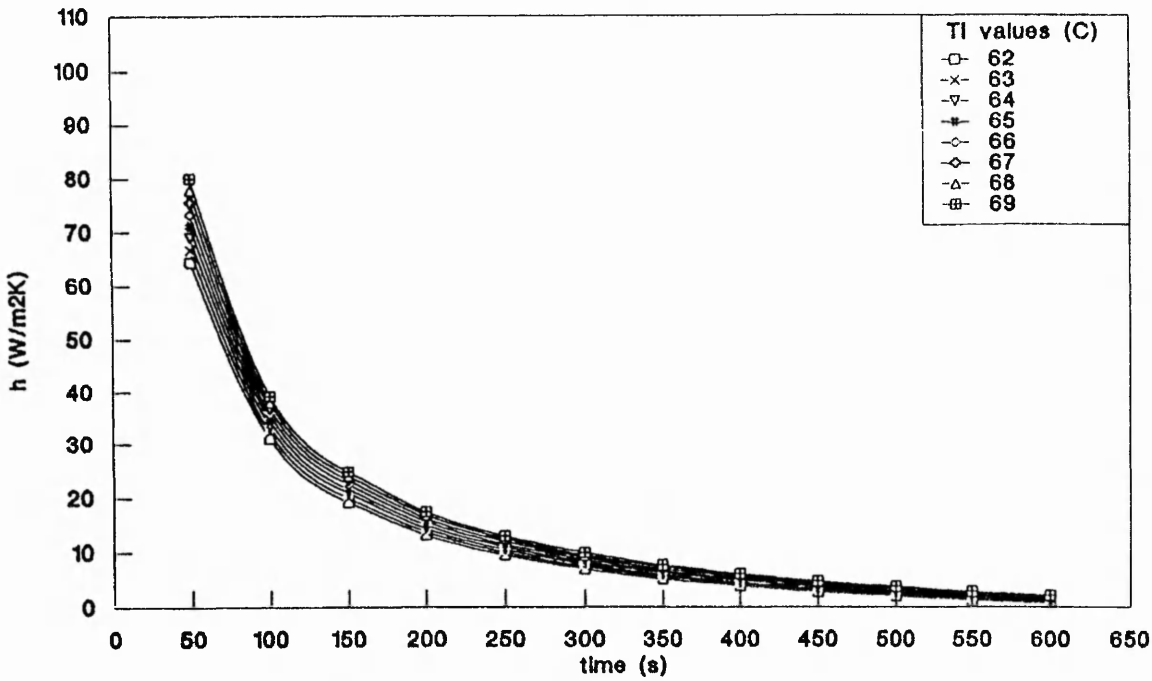

FIGURE 4-4 Estimated h for varying initial temperature

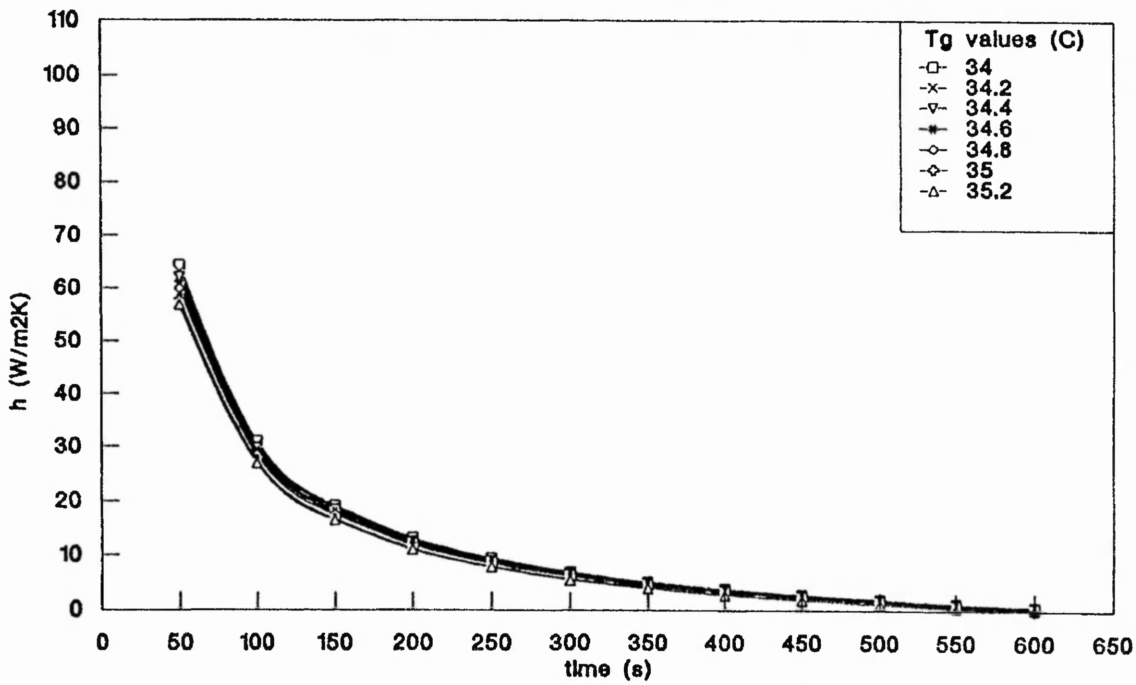

FIGURE 4-5 Estimated h for varying crystal melt temperature

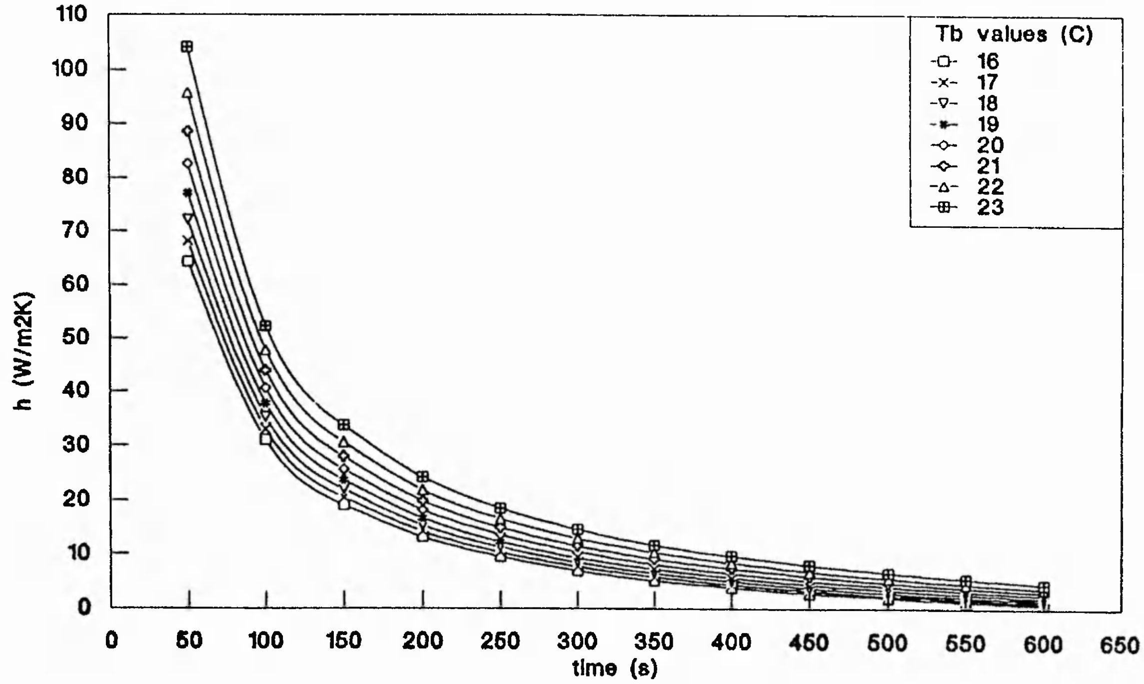

FIGURE 4-6 Estimated h for varying bulk fluid temperature

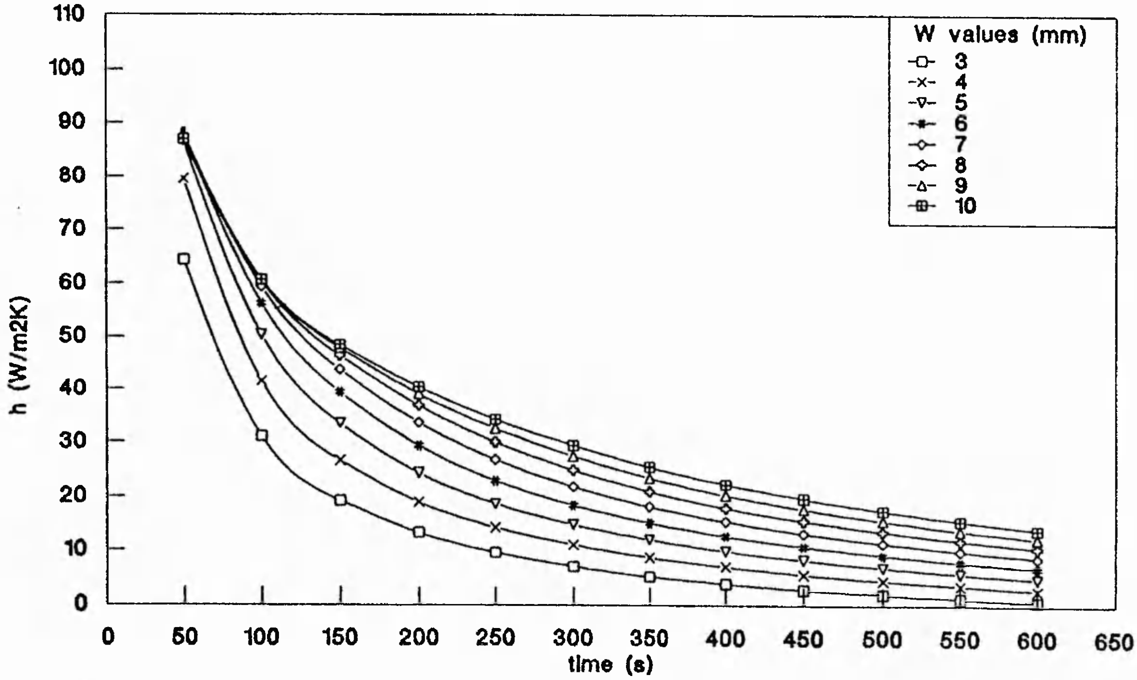

FIGURE 4-7 Estimated h for varying wall thickness

The value of the constant (C), for the reference curve, is calculated using the formula outlined in Appendix B (B.3) and the values given in *(4.2.13)* to *(4.2.16)*. This gives an equation of,

$$\mathbf{h\,t = 3019.4} \tag{4.2.22}$$

Plotting the difference in C, for the variables listed in *(4.2.17)* to *(4.2.20)*, results in a series of curves which relate to the parallel shift. Figure (4-8) shows the correlations for ΔC corresponding to ΔT_I, ΔT_g, ΔT_b and ΔW. Approximating each of the curves, to a linear form, gives a series of equations showing the value of the parallel shift, where

$$\mathbf{\Delta C = 115.5\ (T_I - 335.2) - 14.3} \tag{4.2.23}$$

$$\mathbf{\Delta C = -248.5\ (T_g - 307.2) - 4.1} \tag{4.2.24}$$

$$\mathbf{\Delta C = 290.3\ (T_b - 289.2) - 125.3} \tag{4.2.25}$$

$$\mathbf{\Delta C = 307.4\ (W - 0.003) + 552.8} \tag{4.2.26}$$

Combining these equations, into *(4.2.22)*, gives a correlation for estimating the value of the local heat transfer coefficient, for an acrylic model in free convection of,

$$\mathbf{h = \frac{-43033 + 115T_I - 248T_g + 290T_b + 307W}{t}} \tag{4.2.27}$$

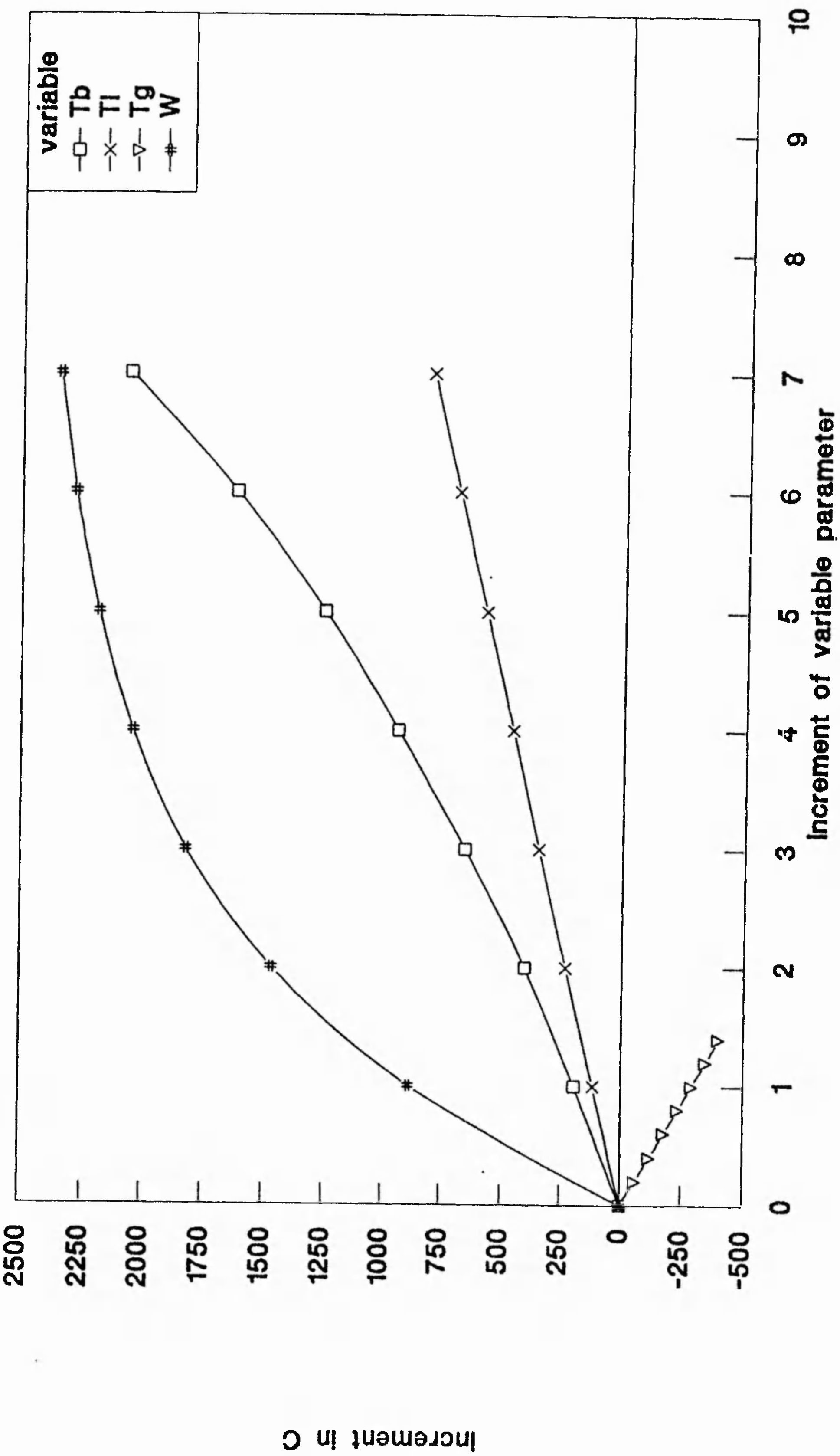

FIGURE 4-8 correlation of model variables for estimated equation of h

The program flow chart is given in Figure (4-9), and shows the steps taken to determine the value of the local heat transfer coefficient. The full program listing, for the 1-D transient analysis technique, is given in Appendix C (1).

4.3 Steady state analysis

4.3.1 2-D finite difference

Two dimensional (2-D) steady state analysis is used to determine the heat transfer through the heat exchanger, given set values of internal temperature, bulk fluid temperature and thermal conductivity, as defined in *(3.4.5)* to *(3.4.7)*. The solution of the general equation is formed by replacement of the partial differentials, by finite difference equations. In the case of the finned heat exchanger, the section analysed, by the 1-D transient method, is partitioned into a grid formation as shown in Figure (4-10). The internal nodes, for the grid formation, are governed by conduction, where Poissons equation gives,

$$\mathbf{k\ \nabla^2 T + H = 0} \tag{4.3.1}$$

Where no internal heat generation occurs equation *(4.3.1)* is modified to the Laplace form of,

$$\mathbf{k\ \nabla^2 T = 0} \tag{4.3.2}$$

For the 2-D form, of the partial differential equation, *(4.3.2)* becomes,

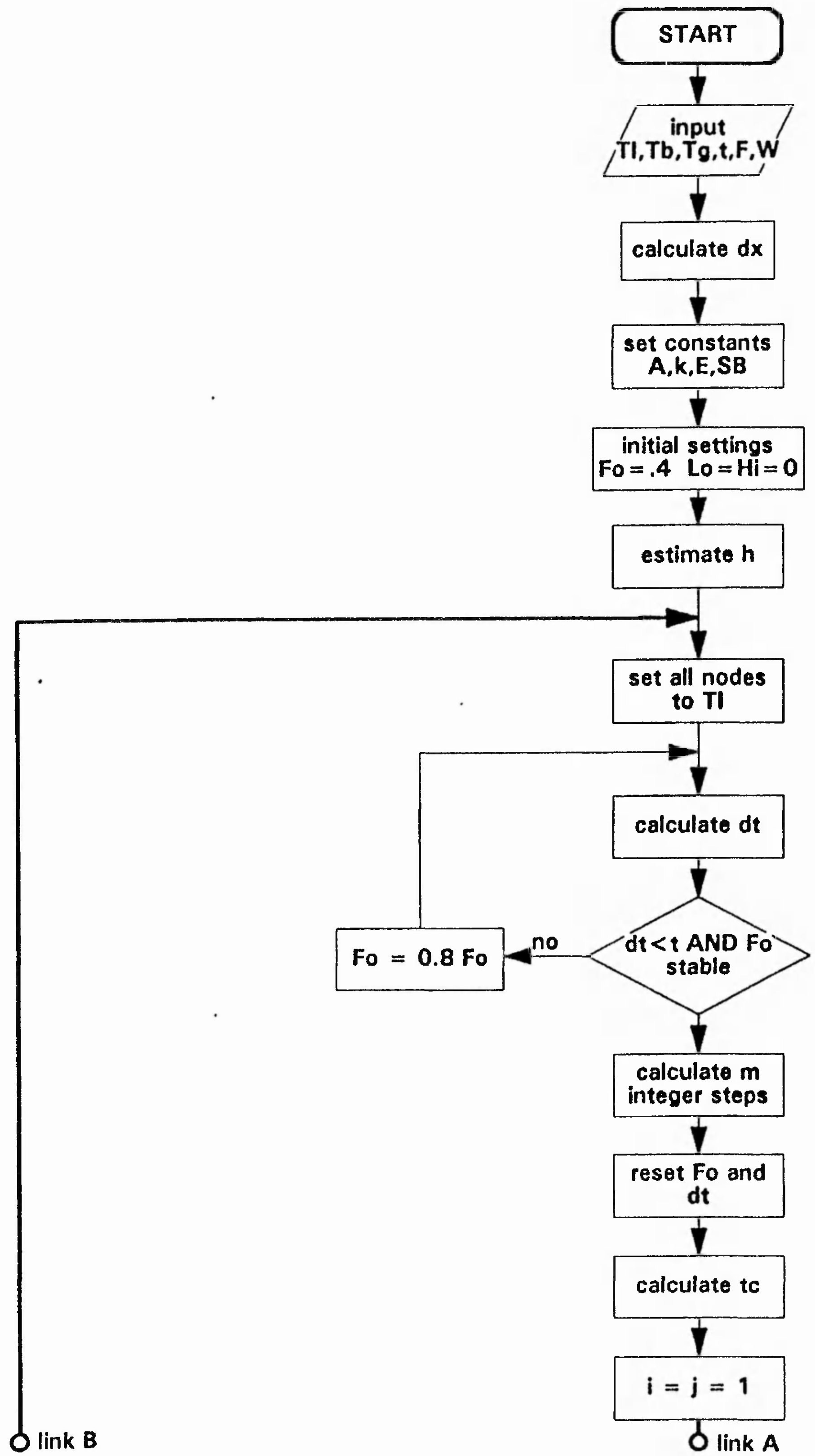

FIGURE (4-9) 1-D transient analysis program flow chart Cont...

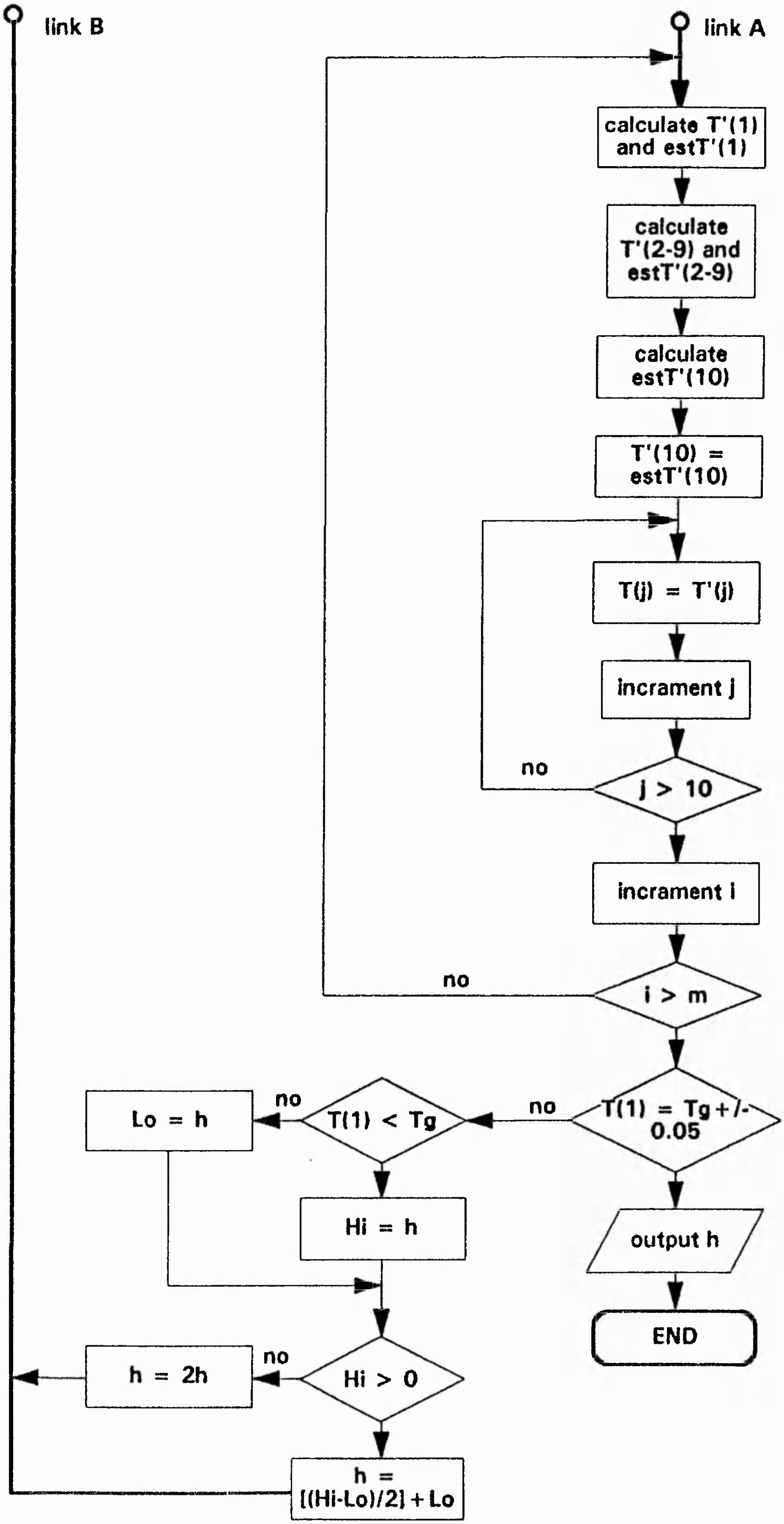

FIGURE (4-9) Continued

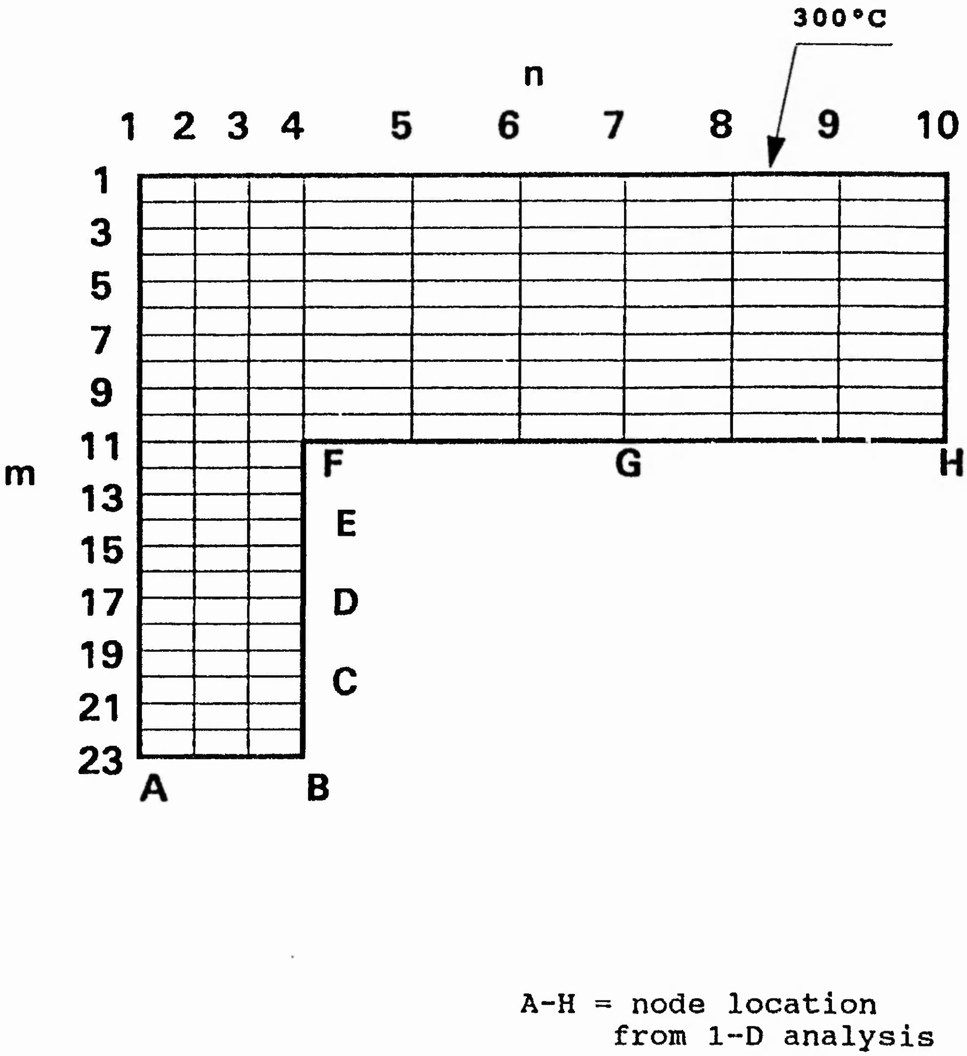

FIGURE 4-10 2-D TRANSIENT GRID FORMATION

$$k\left(\frac{\partial^2 T}{\partial x^2} + \frac{\partial^2 T}{\partial y^2}\right) = 0 \tag{4.3.3}$$

Referring to Figure (4-11), replacing the partial differentials with finite difference terms gives

$$\frac{\partial^2 T}{\partial x^2} = \frac{T_{m+1,n} + T_{m-1,n} - 2T_{m,n}}{\Delta x^2} \tag{4.3.4}$$

$$\frac{\partial^2 T}{\partial y^2} = \frac{T_{m,n+1} + T_{m,n-1} - 2T_{m,n}}{\Delta y^2} \tag{4.3.5}$$

giving the 2-D finite difference equation for conduction at an internal node of

$$\frac{T_{m+1,n} + T_{m-1,n} - 2T_{m,n}}{\Delta x^2} + \frac{T_{m,n+1} + T_{m,n-1} - 2T_{m,n}}{\Delta y^2} = 0 \tag{4.3.6}$$

From Figure (4-10), the inner surface temperature is known (Dirichlet boundary condition), hence no calculation is required. For the surface, exposed to the bulk fluid, both convection and radiation modes of heat transfer takes place. At these nodal points, energy balance requires the rate of heat transfer due to conduction to be equal to the rate of heat transfer from both transfer modes. Using shape factors from Chapman [47], Appendix D (1), and Figure (4-12),

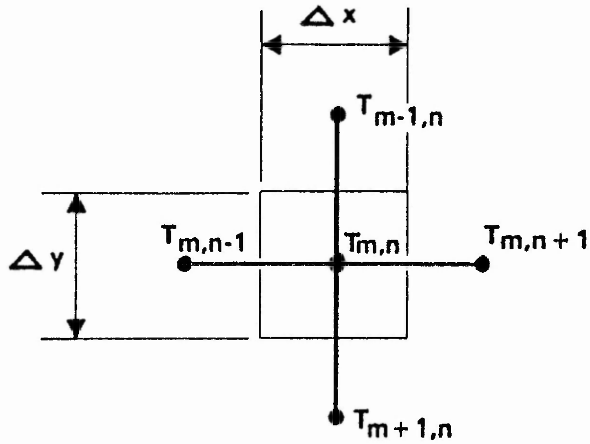

FIGURE (4-11) Internal conduction node

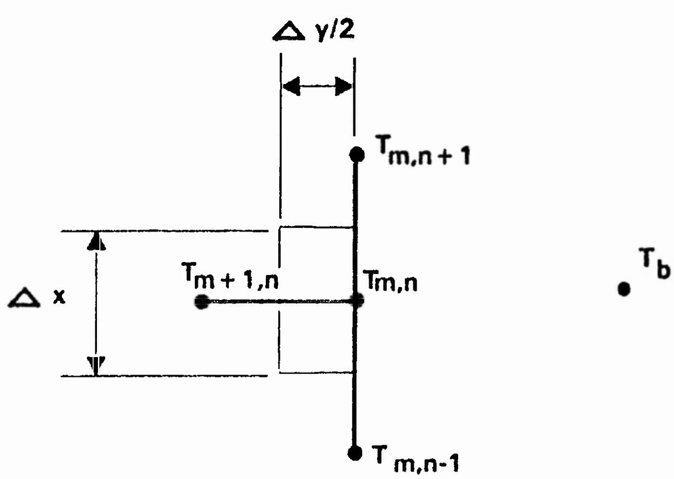

FIGURE (4-12) Flat surface node

$$\frac{k\Delta x}{\Delta y}(T_{m+1,n}-T_{m,n}) + \frac{k\Delta y}{2\Delta x}(T_{m,n-1}+T_{m,n+1}-2T_{m,n}) =$$

$$-h\Delta x\,(T_b-T_{m,n}) - F\epsilon\sigma\Delta x\,(T_b^4-T_{m,n}^4) \qquad (4.3.7)$$

Figure (4-13) shows an externally facing corner node position under the influence of both convection and radiation. Energy balance for this node type gives,

$$\frac{k\Delta x}{2\Delta y}(T_{m-1,n}-T_{m,n}) + \frac{k\Delta y}{2\Delta x}(T_{m,n-1}-T_{m,n}) =$$

$$-\frac{h}{2}(T_b-T_{m,n})(\Delta x+\Delta y) - \epsilon\sigma\,(T_b^4-T_{m,n}^4)\left(F_1\frac{\Delta x}{2}+F_2\frac{\Delta y}{2}\right) \qquad (4.3.8)$$

and an internal corner, as described in Figure (4-14), becomes,

$$\frac{k\Delta x}{\Delta y}\left(T_{m-1,n} + \frac{1}{2}T_{m+1,n}-\frac{3}{2}T_{m,n}\right) + \frac{k\Delta y}{\Delta x}\left(T_{m,n-1}+\frac{1}{2}T_{m,n+1}-\frac{3}{2}T_{m,n}\right) =$$

$$-\frac{h}{2}(T_b-T_{m,n})(\Delta x+\Delta y) - \epsilon\sigma\,(T_b^4-T_{m,n}^4)\left(F_1\frac{\Delta x}{2}+F_2\frac{\Delta y}{2}\right) \qquad (4.3.9)$$

4.3.2 2-D steady state program development

The grid formation, for the program, is outlined in Figure (4-10). The local convective heat transfer coefficients A to H, from the 1-D analysis, are used to preset the surface node values, on this grid, at locations relating to the positions given in Figure (3-7). To reduce the discretisation error, the number of surface nodes have

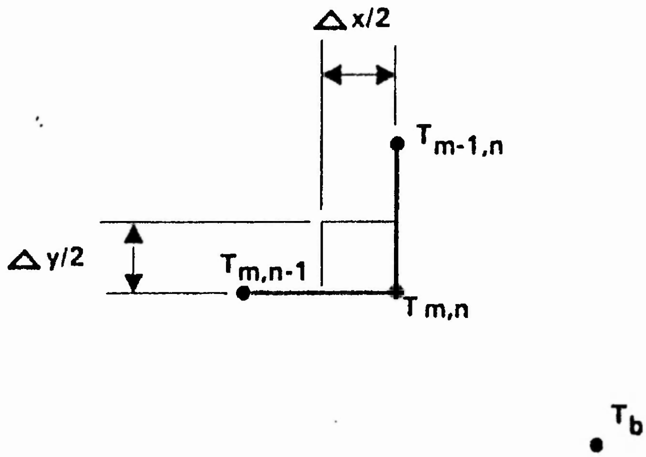

FIGURE (4-13) External corner node

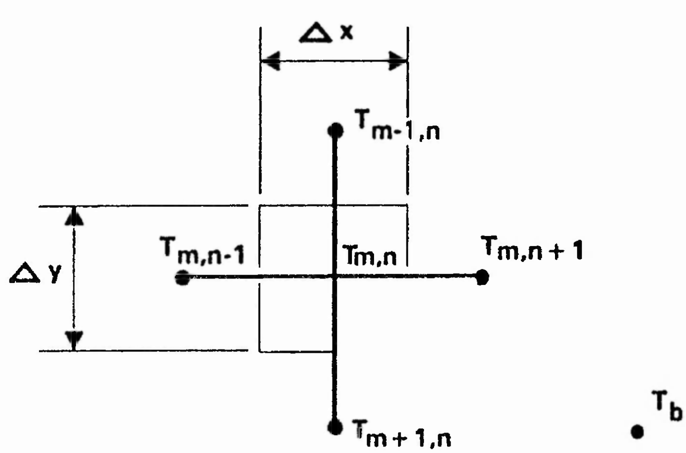

FIGURE (4-14) Internal corner node

been increased by a factor of 3. A linear interpolation, between adjacent preset nodes is used to estimate the local convective heat transfer coefficient at the extra nodes. This results in a rectangular cartesian grid array, where the distance between the nodes is given by,

For $n < 4$

$$\Delta x = \frac{W}{6} \qquad (4.3.10)$$

For $n = 4$

$$\Delta x = \frac{W}{12} + \frac{S}{24} \qquad (4.3.11)$$

For $n > 4$

$$\Delta x = \frac{S}{12} \qquad (4.3.12)$$

For $m < 11$

$$\Delta y = \frac{D}{10} \qquad (4.3.13)$$

For $m = 11$

$$\Delta y = \frac{D}{20} + \frac{H}{24} \qquad (4.3.14)$$

For $m > 11$

$$\Delta y = \frac{H}{12} \qquad (4.3.15)$$

The iterative solution, for the steady state analysis, uses a Gauss-Seidal procedure and tests for a maximum residual value. This value is the largest residual amplitude, calculated from the nodal equations, hence

$$r_{max} = | \, r \, | \qquad (4.3.16)$$

The residual value is the deflection from zero for equations *(4.3.6)* to *(4.3.9)*, and gives rise to modified equations for the four transfer modes. For conduction, Figure (4-15), the equation takes the form,

$$\frac{a+b}{2c} T_{m+1,n} + \frac{a+b}{2d} T_{m-1,n} + \frac{c+d}{2b} T_{m,n+1} +$$

$$\left.\frac{c+d}{2a} T_{m,n-1}\right) - P \, T_{m,n} = r \qquad (4.3.17)$$

where,

$$P = \frac{a+b}{2c} + \frac{a+b}{2d} + \frac{c+d}{2b} + \frac{c+d}{2a} \qquad (4.3.18)$$

For a horizontal surface, Figure (4-16),

$$\frac{a+b}{2a} T_{m-1,n} + \frac{d}{2b} T_{m,n+1} + \frac{d}{2a} T_{m,n-1} + \frac{h(a+b)}{k} T_b +$$

$$\frac{F\epsilon\sigma(a+b)}{k} T_b^4 - P \, T_{m,n} = r \qquad (4.3.19)$$

where,

$$P = \frac{a+b}{2d} + \frac{d}{2a} + \frac{d}{2b} + \frac{h(a+b)}{k} + \frac{F\epsilon\sigma(a+b)}{k} T^3_{m,n} \qquad (4.3.20)$$

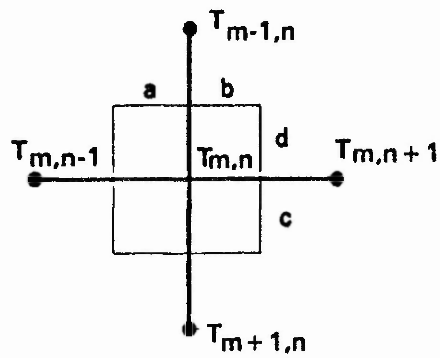

FIGURE (4-15) Internal conduction node

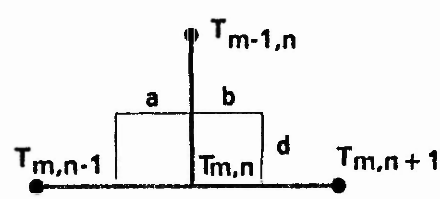

FIGURE (4-16) Horizontal surface node

for a vertical surface, Figure (4-17):

$$\frac{a}{2c} T_{m+1,n} + \frac{a}{2d} T_{m-1,n} + \frac{c+d}{2a} T_{m,n-1} + \frac{h(c+d)}{k} T_b +$$

$$\frac{F\epsilon\sigma(c+d)}{k} T_b^4 - P\, T_{m,n} = r \qquad (4.3.21)$$

where,

$$P = \frac{a}{2c} + \frac{a}{2d} + \frac{c+d}{2a} + \frac{h(c+d)}{k} + \frac{F\epsilon\sigma(c+d)}{k} T^3_{m,n} \qquad (4.3.22)$$

for an external corner, Figure (4-18):

$$\frac{a}{2d} T_{m-1,n} + \frac{d}{2a} T_{m,n-1} + \frac{h(a+d)}{k} T_b +$$

$$\frac{F\epsilon\sigma(a+d)}{k} T_b^4 - P\, T_{m,n} = r \qquad (4.3.23)$$

where,

$$P = \frac{a}{2d} + \frac{d}{2a} + \frac{h(a+d)}{k} + \frac{F\epsilon\sigma(a+d)}{k} T^3_{m,n} \qquad (4.3.24)$$

for an internal corner, Figure (4-19):

$$\frac{a}{2c} T_{m+1,n} + \frac{a+b}{2d} T_{m-1,n} + \frac{d}{2b} T_{m,n+1} + \frac{c+d}{2a} T_{m,n-1} +$$

$$\frac{h(b+c)}{k} T_b + \frac{F\epsilon\sigma(b+c)}{k} T_b^4 - P\, T_{m,n} = r \qquad (4.3.25)$$

where,

$$P = \frac{a}{2c} + \frac{a+b}{2d} + \frac{d}{2b} + \frac{c+d}{2a} + \frac{h(b+c)}{k} +$$

$$\frac{F\epsilon\sigma(b+c)}{k} T^3_{m,n} \qquad (4.3.26)$$

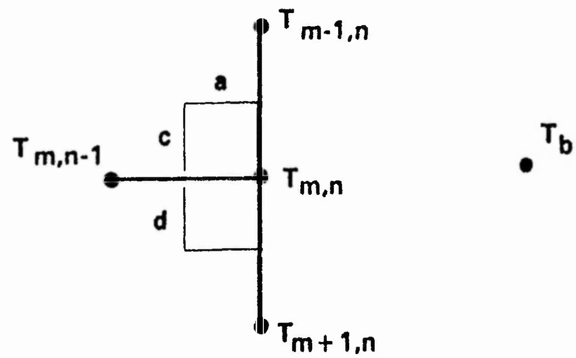

FIGURE (4-17) Vertical surface node

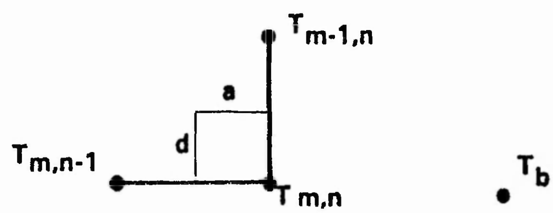

FIGURE (4-18) External corner node

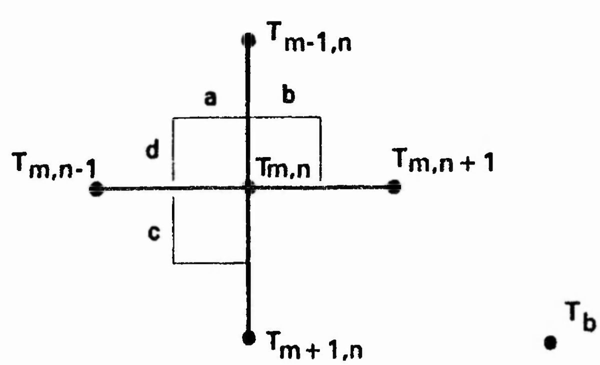

FIGURE (4-19) Internal corner node

The new nodal temperature for the above equations are calculated from,

$$\mathbf{T'_{m,n} = \frac{r}{P} + T_{m,n}} \qquad (4.3.27)$$

Taking $F_1 = F_2 = F$, and the fin and base temperatures nearly equal (found by measurements on the true casting), the value for the shape factor approximates to,

$$\mathbf{F \approx 1} \qquad (4.3.28)$$

On completion of the iteration process, to determine the maximum residual, a test for convergence is made. The test criteria has been determined by undertaking numerous computations using set input parameters, and solving for a value that balances accuracy with computational time. The determined criteria to test for convergence is,

$$\mathbf{r_{max} <= 0.001} \qquad (4.3.29)$$

On convergence, of the iteration process, the heat transfer through the heat exchanger section is calculated. An estimation of the computational error is made by comparison of the heat transfer into the body by conduction, to the heat transfer out of the body by convection and radiation. The conduction heat transfer is given by the summation of the nodal heat fluxes at the Dirichlet boundary, the equation for this taking the form of,

$$Q_{in} = \sum_{n=1,10} Q_{1,n} \tag{4.3.30}$$

and the heat transfer emanating from the heat exchanger, at the surface exposed to the bulk fluid, found by,

$$Q_{out} = Q_{23,1} + \sum_{m=14,23,3} Q_{m,4} + \sum_{n=4,10,3} Q_{11,n} \tag{4.3.31}$$

The output from the program, stored in a user defined file, gives the local heat transfer coefficients and temperature profile, in digital format. The program flow chart is given in Figure (4-20) and the Fortran 77 program listed in Appendix C (2).

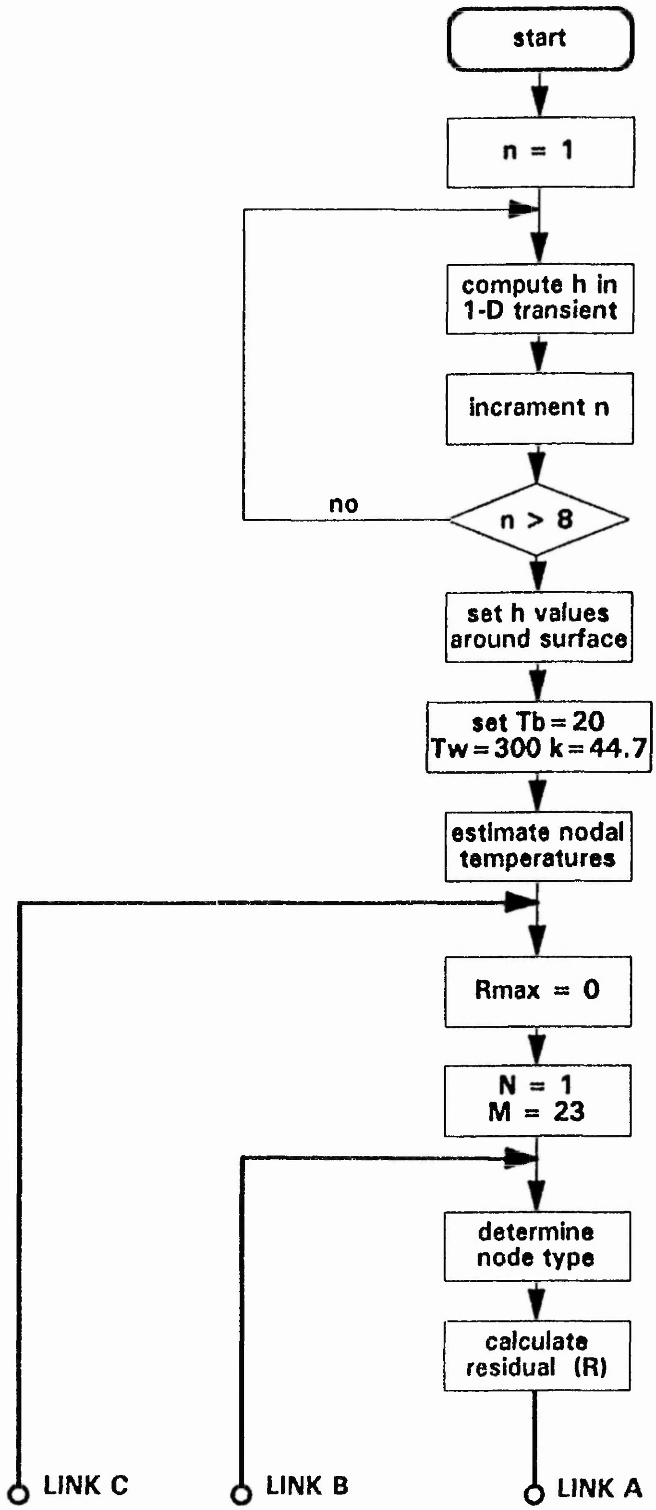

<u>FIGURE 4-20 2-D STEADY STATE FLOW CHART Cont...</u>

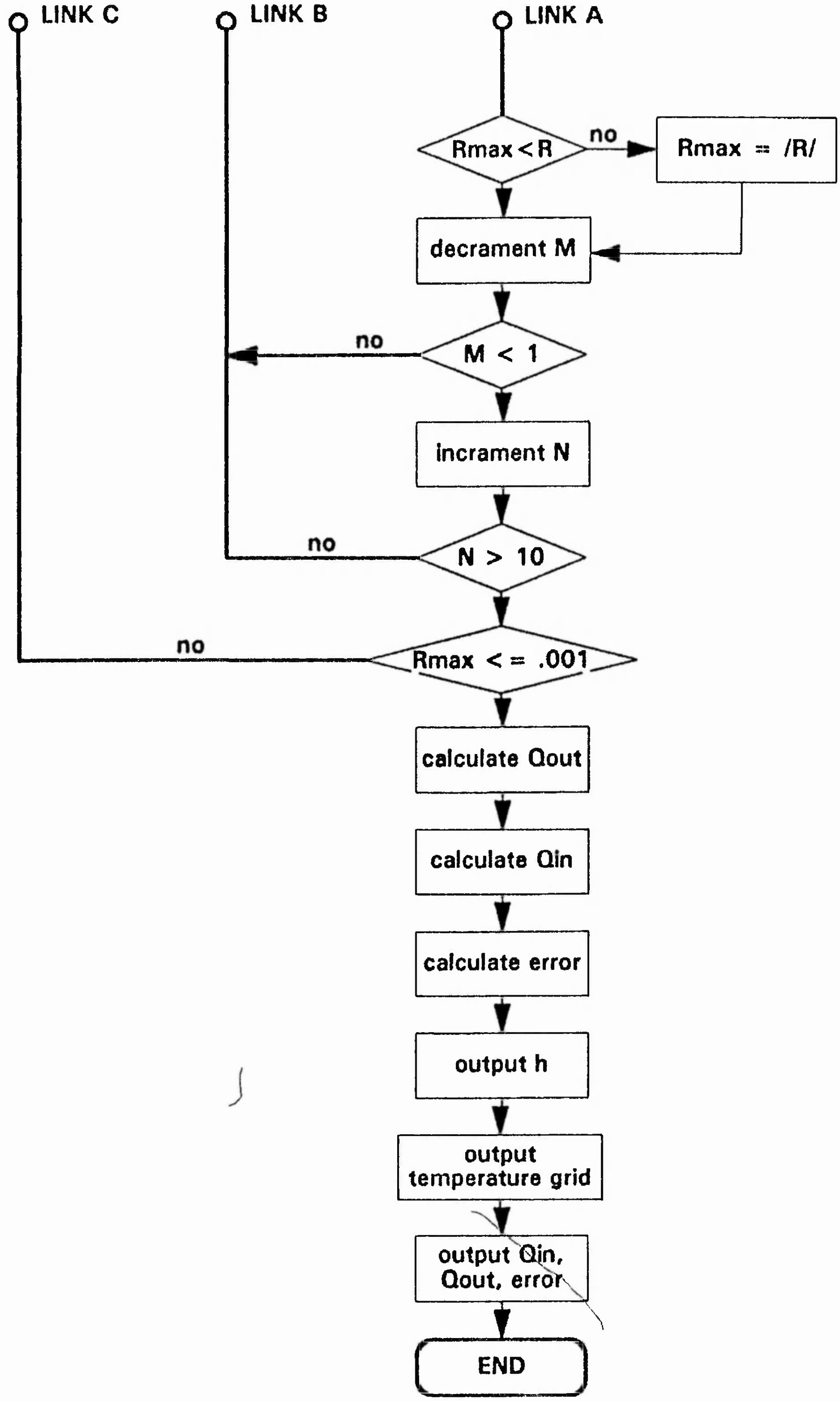

FIGURE 4-20 CONTINUED

CHAPTER 5

EXPERIMENTAL RESULTS

5.1 Introduction

The results are split into four parts, the first three each containing subsections for the appertaining results and concluding remarks, the forth part being a general conclusion for the finned heat exchanger investigation. The first part (5.2), is the investigation of a vertical flat plate. Comparisons for the theoretical internal temperature decay, against measured values on a model, are made, and local heat transfer coefficients, from the transient analysis program, determined. The correlation deduced, for the local Nusselt number, is compared to published ones, and used as a basis for proving the methodology.

The second part (5.3), gives the investigation of extended surfaces with uniform fin length and variable inter fin spacing. The timing results, from the models, are given in tabular form and the resultant values of the local heat transfer coefficients, and total heat transfer value, given in graphical form. The recommended inter fin spacing is given based upon these results.

The third part (5.4) utilises the recommended inter fin spatial separation as the set dimension for varying the fin length. The results of this investigation are again given in a graphical format. The results from both this section and the section (5.3) are used to derive the final conclusions. The liquid crystals used throughout the investigations have a colour change temperature of 36.4 °C as specified in section (3.3.2), equation *(3.3.2)*.

5.2 Vertical flat plate

5.2.1 Internal temperature decay

The vertical flat plate, used for the investigation, has dimensions as given in Appendix A (A-3), and a K-type thermocouple placed volumetrically central within it. The plate was heated, in the thermal tunnel, under the conditions given in Table 5-A, until equilibrium was reached. The plate was then removed from the tunnel and placed on the stand for free convection to take place.

VARIABLE	CONDITION
T_I	60
T_b	18.2

TABLE 5-A INITIAL CONDITIONS

The recorded decay in the internal temperature, and the calculated value from the 1-D transient analysis program, are given in Figure (5-1). The recorded results show that, for a model with finite thickness, a decay in its internal temperature takes place, and must be accounted for. The difference between the computed curve, accounting for the decay, and the measured curve is explained by the placement and mass of the thermocouple, interfering with the system.

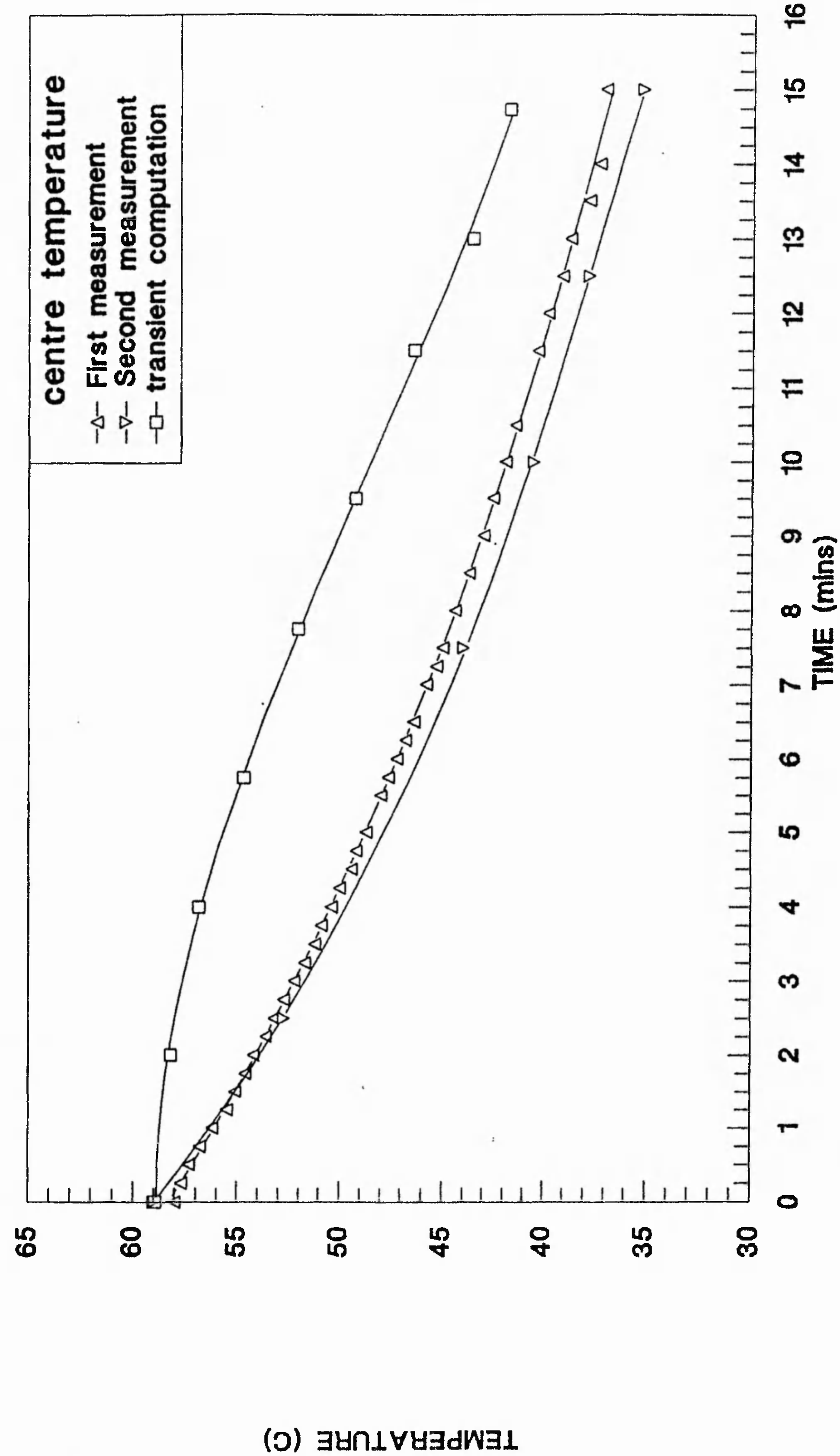

FIGURE 5-1 Comparison of actual internal temperature decay to computed value

5.2.2 Vertical plate correlation

Previously defined correlations are available for the determination of local heat transfer coefficients, for a vertical flat plate in free convection. To validate the 1-D transient program, the output of the program is compared to six of the previously defined correlations, these being,

Chapman [47]

$$\mathbf{Nu_x = 0.508\, Gr_x^{1/4}\, Pr^{1/2}\, (0.952 + Pr)^{-1/2}} \tag{5.2.1}$$

Kreith and Bohn [48]

$$\mathbf{h_x = 0.508\, Pr^{1/2}\, \frac{Gr_x^{1/4}}{(0.952 + Pr)^{1/4}}\, \frac{k}{x}} \tag{5.2.2}$$

Kays and Crawford [49]

$$\mathbf{Nu_x = 0.332\, Pr^{1/3}\, Re_x^{1/2}} \tag{5.2.3}$$

Chen et al. [50]

$$\mathbf{Nu_x = \frac{3}{4}\, Pr^{1/2}\, [2.5(1 + 2Pr^{1/2} + 2Pr)]^{-1/4}\, Gr_x^{1/4}} \tag{5.2.4}$$

Cranfield [51]

$$\mathbf{Nu_x = 0.509\, Pr^{1/4}\, (Pr + \frac{20}{21})^{-1/4}\, Gr_x^{1/4}} \tag{5.2.5}$$

Eckert [52]

$$\mathbf{Nu_x = 0.508\left(\frac{Pr}{Pr+0.952}\,Gr_x\,Pr\right)^{1/4}} \qquad (5.2.6)$$

The above correlations are for laminar flow; laminar flow occurs in the region of, (from Simonson [46])

$$\mathbf{10^4 < GrPr < 10^9} \qquad (5.2.7)$$

The model tested is a vertical flat plate, the design, and dimensions, being given in Appendix A (A-3). The test conditions, Table (5-B), apply and laminar flow tested for using values read from the property table in Appendix D (D-2) (from Chapman [47]).

VARIABLE	CONDITION
T_I	72.2
T_b	18.2

TABLE 5-B INITIAL CONDITIONS OF VERTICAL FLAT PLATE

The property values from the test are given in Table (5-C), and the equations to test for laminar flow given by *(5.2.8)* to *(5.2.10)*. Laminar flow is confirmed by the value of (Gr.Pr) being in the range given by *(5.2.7)*.

PROPERTY	VALUE
μ	0.0000193
ρ	1.10985
c_p	1007.1
k_F	0.02745
ν	0.0000175

TABLE 5-C PROPERTY VALUES FOR LAMINAR FLOW TEST

taking,

$$\beta = \frac{1}{((72.2+18.2)/2)+273.15} = \underline{3.141\times10^{-3}\ K^{-1}} \qquad (5.2.8)$$

$$x = \underline{0.16\ m} \qquad (5.2.9)$$

the laminar flow test value is calculated at,

$$(Gr.Pr) = \underline{14\times10^{6}} \qquad (5.2.10)$$

The timing values, for the 1-D transient analysis program, are taken from the video recording of the vertical flat plate model. The recorded timing values are given in Table (5-D). The computed values for the local heat transfer coefficients, from the 1-D transient analysis program, are given in graphical form in Figures (5-2) and (5-3).

Figure (5-2) shows the computed curve for the local heat transfer coefficients computed with no internal temperature decay. This assimilates an infinite thickness plate, and gives a comparison to the previously defined correlation of equations *(5.2.1)* to *(5.2.6)*. Figure (5-3) shows the effect of a finite thickness model, allowing for the internal temperature decay.

dH	t
0.0065	560
0.0130	710
0.0195	790
0.0260	860
0.0325	903
0.0390	938
0.0455	955
0.0520	984

TABLE 5-D VIDEO TIMING DATA FOR THE VERTICAL FLAT PLATE

From Figure (5-2) a correlation for an infinite vertical flat plate, based upon the Nusselt number, has been formulated.

$$\mathbf{Nu_x = 0.805\ Pr^{1/4}\ Gr_x^{1/6}} \qquad (5.2.11)$$

Plotting the log of the Nusselt number against the log of the distance from the lower edge of the plate, and the log of the Nusselt number against the log of the Rayleigh number, gives two linear correlations. These correlations are shown in Figures (5-4) and (5.5) respectively, along with plots of *(5.2.1)*, *(5.2.3)* and *(5.2.6)*.

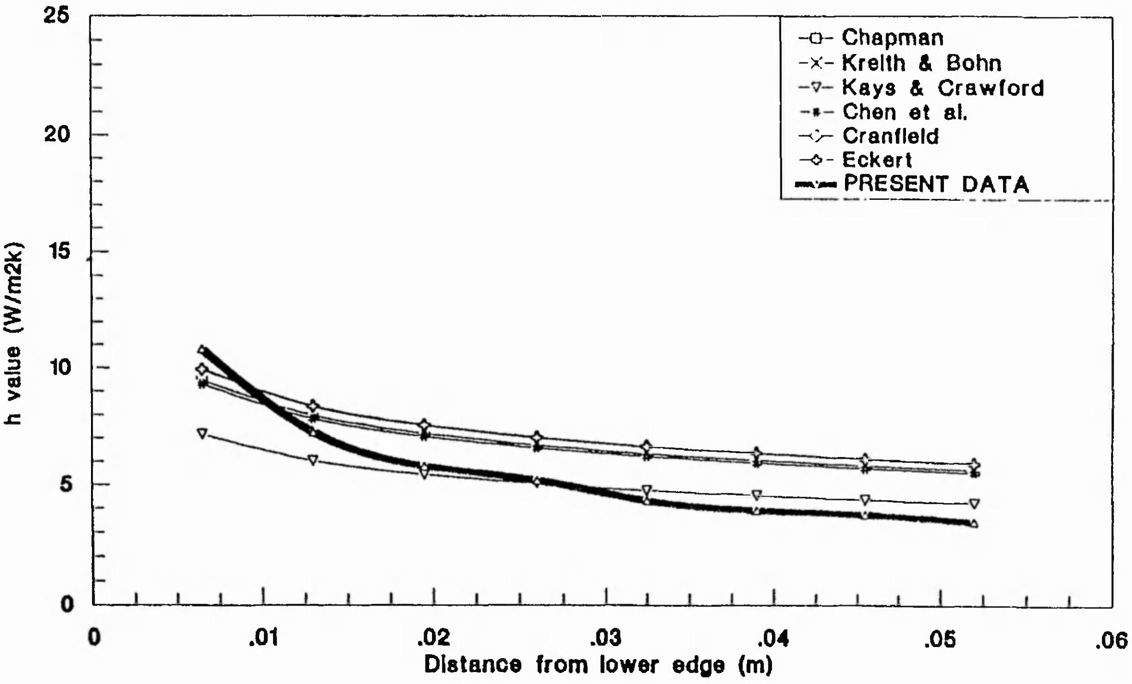

FIGURE 5-2 Vertical flat convection surface with infinite thickness

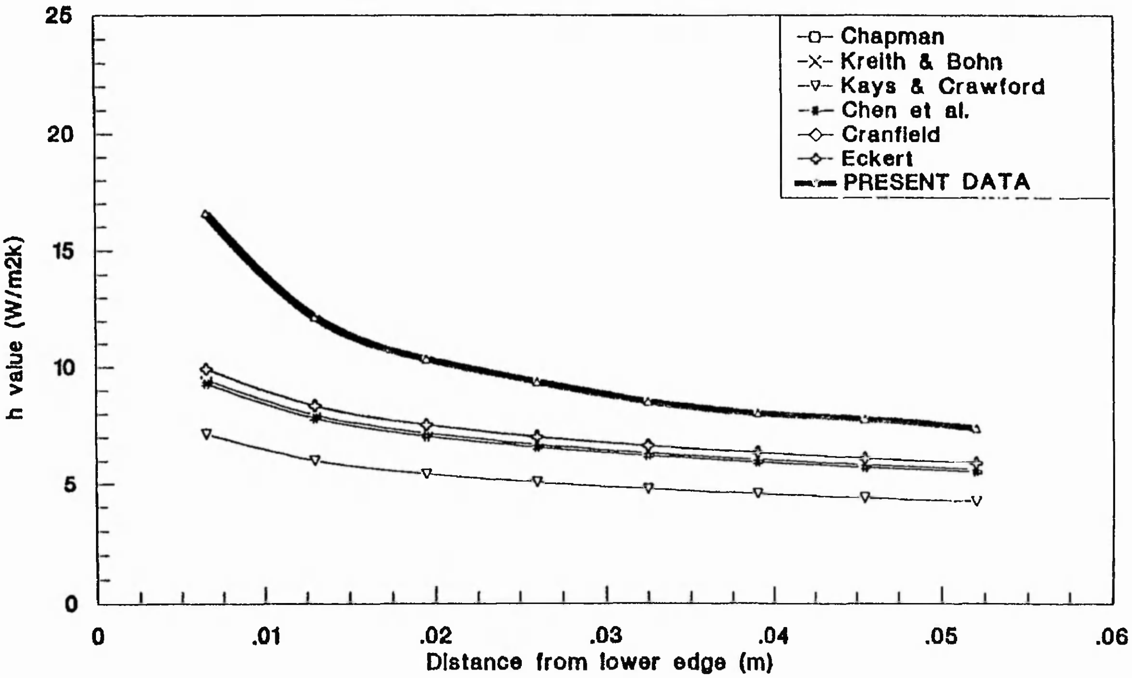

FIGURE 5-3 Vertical flat convection surface with finite thickness

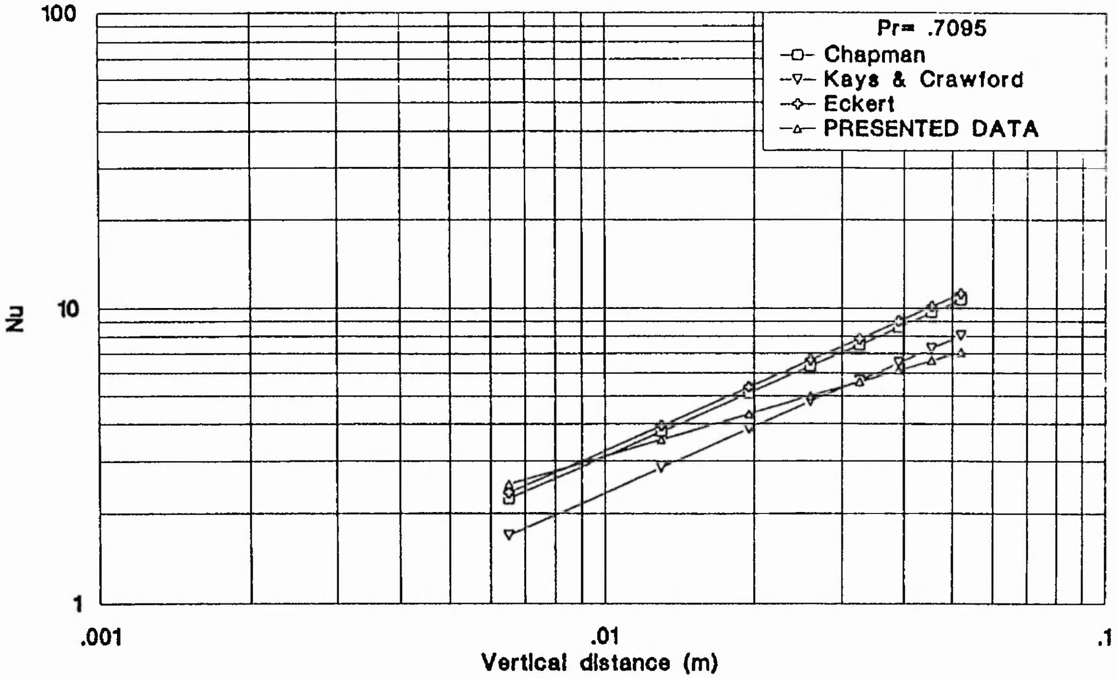

FIGURE 5-4 Change in local Nusselt number over vertical distance

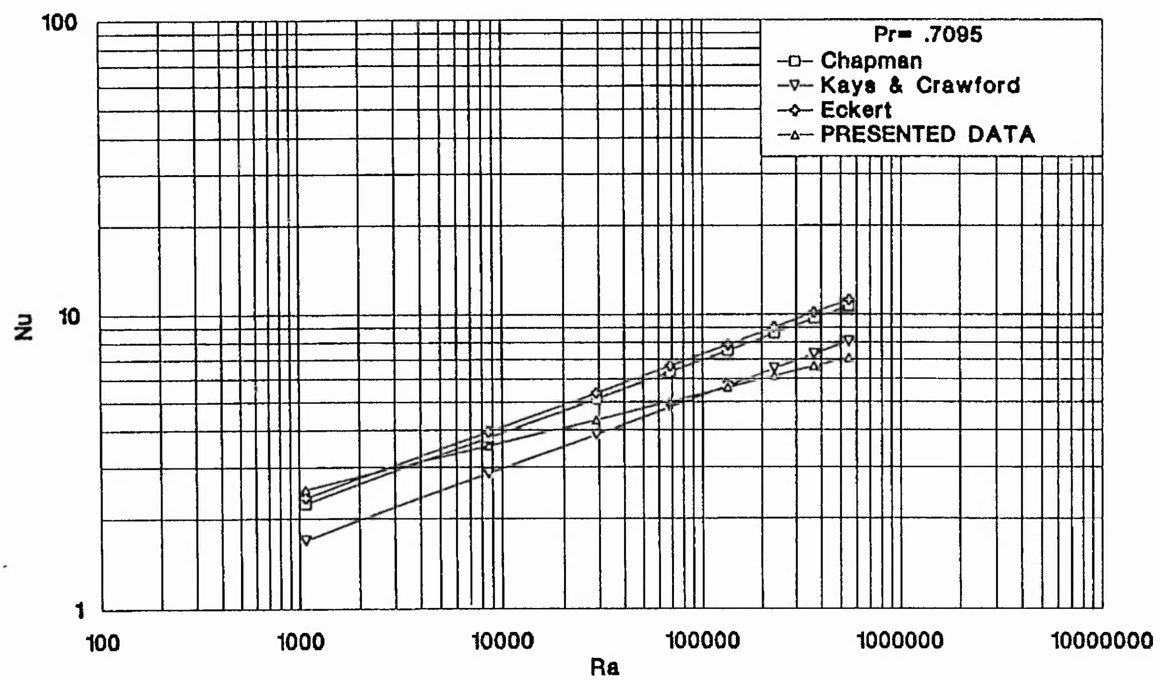

FIGURE 5-5 Correlation for vertical flat plate in laminar free convection flow

5.2.3 Summary

The methodology used, with the liquid crystal technique and 1-D transient analysis, has been validated against previously defined correlations. This is in respect to an infinite vertical flat plate.

It is shown that the introduction of a finite thickness, and hence an internal temperature decay, gives a marked variation in the computed local heat transfer coefficient. The variation is explained by the addition of convection and radiation on the rear surface of the plate.

There is a difference in the gradient of the presented data to that of the previously defined correlation data, under the same conditions. The difference in the gradient is due to the tested model only assimilating an infinite plate thickness, by not allowing for the fall in the centre temperature of the finite thickness plate. The results presented do, nevertheless fall within the correct order of magnitude.

The heat transfer from this surface, calculated from 2-D steady state analysis, is

$$Q = 289 \;\; W \tag{5.2.12}$$

5.3 Finned section of varying separation

The standard fin length of the Brazilia slimline 5 is used as the reference length for the investigation of variable fin spatial separation. This gives a set dimension for the length (L) of 25 mm. The tests are undertaken with separations (S) ranging from 37 mm to 11 mm, in 3 mm decrements. The timing data for the mid and end sections, as depicted in Figure (3-6), are given in tabular form, with the resultant local heat transfer coefficients in graphical form. Two types of graphical representation is used, the first showing the local heat transfer coefficient against its horizontal location, the second showing the local heat transfer coefficient against its vertical position (dH). The horizontal locations are given in Figure (3-7). The computed value for the heat transfer through each heat exchanger is based upon equations *(3.4.1)* and *(3.4.2)*. The resultant values of each heat exchanger sub section is given in tabular form, and the total heat transfer, from each heat exchanger tested, displayed graphically.

5.3.1 37 mm spatial separation

Test conditions

VARIABLE	CONDITION
No. fins	5
T_I	67
T_b	20.2

TABLE 5-E INITIAL CONDITIONS FOR S=37 mm

Timing data (s)

dH(mm)	A	B	C	D	E	F	G	H
160	129	125	260	411	623	1100	1036	1004
142.2	220	215	343	516	803	1328	1305	1277
124.4	231	230	321	516	803	1391	1392	1357
106.7	243	240	311	516	803	1431	1399	1387
88.9	243	240	311	516	803	1383	1374	1374
71.1	243	240	311	487	773	1300	1359	1281
53.3	235	230	311	437	733	1169	1136	1094
35.6	213	210	294	391	623	1036	999	965
17.8	175	170	294	327	451	841	773	773
0	74	70	111	154	245	394	394	394

TABLE 5-F MIDDLE FIN FOR S=37 mm

dH(mm)	A	B	C	D	E	F	G	H
160	159	155	279	413	578	905	626	200
142.2	221	220	420	545	800	1087	935	481
124.4	248	246	435	545	800	1140	938	481
106.7	248	246	425	545	800	1140	935	481
88.9	232	230	420	510	800	1119	930	481
71.1	226	224	413	485	800	1073	910	481
53.3	204	200	372	458	664	1027	875	481
35.6	189	185	326	415	585	947	820	481
17.8	179	175	259	336	411	820	694	409
0	78	76	150	236	256	368	341	186

TABLE 5-G END FIN FOR S=37 mm

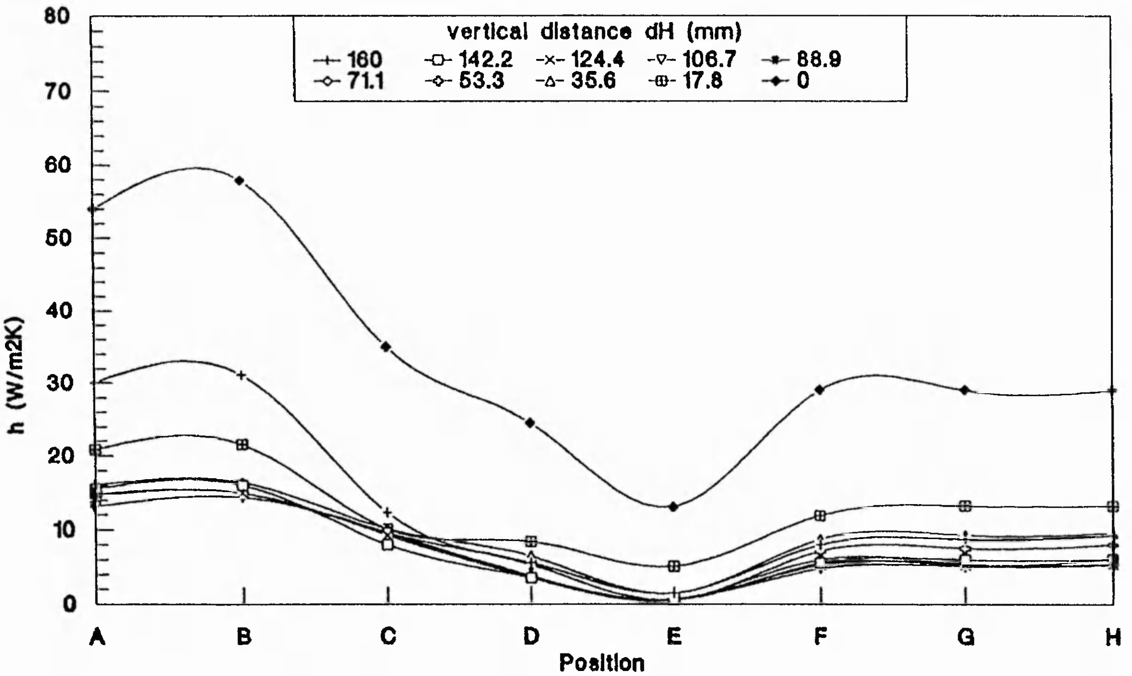

FIGURE 5-6 Mid section horizontal heat transfer coefficient map for S=37mm

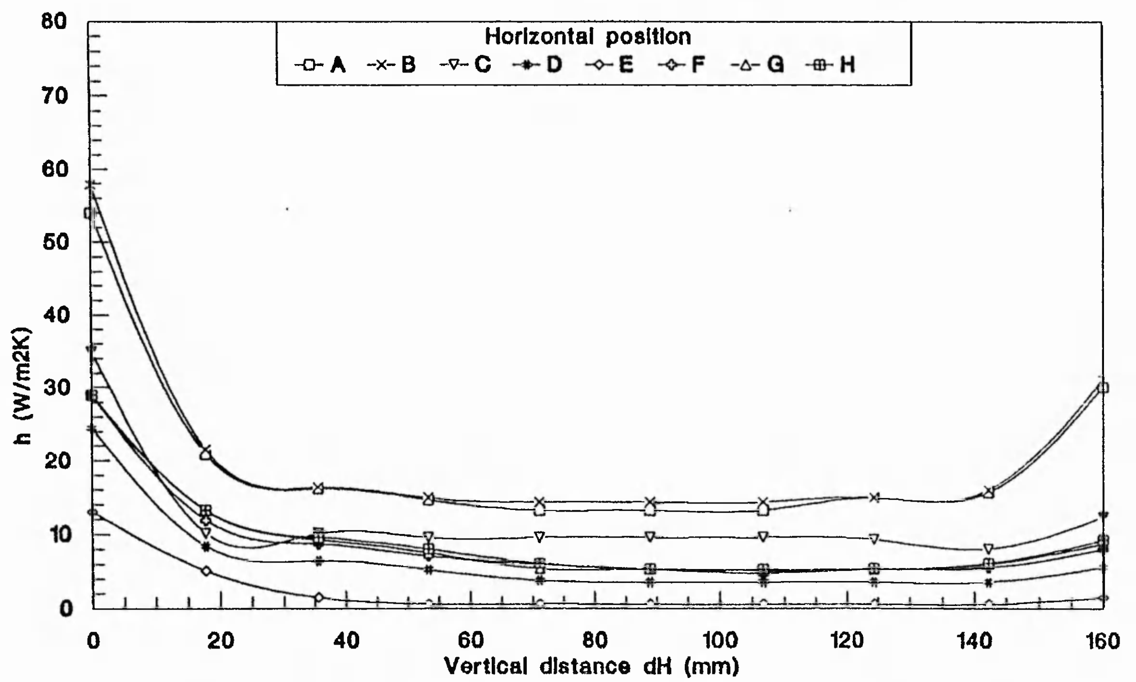

FIGURE 5-7 Mid section vertical heat transfer coefficient map for S=37mm

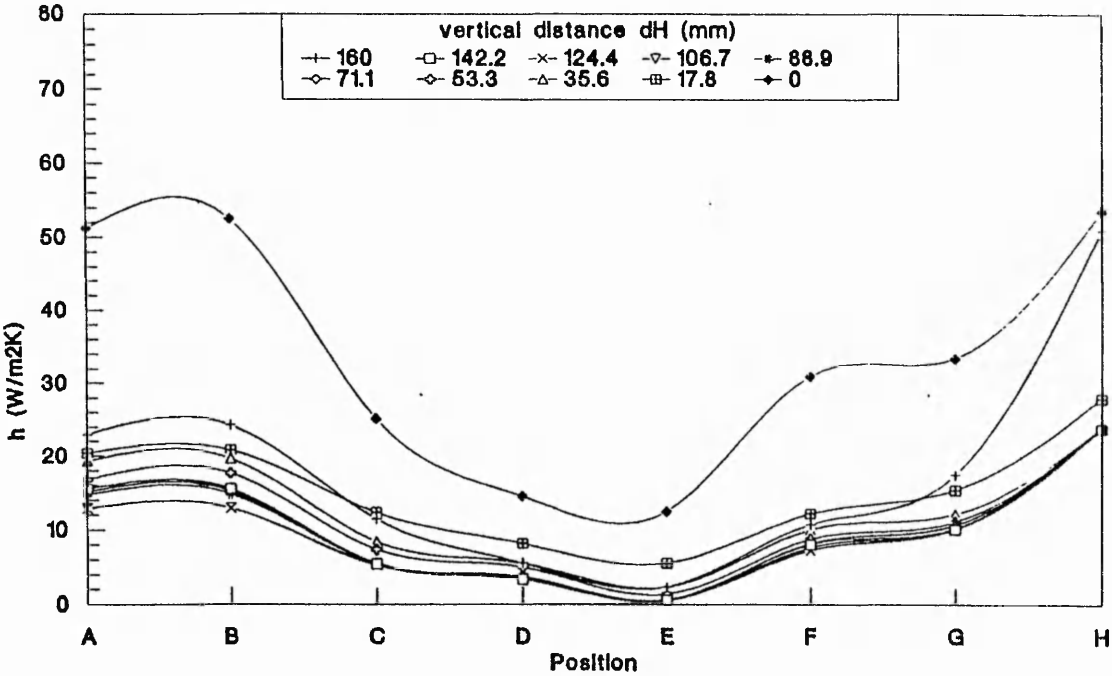

FIGURE 5-8 End section horizontal heat transfer coefficient map for S=37mm

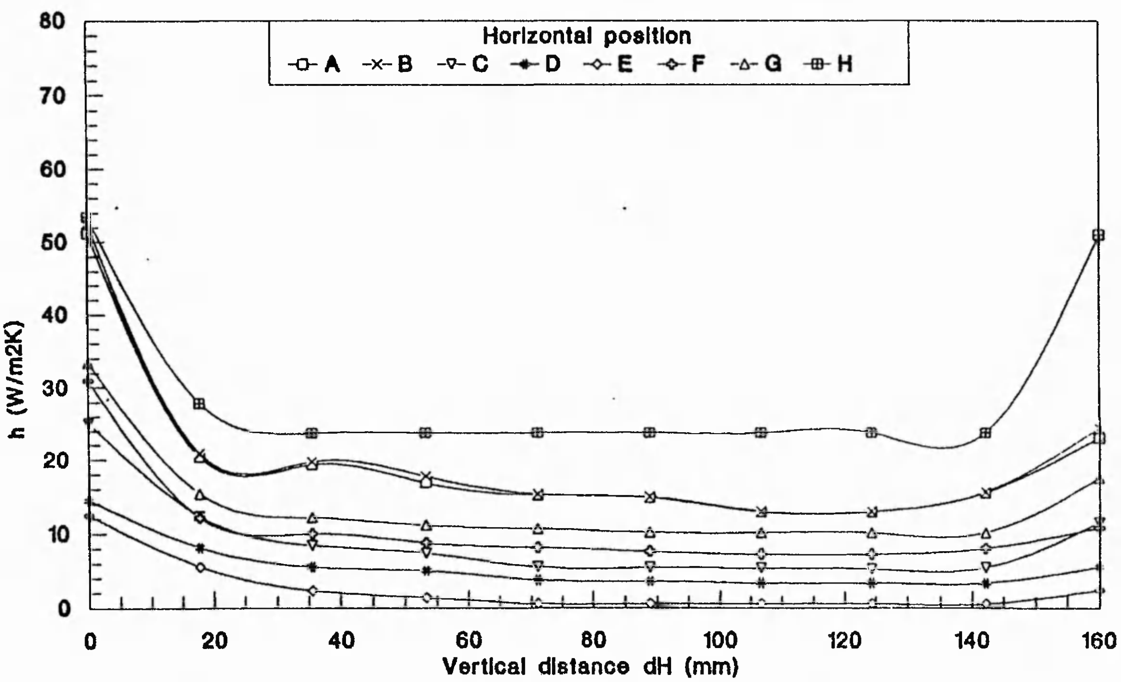

FIGURE 5-9 End section vertical heat transfer coefficient map for S=37mm

Heat transfer through each sub section (W)

SECTION No.	MID SECTION	END SECTION
1	2.884	2.556
2	5.103	4.230
3	5.057	4.165
4	5.022	4.168
5	5.054	4.215
6	5.105	4.252
7	5.331	4.400
8	5.587	4.544
9	6.169	4.953
10	4.659	3.538

TABLE 5-H COMPUTED SUB SECTION HEAT FLOWS FOR S=37 mm

The total heat transfer through the heat exchanger is,

$$\mathbf{Q_{TOT} = 478 \pm 3 \quad W} \tag{5.3.1}$$

The heat exchange area and volume are,

$$\mathbf{A = 0.072 \quad m^2} \tag{5.3.2}$$

$$\mathbf{V = 3.8 \times 10^{-4} \quad m^3} \tag{5.3.3}$$

5.3.2 34 mm spatial separation

Test conditions

VARIABLE	CONDITION
No. fins	5
T_I	70.5
T_b	15.9

TABLE 5-I INITIAL CONDITIONS FOR S=34 mm

Timing data (s)

dH(mm)	A	B	C	D	E	F	G	H
160	103	100	239	349	504	858	762	716
142.2	171	165	341	454	646	1070	1022	942
124.4	185	180	371	468	672	1131	1093	999
106.7	208	204	371	468	672	1137	1093	1003
88.9	221	214	367	477	668	1113	1083	999
71.1	225	220	358	470	648	1070	1024	952
53.3	256	250	343	413	604	1029	955	906
35.6	189	186	311	379	538	922	863	830
17.8	167	165	275	313	445	762	708	689
0	50	50	87	128	161	258	205	205

TABLE 5-J MIDDLE FIN FOR S=34 mm

dH(mm)	A	B	C	D	E	F	G	H
160	88	88	216	288	413	781	610	199
142.2	155	154	277	408	574	990	813	413
124.4	168	166	311	423	589	1009	838	413
106.7	176	174	311	423	589	1002	826	413
88.9	176	174	311	423	589	998	817	413
71.1	185	183	308	398	582	990	808	413
53.3	185	183	302	378	566	949	772	413
35.6	167	164	286	340	478	887	734	339
17.8	155	152	238	290	408	755	617	246
0	60	59	89	103	150	247	229	141

TABLE 5-K END FIN FOR S=34 mm

Heat transfer through each sub section (W)

SECTION No.	MID SECTION	END SECTION
1	2.930	2.987
2	5.039	4.921
3	4.923	4.815
4	4.874	4.812
5	4.888	4.821
6	4.935	4.825
7	5.026	4.872
8	5.306	5.099
9	5.783	5.583
10	5.257	4.612

TABLE 5-L COMPUTED SUB SECTION HEAT FLOWS FOR S=34 mm

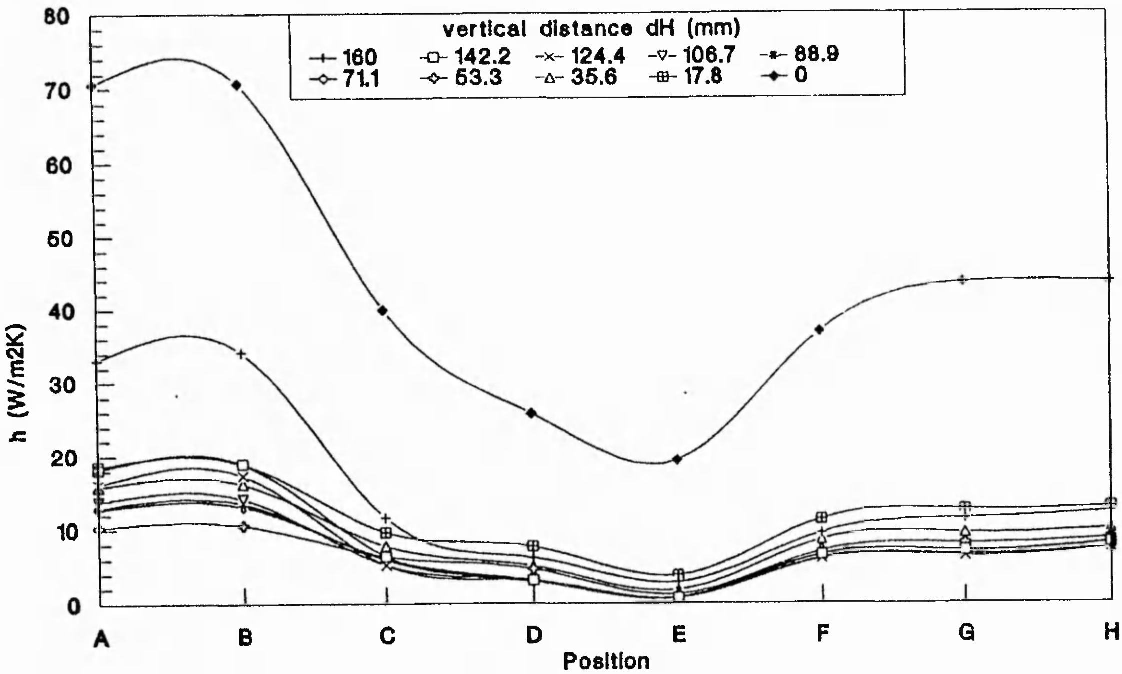

FIGURE 5-10 Mid section horizontal heat transfer coefficient map for S=34mm

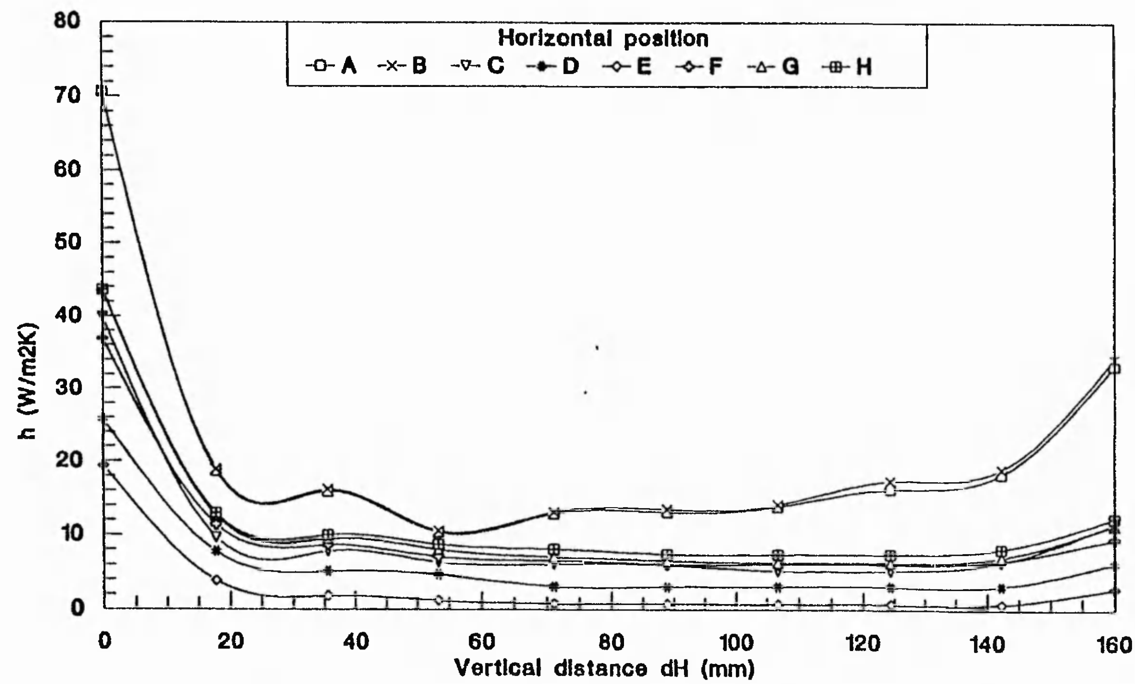

FIGURE 5-11 Mid section vertical heat transfer coefficient map for S=34mm

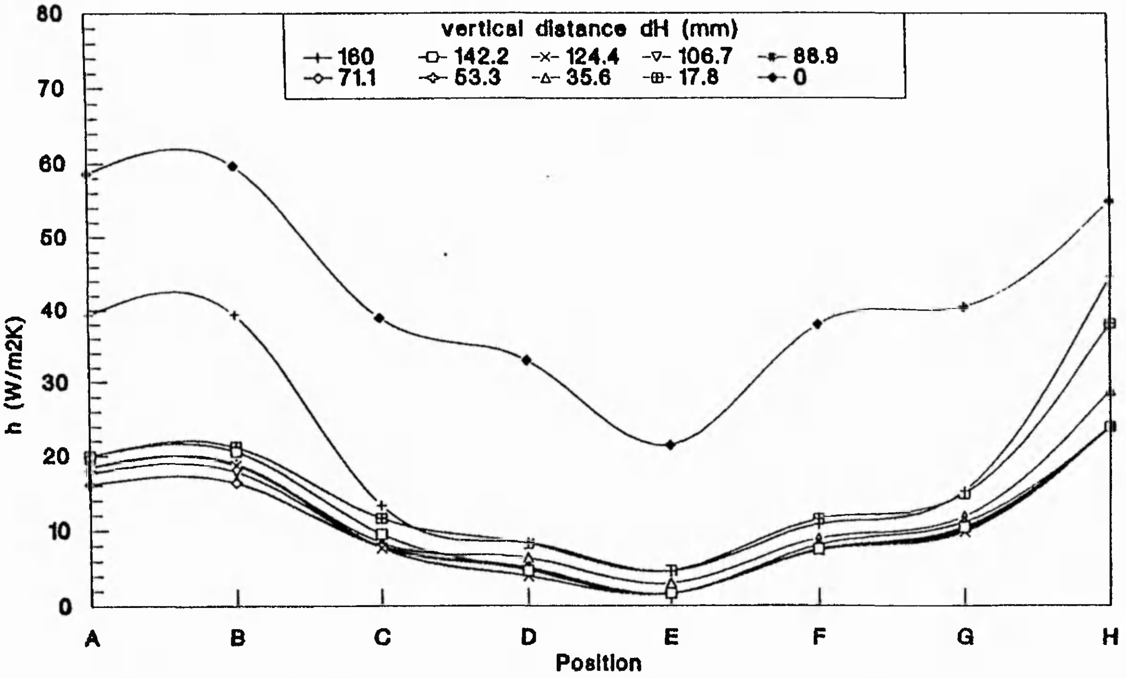

FIGURE 5-12 End section horizontal heat transfer coefficient map for S=34mm

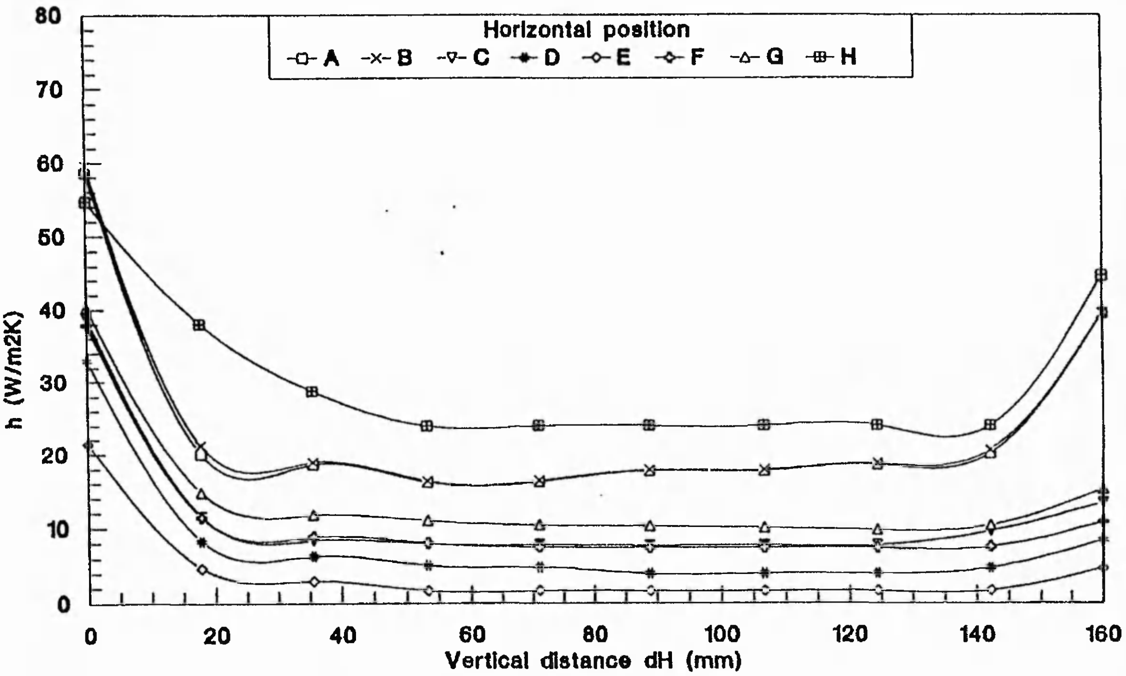

FIGURE 5-13 End section vertical heat transfer coefficient map for S=34mm

The total heat transfer through the heat exchanger is,

$$\mathbf{Q_{TOT} = 482 \pm 3 \quad W} \tag{5.3.4}$$

The heat exchange area and volume are,

$$\mathbf{A = 0.072 \quad m^2} \tag{5.3.5}$$

$$\mathbf{V = 3.8 \times 10^{-4} \quad m^3} \tag{5.3.6}$$

5.3.3 31 mm spatial separation

Test conditions

VARIABLE	CONDITION
No. fins	5
T_I	67.6
T_b	17.4

TABLE 5-M INITIAL CONDITIONS FOR S=31 mm

Timing data (s)

dH(mm)	A	B	C	D	E	F	G	H
160	120	115	250	319	570	1109	961	960
142.2	194	190	295	469	700	1239	1216	1112
124.4	204	200	295	469	700	1280	1222	1149
106.7	207	200	295	469	700	1273	1222	1099
88.9	217	200	295	469	700	1233	1204	1070
71.1	217	200	295	461	670	1204	1092	1010
53.3	204	200	295	420	651	1104	1008	960
35.6	188	180	278	382	566	983	921	853
17.8	158	150	239	309	438	754	683	646
0	61	60	93	105	110	234	230	221

TABLE 5-N MIDDLE FIN FOR S=31 mm

dH(mm)	A	B	C	D	E	F	G	H
160	160	155	258	418	492	949	703	123
142.2	258	255	291	462	693	1232	1063	294
124.4	266	260	291	461	693	1238	1065	328
106.7	266	260	291	461	693	1232	1048	328
88.9	266	260	291	462	693	1211	1014	328
71.1	258	255	291	435	693	1168	998	328
53.3	234	230	291	392	615	1109	949	328
35.6	209	200	251	336	465	1003	868	274
17.8	171	165	209	263	368	849	696	267
0	60	58	91	100	106	289	224	98

TABLE 5-O END FIN FOR S=31 mm

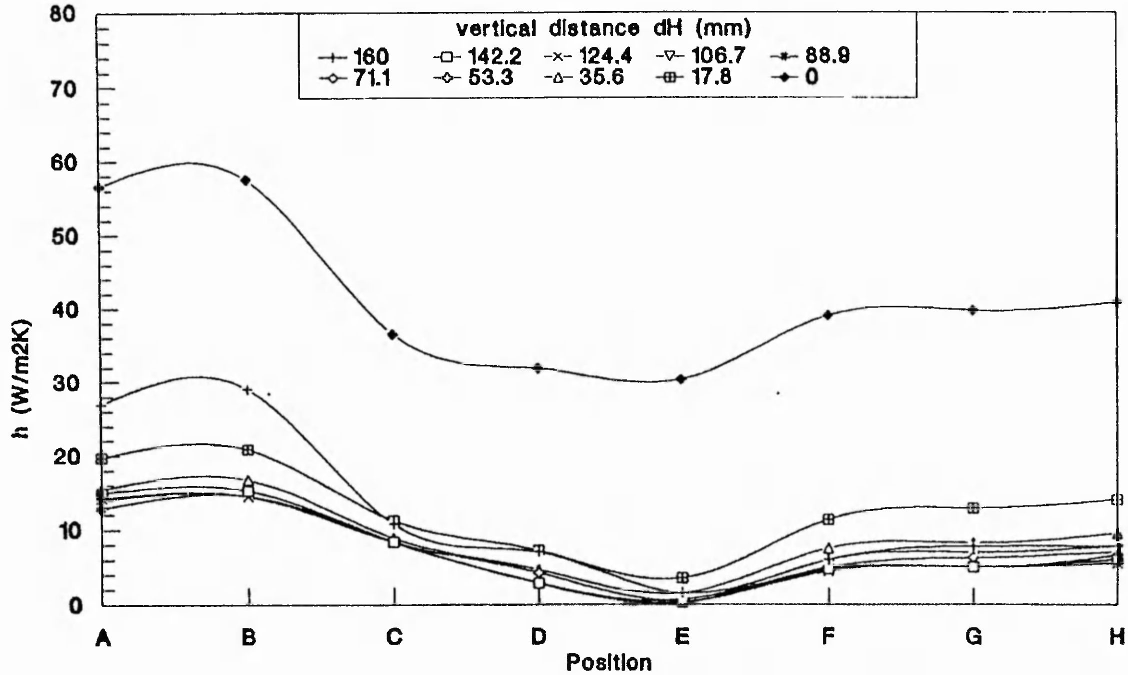

FIGURE 5-14 Mid section horizontal heat transfer coefficient map for S=31mm

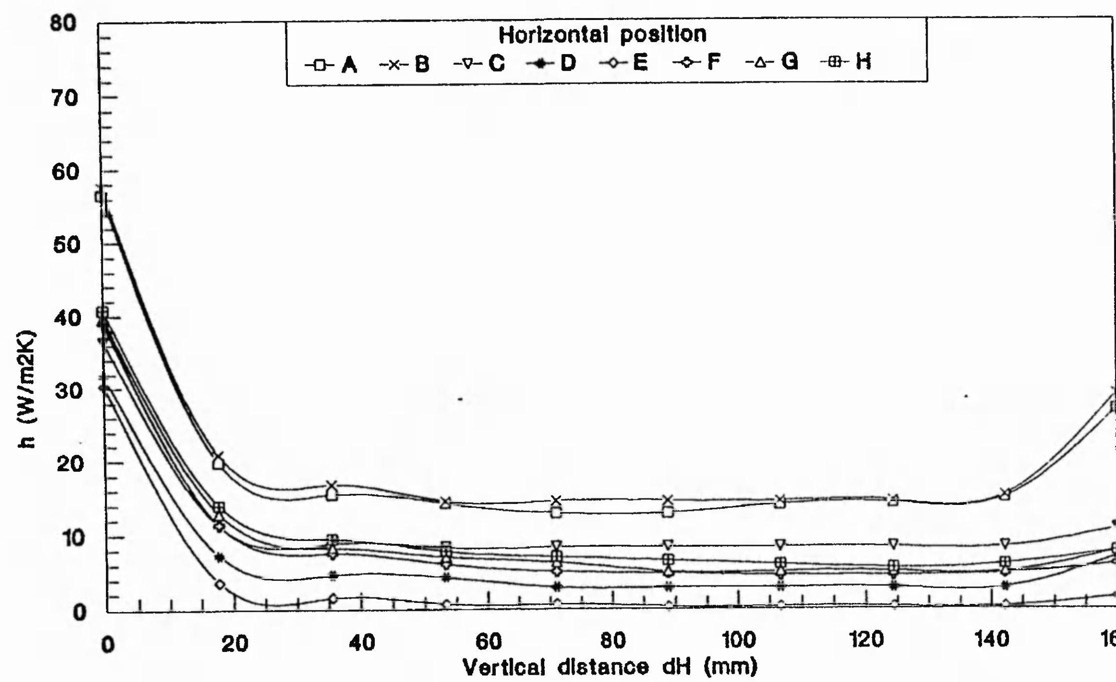

FIGURE 5-15 Mid section vertical heat transfer coefficient map for S=31mm

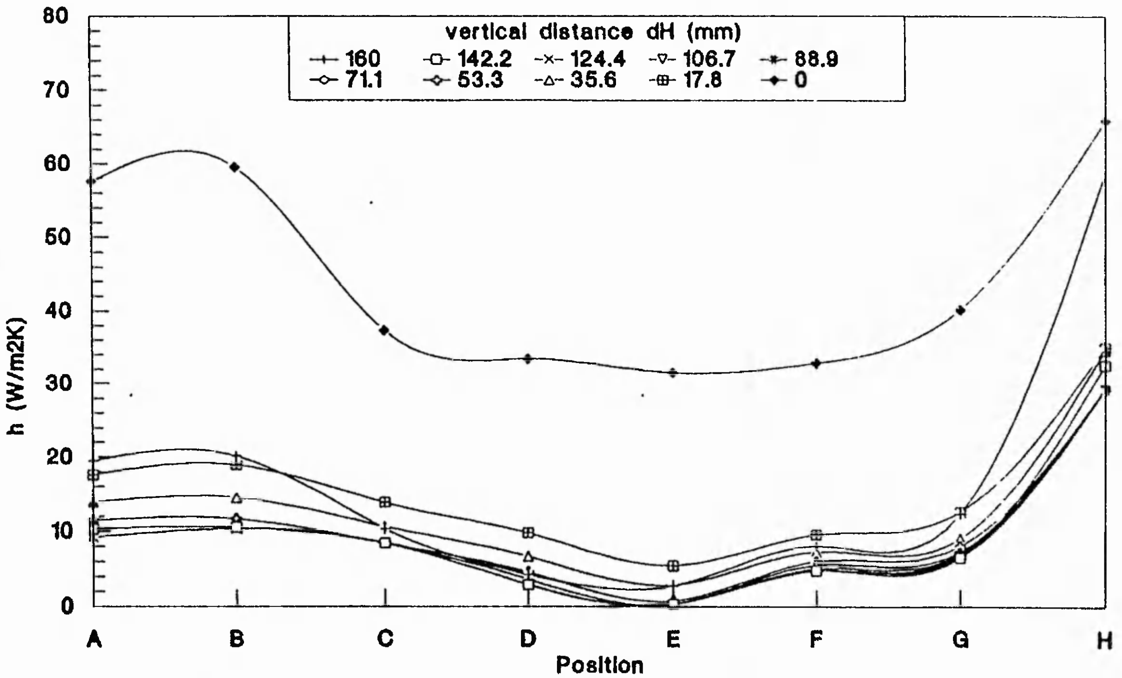

FIGURE 5-16 End section horizontal heat transfer coefficient map for S=31mm

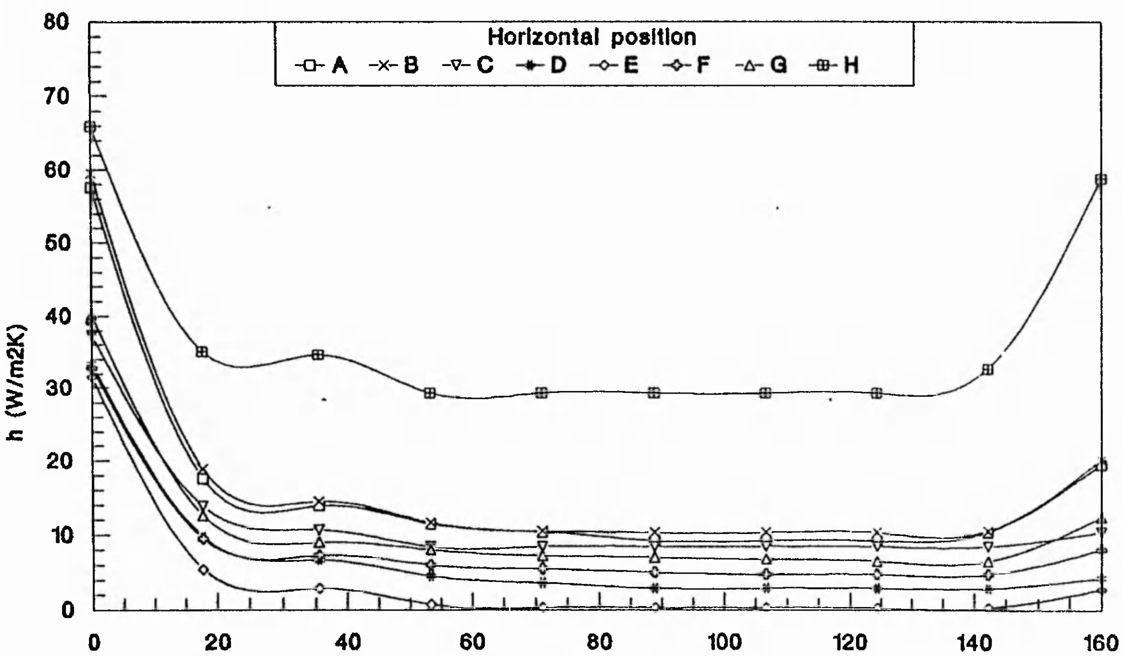

FIGURE 5-17 End section vertical heat transfer coefficient map for S=31mm

Heat transfer through each sub section (W)

SECTION No.	MID SECTION	END SECTION
1	2.599	3.083
2	4.639	5.088
3	4.610	5.020
4	4.619	5.029
5	4.634	5.047
6	4.708	5.094
7	4.820	5.189
8	5.022	5.557
9	5.625	6.036
10	5.039	5.186

TABLE 5-P COMPUTED SUB SECTION HEAT FLOWS FOR S=31 mm

The total heat transfer through the heat exchanger is,

$$\mathbf{Q_{TOT} = 468 \pm 2 \quad W} \tag{5.3.7}$$

The heat exchange area and volume are,

$$\mathbf{A = 0.072 \quad m^2} \tag{5.3.8}$$

$$\mathbf{V = 3.8 \times 10^{-4} \quad m^3} \tag{5.3.3}$$

5.3.4 29 mm spatial separation

Test conditions

VARIABLE	CONDITION
No. fins	5
T_I	68
T_b	17

TABLE 5-O INITIAL CONDITIONS FOR S=29 mm

Timing data (s)

dH(mm)	A	B	C	D	E	F	G	H
160	111	110	185	339	476	839	747	747
142.2	179	178	318	442	651	1117	792	1002
124.4	194	190	318	445	656	1154	1108	1051
106.7	199	195	318	445	656	1161	1108	1051
88.9	204	200	314	437	647	1146	1099	1037
71.1	199	195	302	418	640	1072	1015	1002
53.3	194	190	289	402	552	1025	951	911
35.6	186	182	276	351	494	918	836	825
17.8	169	165	242	293	389	740	667	657
0	55	54	82	97	108	210	210	202

TABLE 5-R MIDDLE FIN FOR S=29 mm

dH(mm)	A	B	C	D	E	F	G	H
160	116	115	235	357	487	822	553	168
142.2	215	214	324	451	705	1027	857	263
124.4	232	230	324	451	699	1053	889	263
106.7	232	230	324	451	691	1043	882	254
88.9	226	224	313	340	579	1027	867	254
71.1	222	220	293	392	531	1002	851	254
53.3	209	207	267	352	476	968	809	226
35.6	200	198	234	303	402	906	765	208
17.8	165	163	215	257	331	765	625	190
0	47	47	89	97	130	296	228	80

TABLE 5-S END FIN FOR S=29 mm

Heat transfer through each sub section (W)

SECTION No.	MID SECTION	END SECTION
1	2.737	3.394
2	4.771	5.655
3	4.583	5.602
4	4.576	5.623
5	4.580	5.755
6	4.677	5.778
7	4.797	5.983
8	5.001	6.255
9	5.480	6.721
10	5.993	5.559

TABLE 5-T COMPUTED SUB SECTION HEAT FLOWS FOR S=29 mm

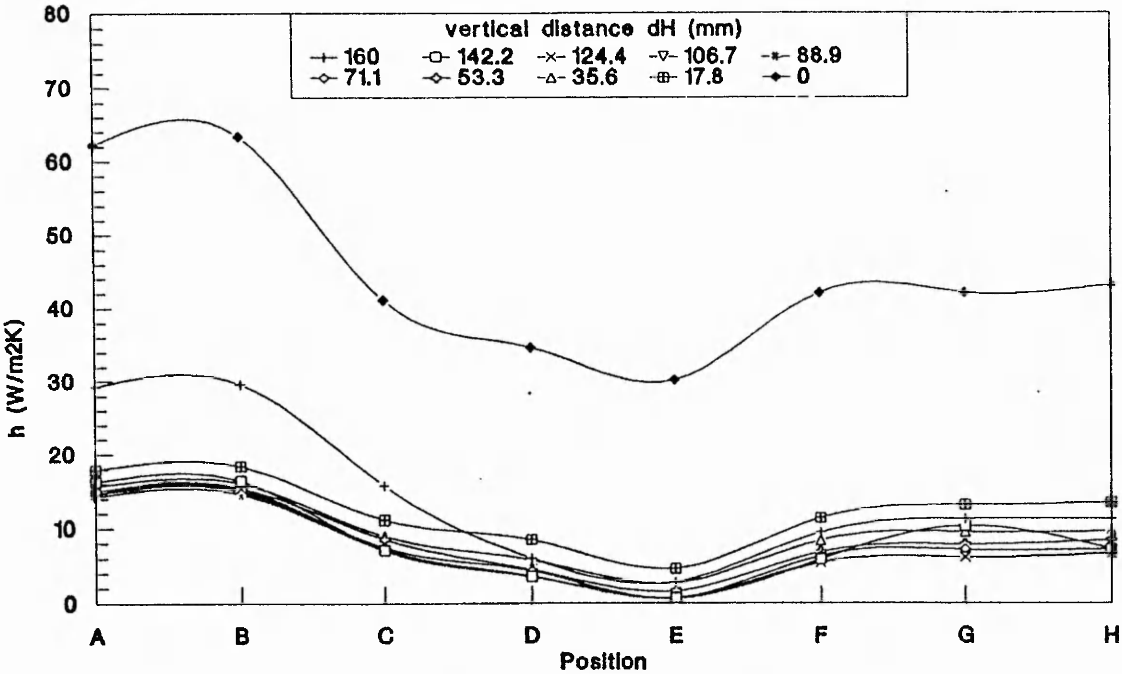

FIGURE 5-18 Mid section horizontal heat transfer coefficient map for S=29mm

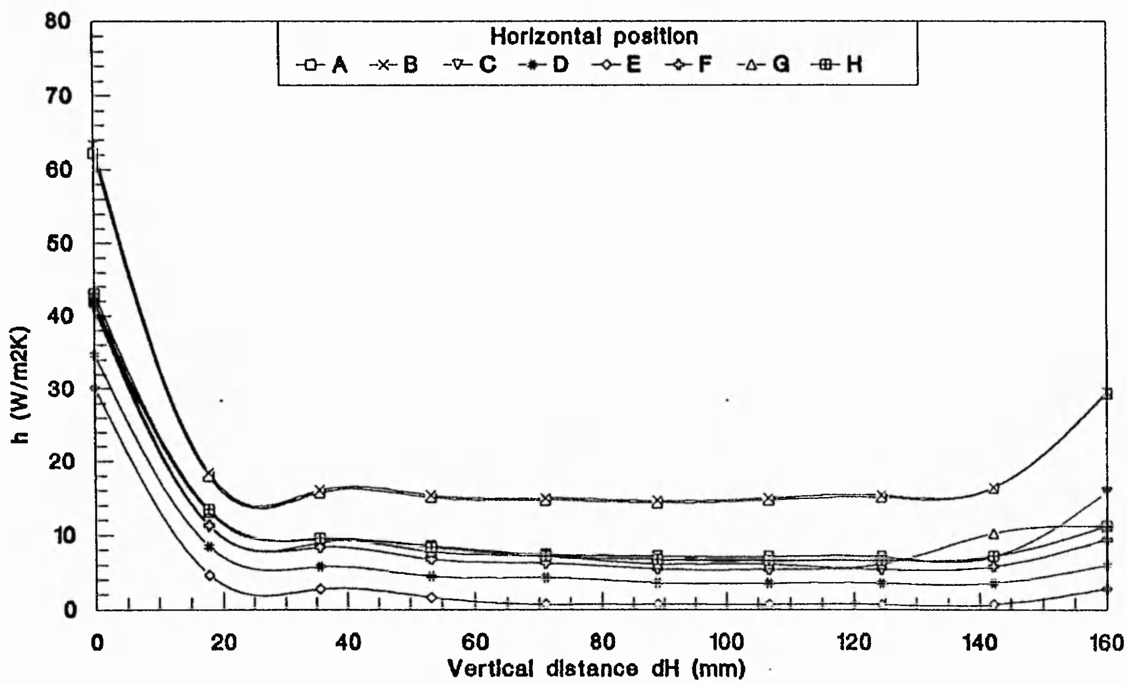

FIGURE 5-19 Mid section vertical heat transfer coefficient map for S=29mm

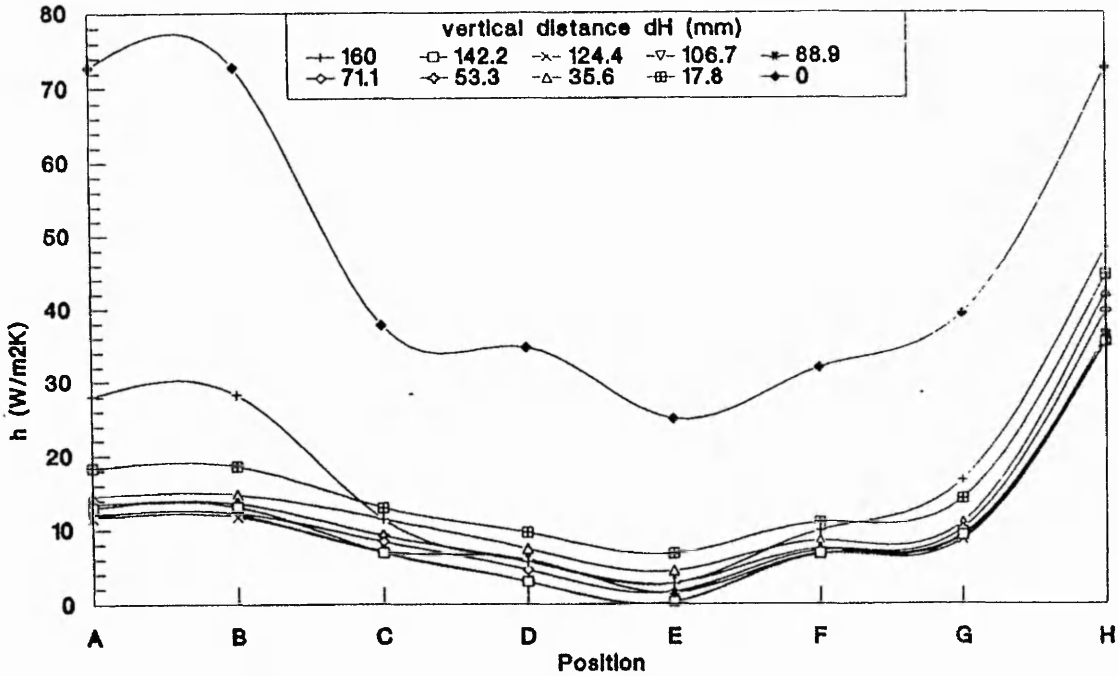

FIGURE 5-20 End section horizontal heat transfer coefficient map for S=29mm

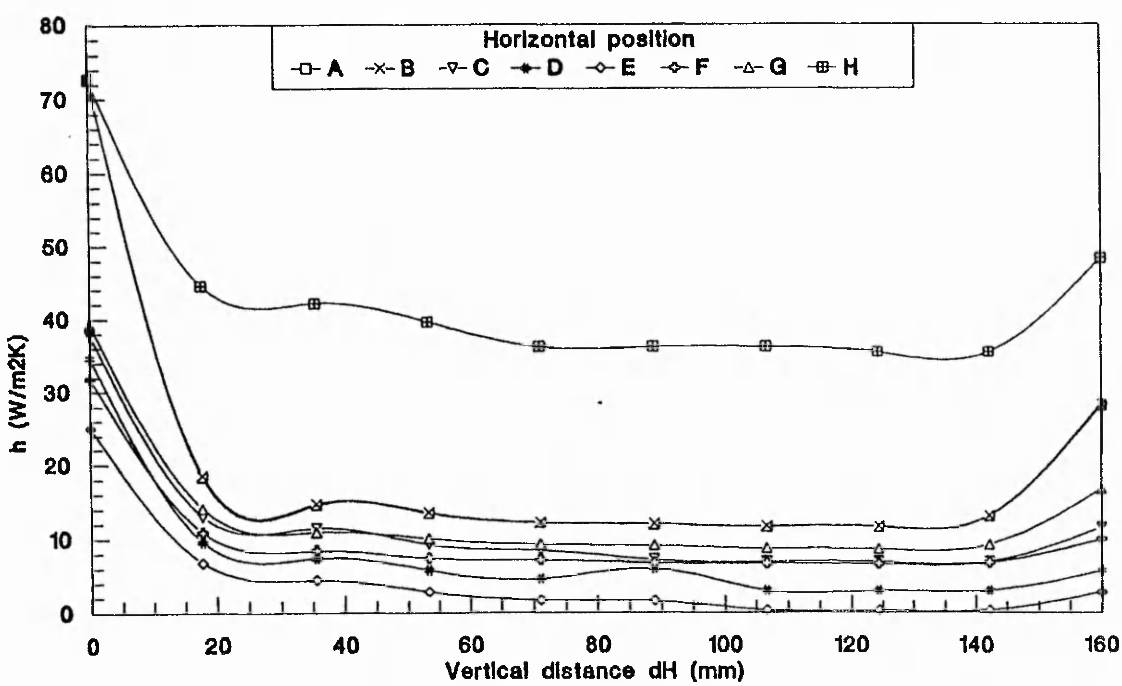

FIGURE 5-21 End section vertical heat transfer coefficient map for S=29mm

The total heat transfer through the heat exchanger is,

$$\mathbf{Q_{TOT} = 479 \pm 2 \quad W} \tag{5.3.10}$$

The heat exchange area and volume are,

$$\mathbf{A = 0.072 \ m^2} \tag{5.3.11}$$

$$\mathbf{V = 3.8 \times 10^{-4} \ m^3} \tag{5.3.12}$$

5.3.5 26 mm spatial separation

Test conditions

VARIABLE	CONDITION
No. fins	7
T_I	70.5
T_b	17.9

TABLE 5-U INITIAL CONDITIONS FOR S=26 mm

Timing data (s)

dH(mm)	A	B	C	D	E	F	G	H
160	106	104	311	423	644	1028	973	943
142.2	211	210	413	544	794	1253	1234	1210
124.4	232	230	413	548	794	1323	1257	1244
106.7	224	234	413	548	794	1330	1321	1244
88.9	234	232	393	511	743	1292	1275	1244
71.1	219	217	384	480	682	1236	1222	1179
53.3	208	204	366	456	602	1133	1124	1102
35.6	196	294	323	384	511	1028	998	969
17.8	169	165	261	312	406	818	794	743
0	52	52	82	125	116	239	239	239

TABLE 5-V MIDDLE FIN FOR S=26 mm

dH(mm)	A	B	C	D	E	F	G	H
160	110	110	241	304	409	736	614	502
142.2	170	169	333	434	562	914	827	624
124.4	179	175	346	450	630	921	827	624
106.7	186	184	350	454	639	925	827	624
88.9	188	186	353	454	639	914	787	624
71.1	190	186	333	434	639	884	757	624
53.3	187	186	316	409	629	836	731	624
35.6	183	180	300	365	535	787	665	472
17.8	170	165	248	292	409	652	566	342
0	63	62	90	102	115	252	220	167

TABLE 5-W END FIN FOR S=26 mm

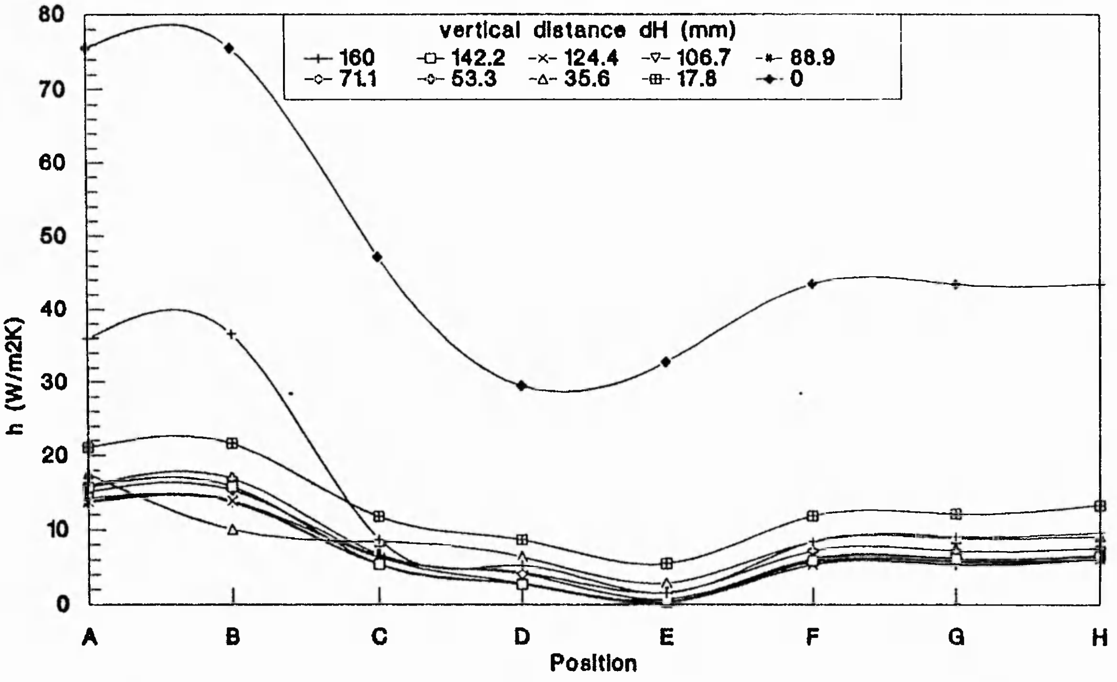

FIGURE 5-22 Mid section horizontal heat transfer coefficient map for S=26mm

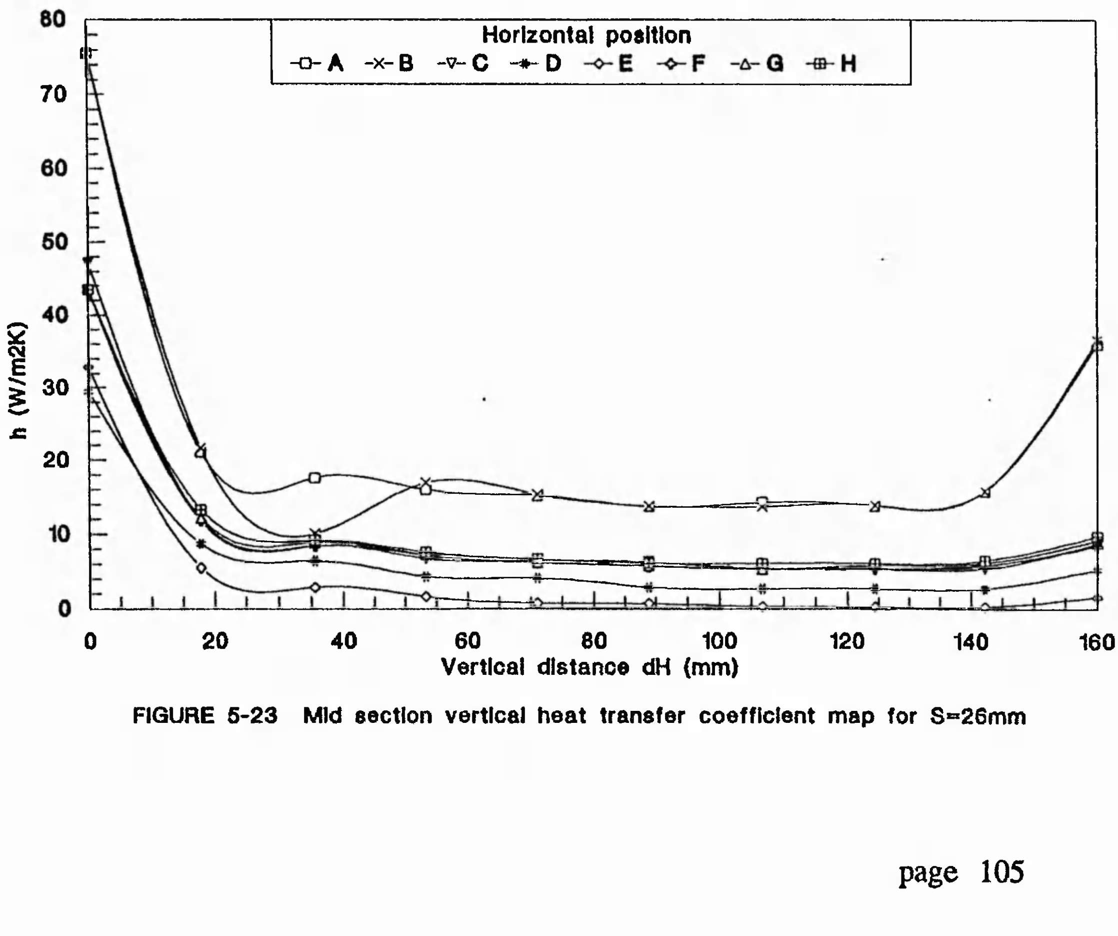

FIGURE 5-23 Mid section vertical heat transfer coefficient map for S=26mm

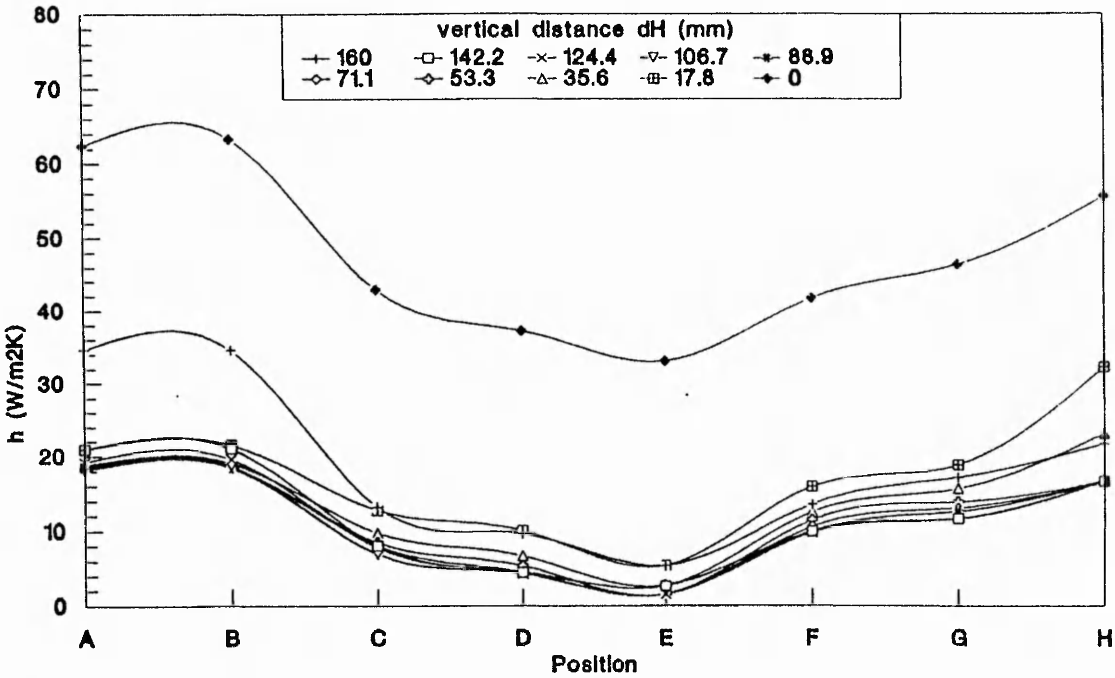

FIGURE 5-24 End section horizontal heat transfer coefficient map for S=26mm

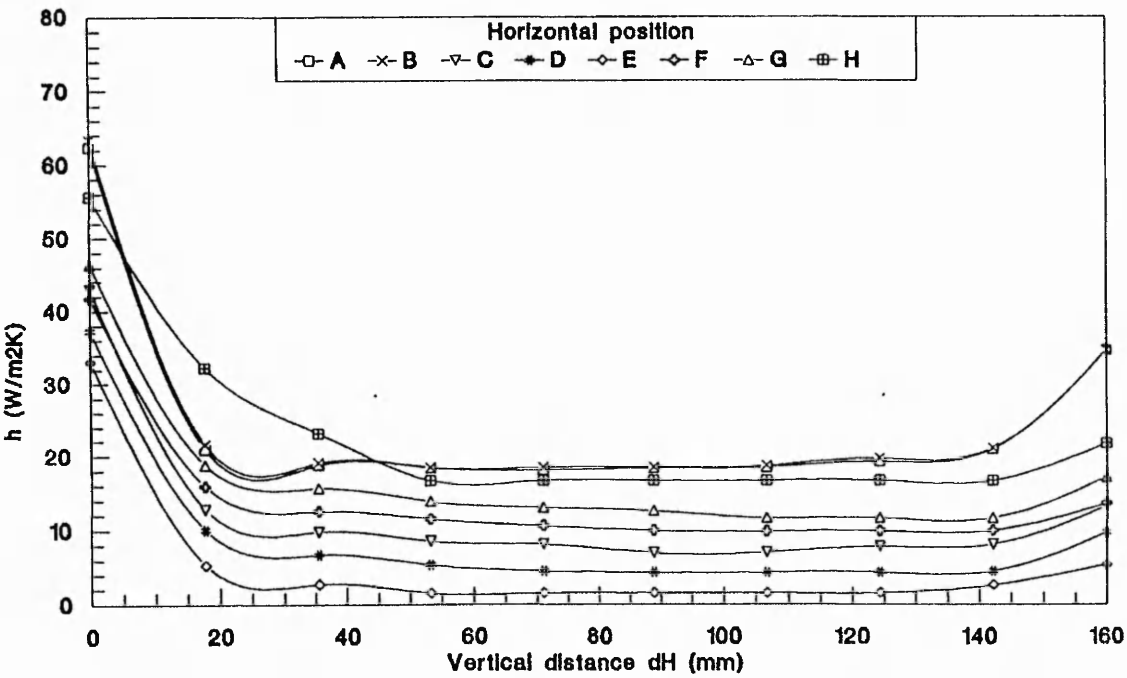

FIGURE 5-25 End section vertical heat transfer coefficient map for S=26mm

Heat transfer through each sub section (W)

SECTION No.	MID SECTION	END SECTION
1	2.519	2.279
2	4.349	3.890
3	4.287	3.831
4	4.270	3.798
5	4.326	3.809
6	4.420	3.857
7	4.553	3.919
8	4.699	4.104
9	5.309	4.519
10	5.003	3.884

TABLE 5-X COMPUTED SUB SECTION HEAT FLOWS FOR S=26 mm

The total heat transfer through the heat exchanger is,

$$\mathbf{Q_{TOT} = 569 \pm 3 \quad W} \tag{5.3.13}$$

The heat exchange area and volume are,

$$\mathbf{A = 0.088 \ \ m^2} \tag{5.3.14}$$

$$\mathbf{V = 4.04 \times 10^{-4} \ \ m^3} \tag{5.3.15}$$

5.3.6 23 mm spatial separation

Test conditions

VARIABLE	CONDITION
No. fins	7
T_I	71.3
T_b	17.5

TABLE 5-Y INITIAL CONDITIONS FOR S=23 mm

Timing data (s)

dH(mm)	A	B	C	D	E	F	G	H
160	89	85	288	398	634	898	898	898
142.2	195	190	358	529	799	1217	1214	1130
124.4	215	210	368	540	804	1291	1277	1229
106.7	224	220	373	540	804	1305	1291	1229
88.9	228	224	358	518	731	1217	1261	1229
71.1	220	210	349	483	677	1201	1199	1171
53.3	209	200	331	462	629	1122	1111	1106
35.6	194	190	299	389	531	1040	1010	966
17.8	166	160	255	318	437	815	771	751
0	58	56	100	113	132	261	261	261

TABLE 5-Z MIDDLE FIN FOR S=23 mm

dH(mm)	A	B	C	D	E	F	G	H
160	90	87	229	360	534	852	579	226
142.2	149	145	336	457	670	1055	845	305
124.4	165	163	358	473	697	1079	852	312
106.7	186	184	358	473	709	1083	852	334
88.9	186	184	353	473	697	1055	805	334
71.1	183	180	336	457	670	1024	789	334
53.3	180	175	327	414	627	970	760	317
35.6	174	170	295	366	538	897	707	305
17.8	148	142	248	299	409	763	579	280
0	59	57	104	120	127	268	230	133

TABLE 5-A1 END FIN FOR S=23 mm

Heat transfer through each sub section (W)

SECTION No.	MID SECTION	END SECTION
1	2.547	2.840
2	4.266	4.817
3	4.172	4.700
4	4.150	4.634
5	4.191	4.666
6	4.282	4.737
7	4.398	4.834
8	4.603	5.006
9	5.085	5.454
10	4.578	4.533

TABLE 5-B1 COMPUTED SUB SECTION HEAT FLOWS FOR S=23 mm

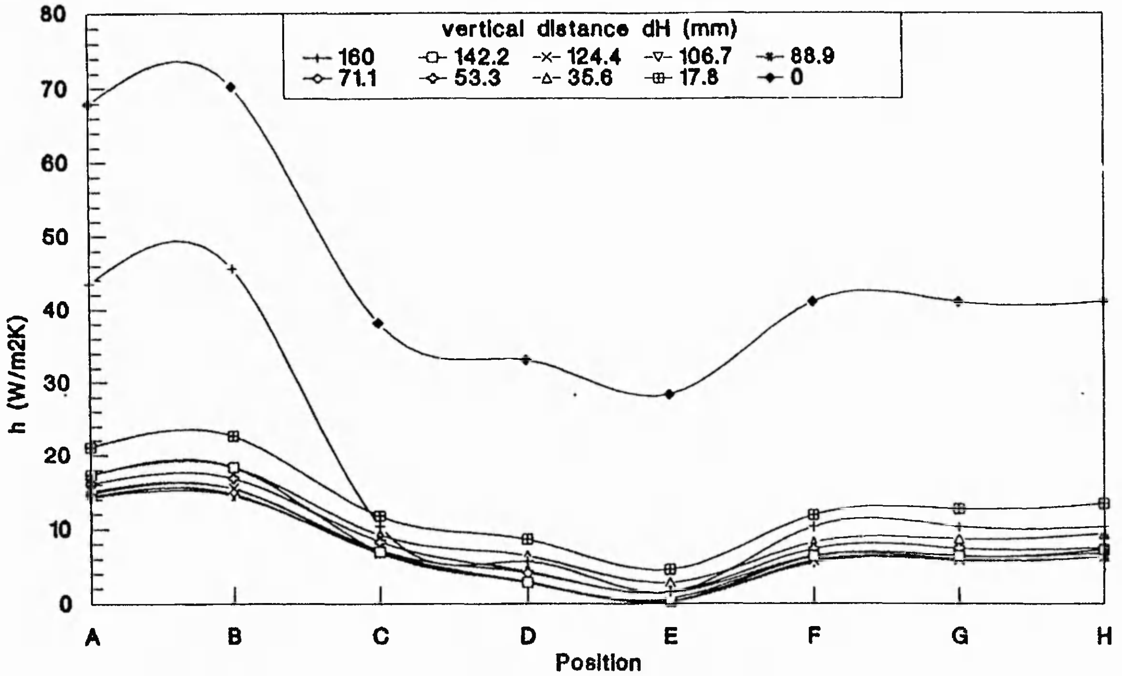

FIGURE 5-26 Mid section horizontal heat transfer coefficient map for S=23mm

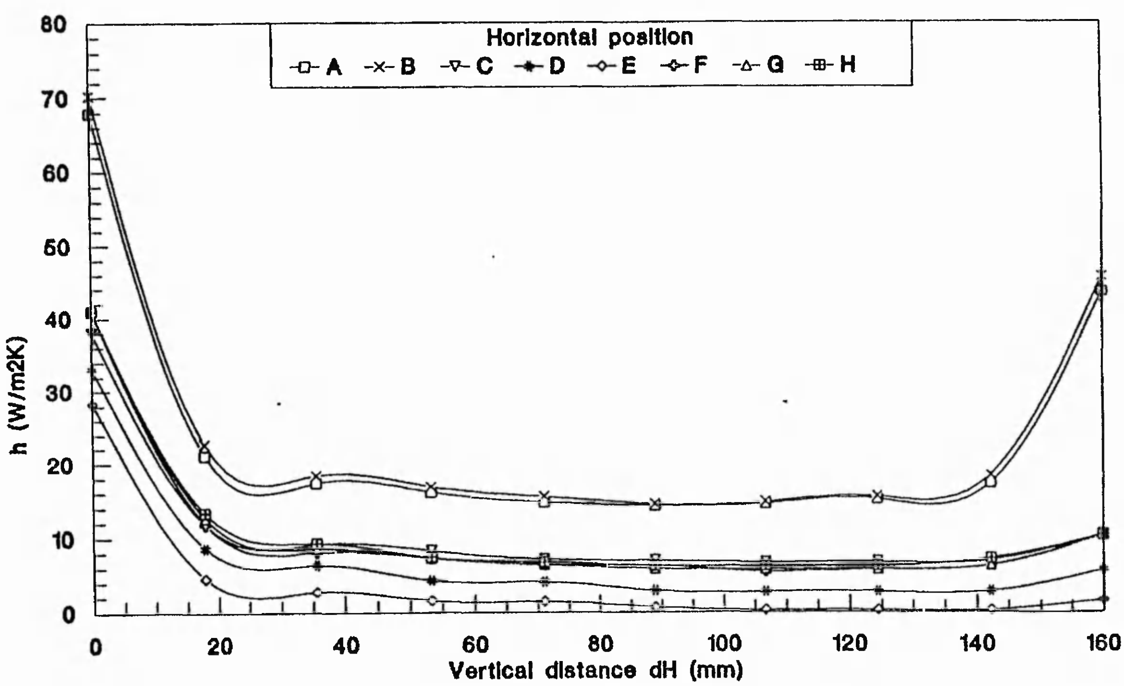

FIGURE 5-27 Mid section vertical heat transfer coefficient map for S=23mm

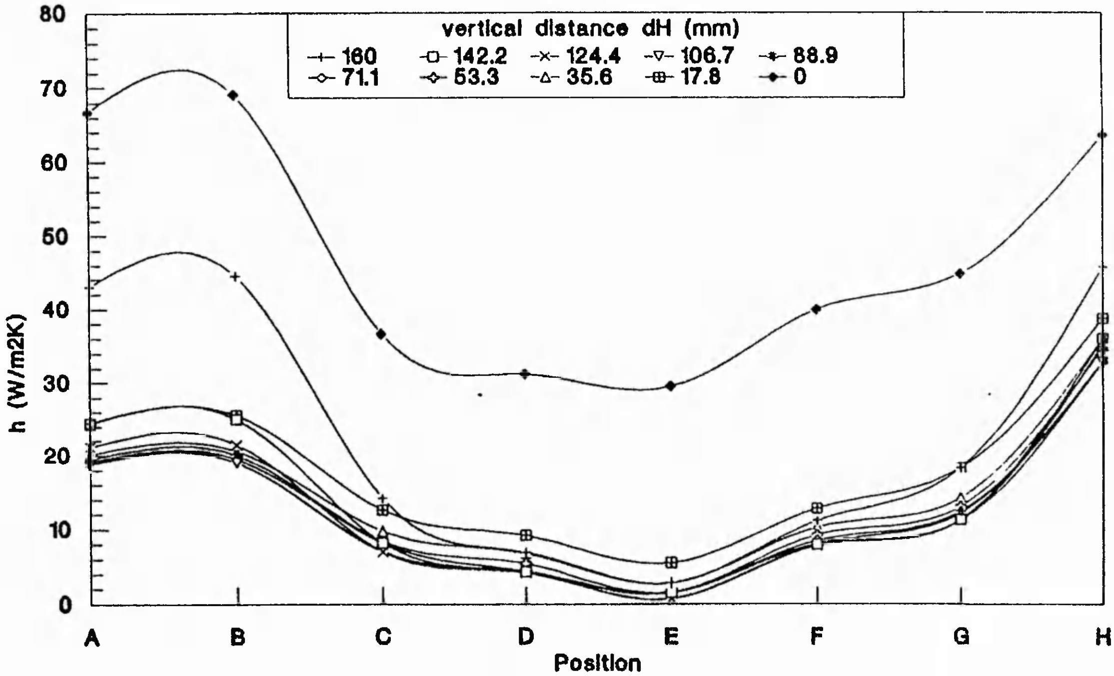

FIGURE 5-28 End section horizontal heat transfer coefficient map for S=23mm

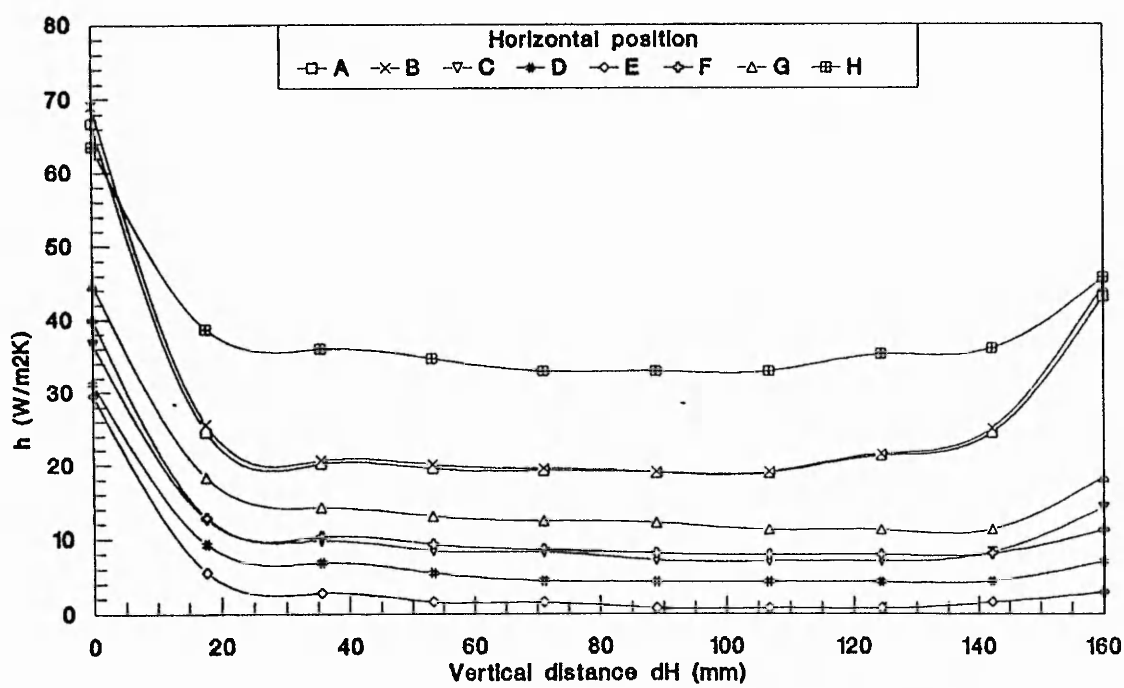

FIGURE 5-29 End section vertical heat transfer coefficient map for S=23mm

The total heat transfer through the heat exchanger is,

$$\mathbf{Q_{TOT} = 595 \pm 3 \quad W} \tag{5.3.16}$$

The heat exchange area and volume are,

$$\mathbf{A = 0.088 \;\; m^2} \tag{5.3.17}$$

$$\mathbf{V = 4.04 \times 10^{-4} \;\; m^3} \tag{5.3.18}$$

5.3.7 20 mm spatial separation

<u>Test conditions</u>

VARIABLE	CONDITION
No. fins	9
T_I	68.5
T_b	17.4

TABLE 5-C1 INITIAL CONDITIONS FOR S=20 mm

Timing data (s)

dH(mm)	A	B	C	D	E	F	G	H
160	113	113	276	422	484	1004	1004	1004
142.2	179	175	304	514	693	1328	1297	1296
124.4	207	206	304	514	693	1322	1342	1328
106.7	204	200	304	514	681	1349	1342	1308
88.9	202	200	304	514	671	1345	1321	1308
71.1	201	200	304	514	647	1327	1257	1247
53.3	201	198	304	504	585	1194	1185	1140
35.6	189	187	254	345	484	1086	1058	1034
17.8	154	152	244	288	345	850	840	793
0	80	79	100	107	110	267	267	267

TABLE 5-D1 MIDDLE FIN FOR S=20 mm

dH(mm)	A	B	C	D	E	F	G	H
160	113	113	169	210	357	648	508	468
142.2	180	179	240	357	520	801	778	687
124.4	206	204	276	360	520	811	790	728
106.7	203	200	276	372	491	811	790	720
88.9	203	200	276	372	491	793	766	687
71.1	202	199	276	372	491	788	733	568
53.3	202	199	276	372	491	767	717	568
35.6	186	184	254	343	425	688	656	537
17.8	153	150	234	284	343	562	511	358
0	80	80	102	107	110	360	217	167

TABLE 5-E1 END FIN FOR S=20 mm

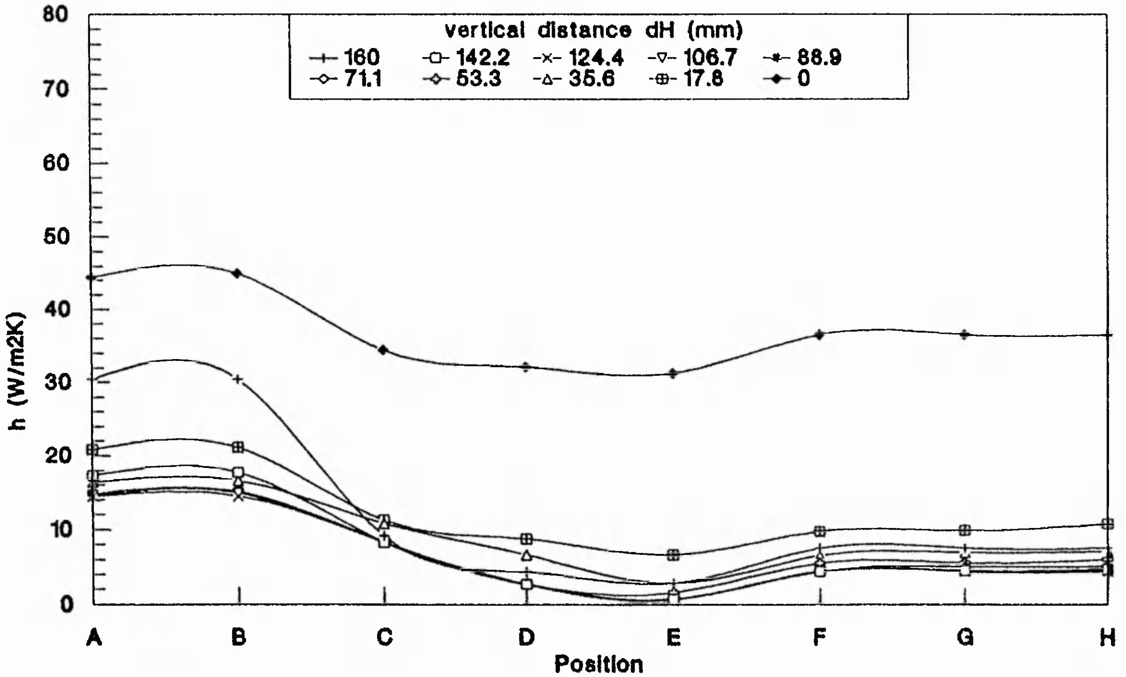

FIGURE 5-30 Mid section horizontal heat transfer coefficient map for S=20mm

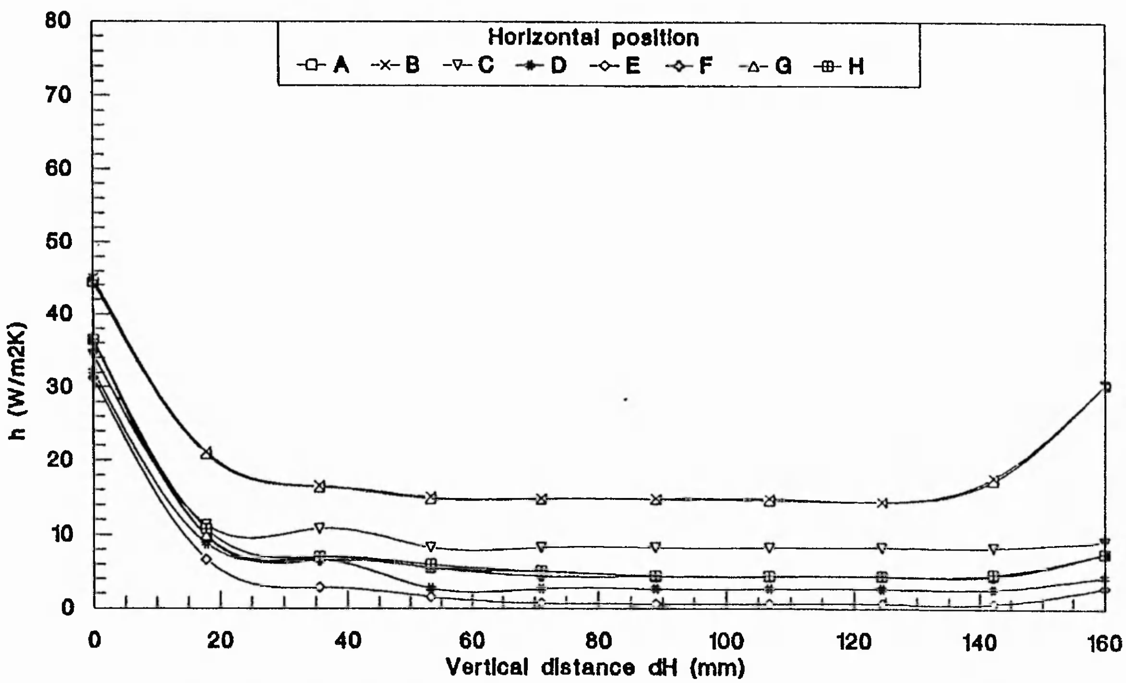

FIGURE 5-31 Mid section vertical heat transfer coefficient map for S=20mm

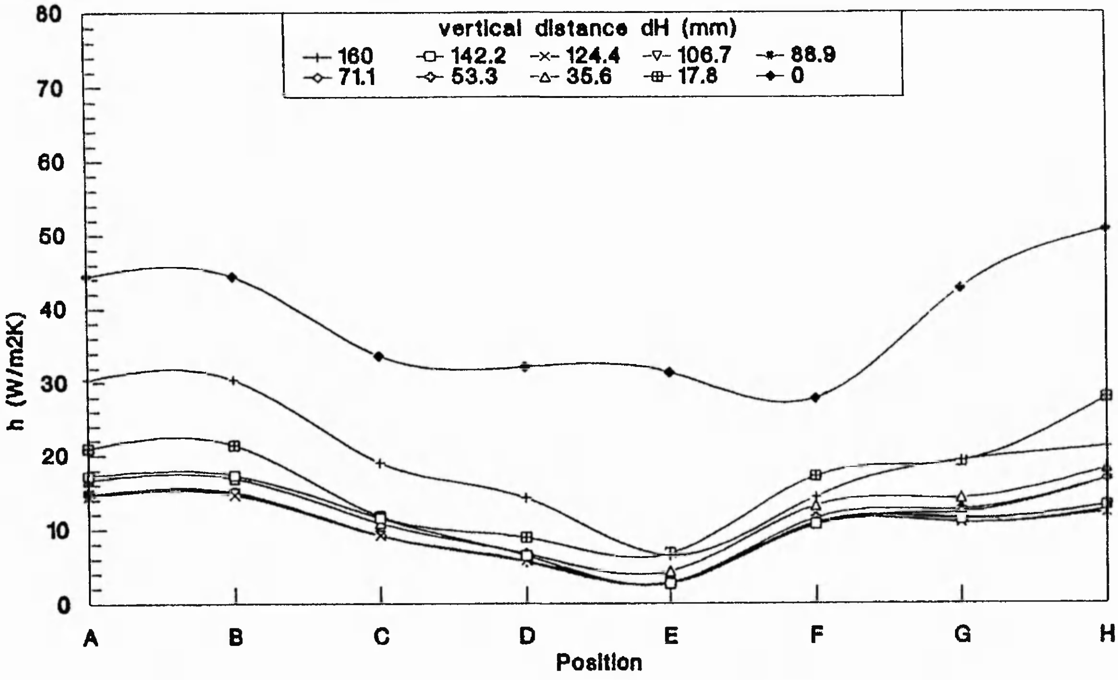

FIGURE 5-32 End section horizontal heat transfer coefficient map for S=20mm

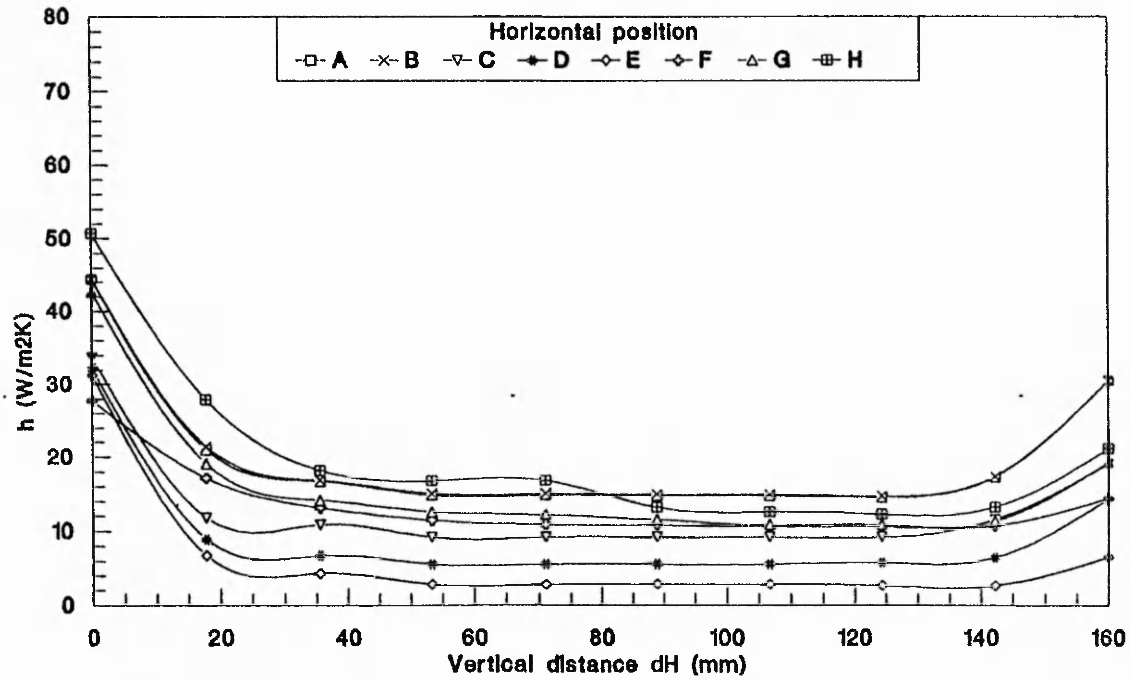

FIGURE 5-33 End section vertical heat transfer coefficient map for S=20mm

Heat transfer through each sub section (W)

SECTION No.	MID SECTION	END SECTION
1	2.230	2.137
2	3.970	3.526
3	3.915	3.413
4	3.920	3.418
5	3.922	3.429
6	3.947	3.450
7	4.023	3.465
8	4.296	3.636
9	4.713	3.971
10	4.064	3.054

TABLE 5-F1 COMPUTED SUB SECTION HEAT FLOWS FOR S=20 mm

The total heat transfer through the heat exchanger is,

$$\mathbf{Q_{TOT} = 687 \pm 3 \quad W} \tag{5.3.19}$$

The heat exchange area and volume are,

$$\mathbf{A = 0.104 \;\; m^2} \tag{5.3.20}$$

$$\mathbf{V = 4.28 \times 10^{-4} \;\; m^3} \tag{5.3.21}$$

5.3.8 17 mm spatial separation

Test conditions

VARIABLE	CONDITION
No. fins	9
T_I	68.5
T_b	19.4

TABLE 5-G1 INITIAL CONDITIONS FOR S=17 mm

Timing data (s)

dH(mm)	A	B	C	D	E	F	G	H
160	94	90	227	374	470	1114	741	994
142.2	176	170	325	470	776	1034	1294	1279
124.4	193	190	300	498	837	1379	1368	1353
106.7	193	190	299	498	837	1405	1391	1361
88.9	184	180	299	498	810	1402	1380	1353
71.1	179	175	299	470	722	1315	1294	1272
53.3	166	164	299	438	609	1192	1184	1160
35.6	154	150	299	402	569	1074	1074	1066
17.8	133	130	242	340	438	865	876	836
0	59	58	109	134	158	342	342	342

TABLE 5-H1 MIDDLE FIN FOR S=17 mm

dH(mm)	A	B	C	D	E	F	G	H
160	94	90	208	322	460	907	580	264
142.2	180	175	366	390	662	1077	833	444
124.4	180	175	366	430	678	1104	833	444
106.7	180	175	366	430	678	1101	833	444
88.9	173	170	366	430	678	1086	833	425
71.1	169	165	349	430	662	1069	823	425
53.3	165	160	331	398	616	1018	813	424
35.6	156	150	324	373	570	956	808	409
17.8	143	140	276	353	450	808	655	365
0	63	62	91	122	167	364	241	138

TABLE 5-I1 END FIN FOR S=17 mm

Heat transfer through each sub section (W)

SECTION No.	MID SECTION	END SECTION
1	2.398	2.781
2	4.032	4.497
3	3.900	4.472
4	3.897	4.472
5	3.914	4.499
6	3.982	4.543
7	4.135	4.597
8	4.266	4.715
9	4.693	5.063
10	3.806	4.226

TABLE 5-J1 COMPUTED SUB SECTION HEAT FLOWS FOR S=17 mm

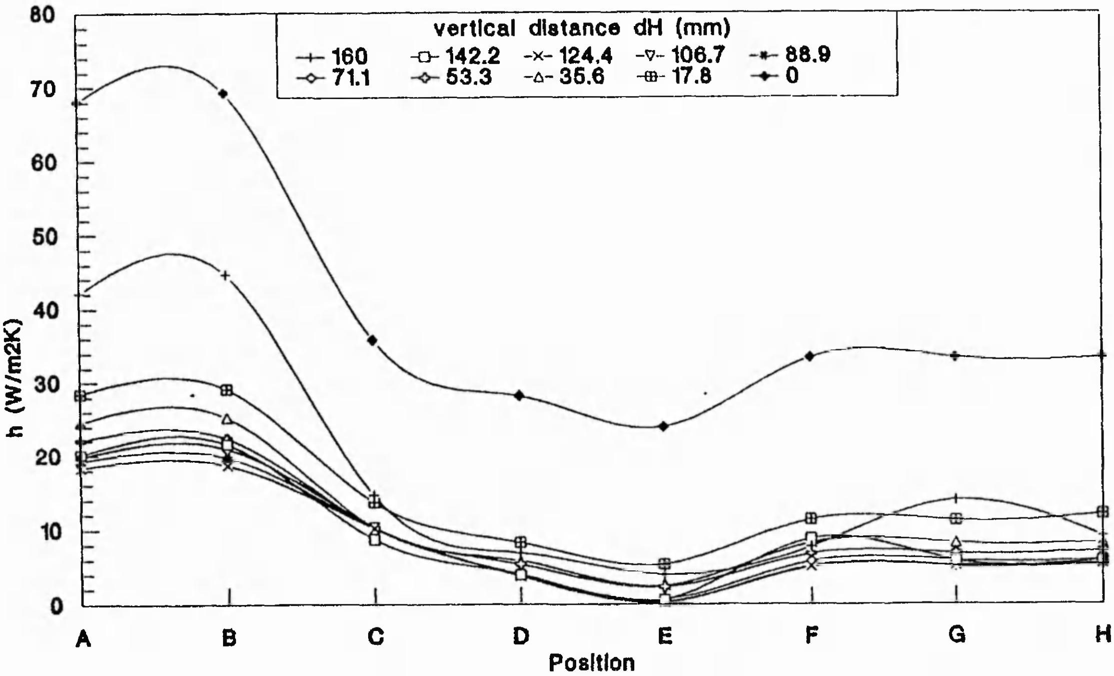

FIGURE 5-34 Mid section horizontal heat transfer coefficient map for S=17mm

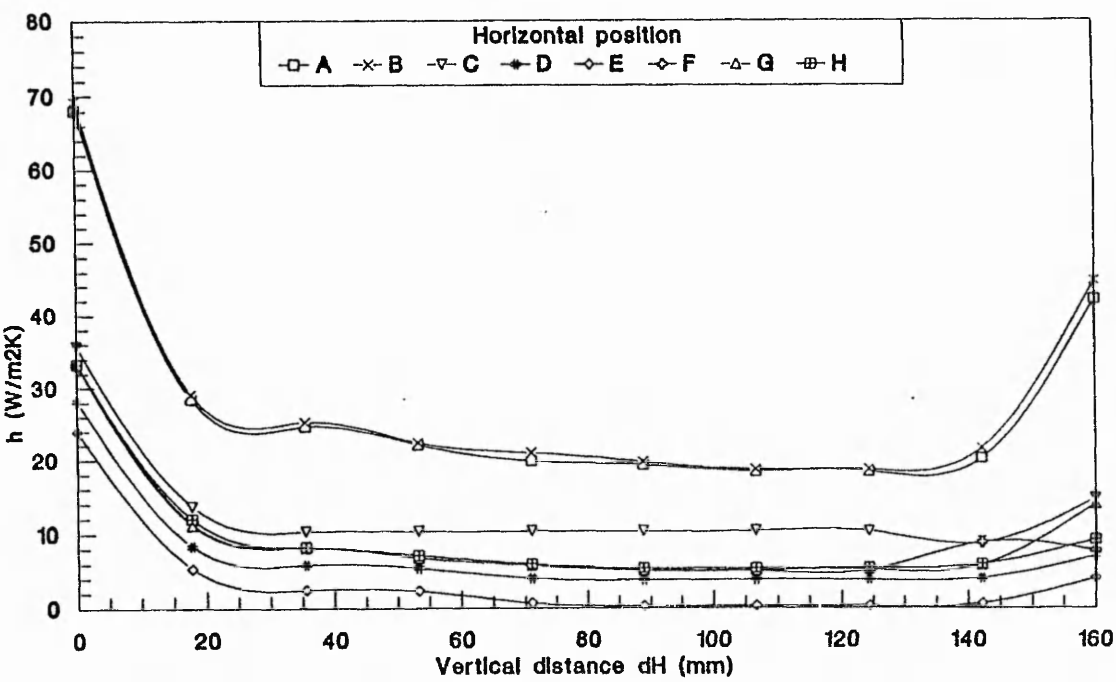

FIGURE 5-35 Mid section vertical heat transfer coefficient map for S=17mm

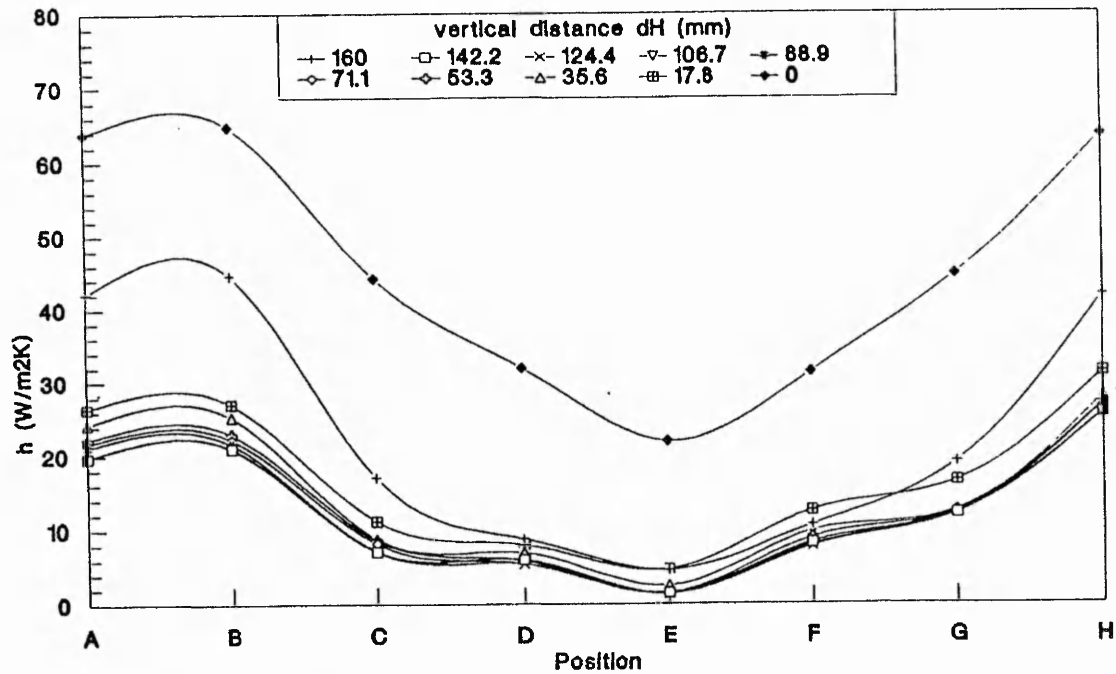

FIGURE 5-36 End section horizontal heat transfer coefficient map for S=17mm

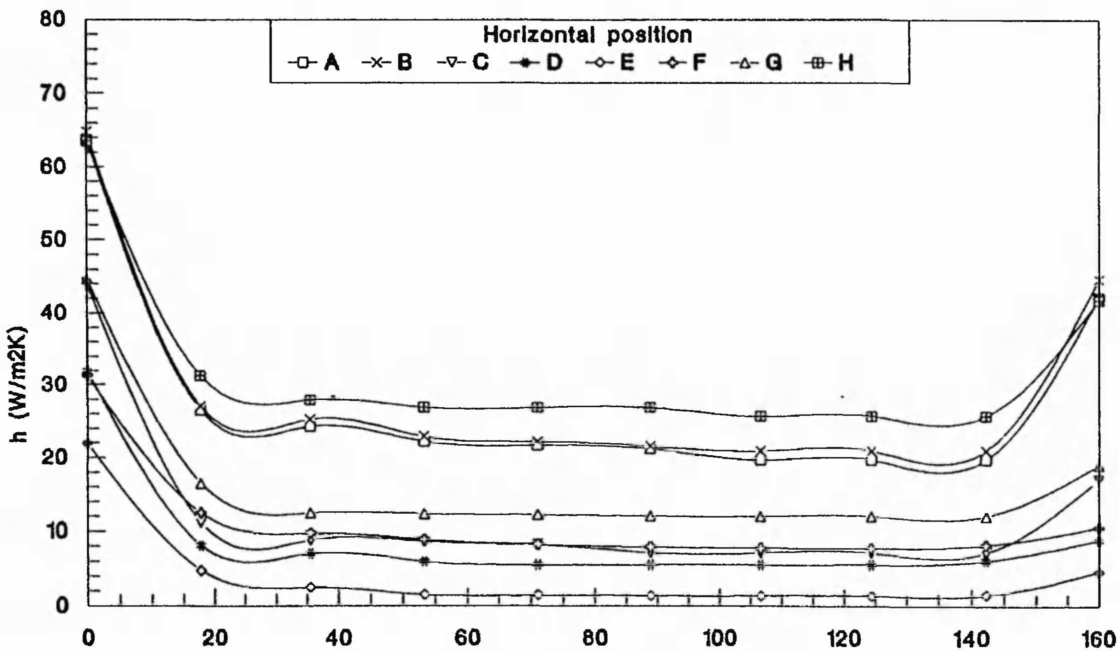

FIGURE 5-37 End section vertical heat transfer coefficient map for S=17mm

The total heat flow through the heat exchanger is,

$$\mathbf{Q_{TOT} = 705 \pm 4 \quad W} \tag{5.3.22}$$

The heat exchange area and volume are,

$$\mathbf{A = 0.104 \ \ m^2} \tag{5.3.23}$$

$$\mathbf{V = 4.28 \times 10^{-4} \ \ m^3} \tag{5.3.24}$$

5.3.9 14 mm spatial separation

Test conditions

VARIABLE	CONDITION
No. fins	11
T_I	53
T_b	22

TABLE 5-K1 INITIAL CONDITIONS FOR S=14 mm

Timing data (s)

dH(mm)	A	B	C	D	E	F	G	H
160	70	68	230	286	450	1005	1005	1005
142.2	135	133	281	407	480	1149	1145	1141
124.4	143	140	281	407	480	1150	1130	1123
106.7	135	133	281	407	480	1130	1121	1108
88.9	131	130	276	392	480	1100	1090	1080
71.1	123	122	270	380	480	1080	1070	1059
53.3	113	112	237	348	435	1040	1015	1005
35.6	92	91	219	323	447	930	925	920
17.8	79	79	190	281	407	739	739	739
0	39	39	70	100	133	304	304	304

TABLE 5-L1 MIDDLE FIN FOR S=14 mm

dH(mm)	A	B	C	D	E	F	G	H
160	112	112	351	477	709	827	562	250
142.2	242	236	406	618	804	1041	800	500
124.4	242	236	416	624	804	1072	800	500
106.7	242	236	416	624	804	1072	800	500
88.9	236	230	416	582	804	1041	800	500
71.1	220	214	298	521	804	1010	796	500
53.3	215	209	370	482	736	966	787	500
35.6	182	180	530	428	639	854	745	459
17.8	165	262	282	350	515	728	593	351
0	73	72	120	112	162	355	250	162

TABLE 5-M1 END FIN FOR S=14 mm

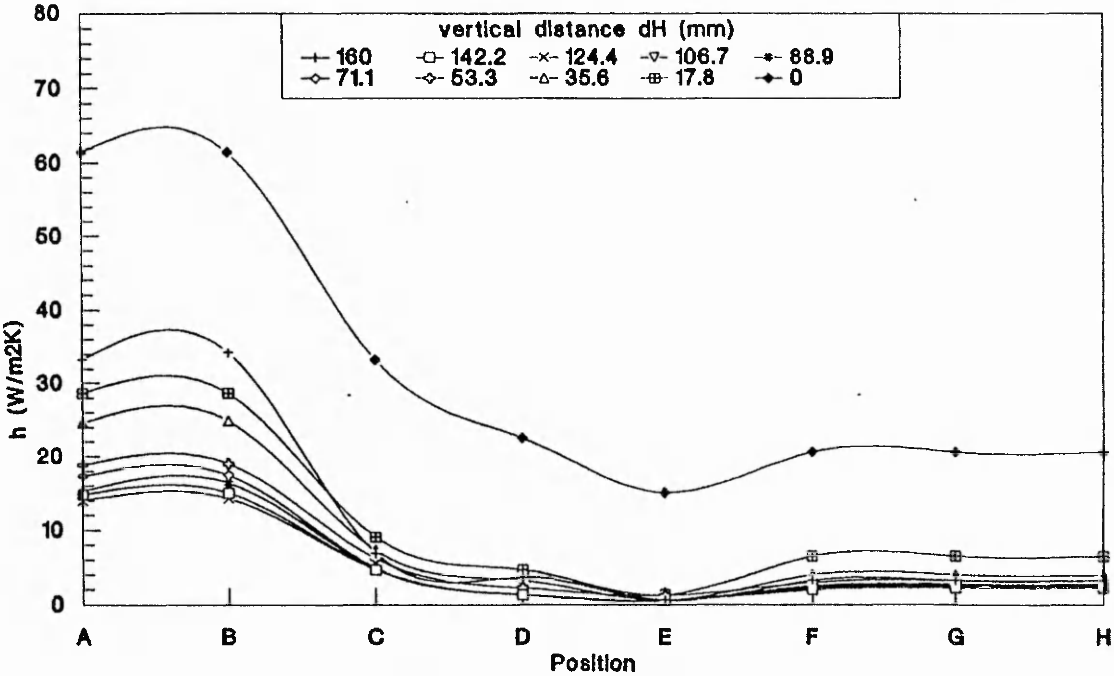

FIGURE 5-38 Mid section horizontal heat transfer coefficient map for S=14mm

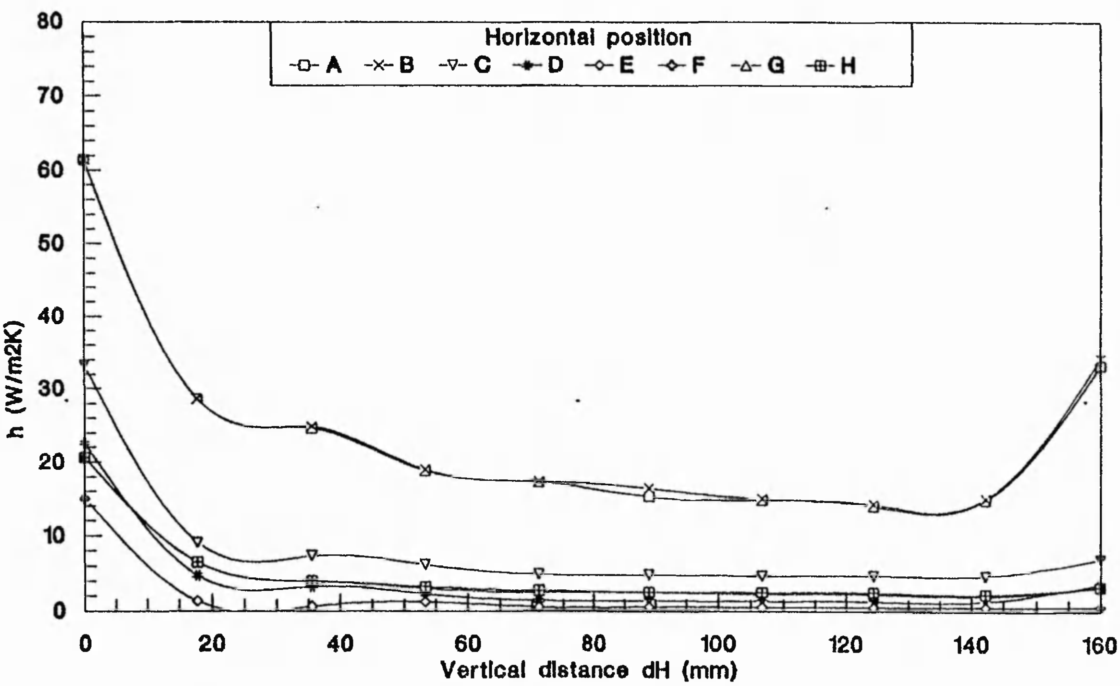

FIGURE 5-39 Mid section vertical heat transfer coefficient map for S=14mm

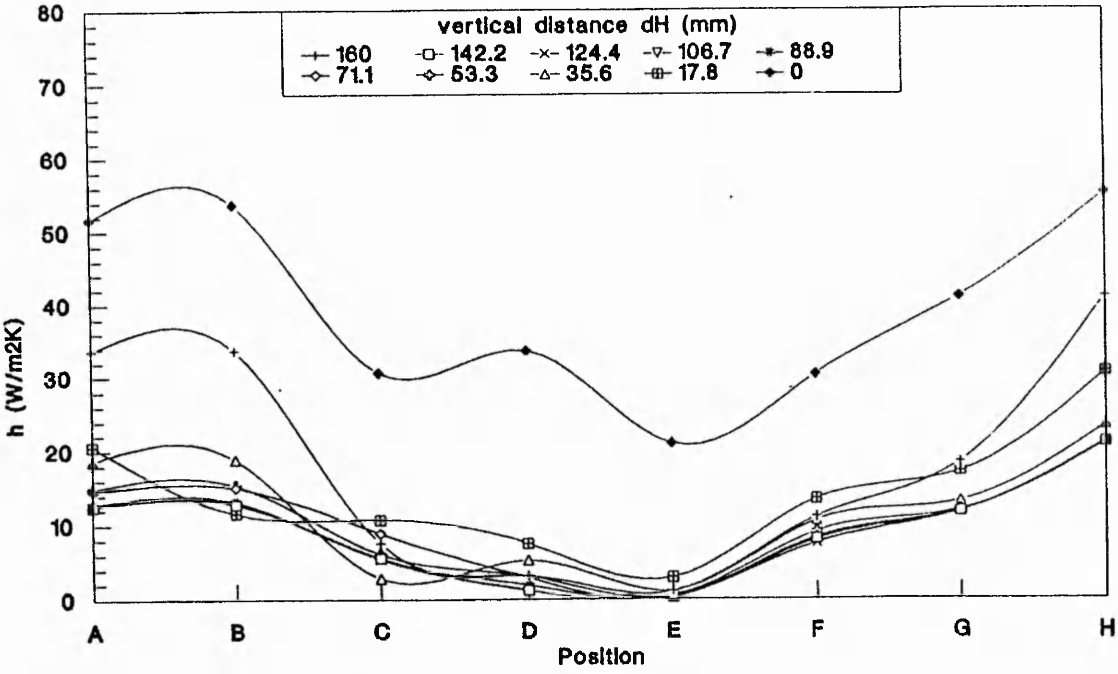

FIGURE 5-40 End section horizontal heat transfer coefficient map for S=14mm

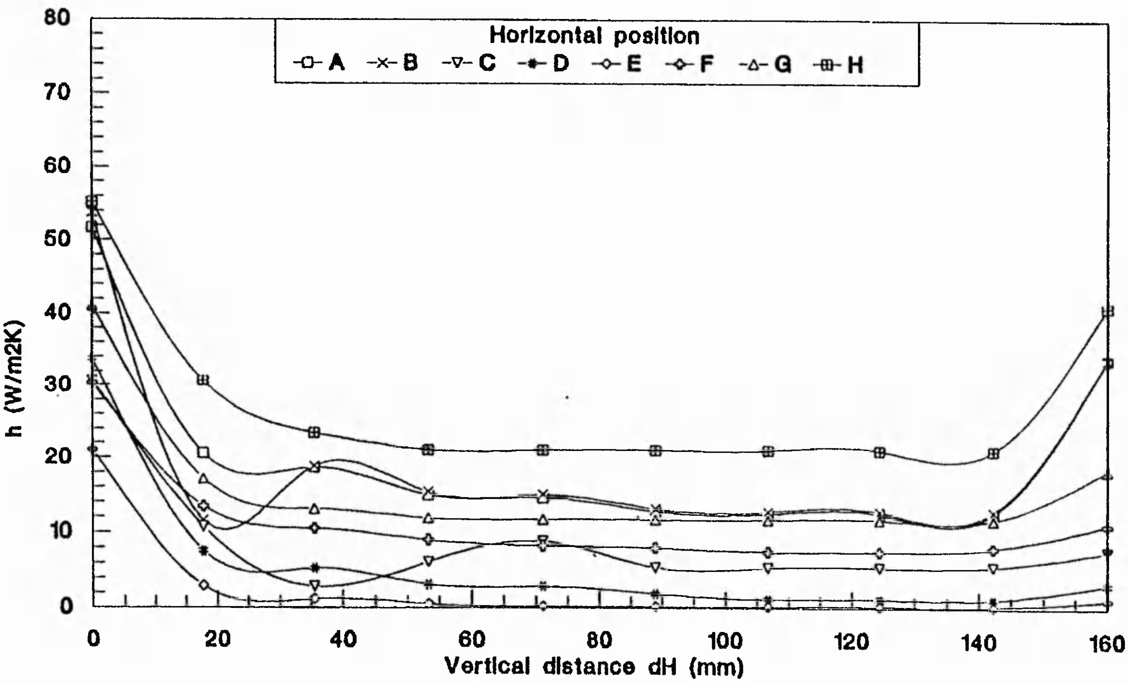

FIGURE 5-41 End section vertical heat transfer coefficient map for S=14mm

Heat transfer through each sub section (W)

SECTION No.	MID SECTION	END SECTION
1	2.254	2.243
2	3.777	3.728
3	3.736	3.714
4	3.745	3.714
5	3.798	3.748
6	3.863	3.880
7	4.020	3.858
8	4.168	3.981
9	4.553	4.342
10	3.739	3.579

TABLE 5-N1 COMPUTED SUB SECTION HEAT FLOWS FOR S=14 mm

The total heat transfer through the heat exchanger is,

$$\mathbf{Q_{TOT} = 817 \pm 5 \quad W} \qquad (5.3.25)$$

The heat exchange area and volume are,

$$\mathbf{A = 0.12 \ m^2} \qquad (5.3.26)$$

$$\mathbf{V = 4.52 \times 10^{-4} \ m^3} \qquad (5.3.27)$$

5.3.10 11 mm spatial separation

Test conditions

VARIABLE	CONDITION
No. fins	13
T_I	65
T_b	21

TABLE 5-O1 INITIAL CONDITIONS FOR S=11 mm

Timing data (s)

dH(mm)	A	B	C	D	E	F	G	H
160	97	97	230	274	449	770	770	770
142.2	186	182	244	405	599	1090	1090	1080
124.4	204	200	244	427	599	1130	1110	1085
106.7	198	194	244	427	599	1130	1110	1080
88.9	180	175	244	427	578	1096	1079	1047
71.1	171	164	244	427	564	1014	1008	1006
53.3	155	150	244	384	546	909	905	900
35.6	145	140	237	352	462	820	815	800
17.8	122	120	217	285	343	690	690	685
0	60	60	91	107	131	257	257	257

TABLE 5-P1 MIDDLE FIN FOR S=11 mm

dH(mm)	A	B	C	D	E	F	G	H
160	240	240	390	547	795	1007	645	243
142.2	338	336	510	659	820	1207	1012	590
124.4	349	345	510	659	820	1220	1007	668
106.7	349	345	510	650	820	1220	1003	668
88.9	338	336	510	645	820	1203	1003	668
71.1	315	310	469	613	800	1168	1002	668
53.3	291	290	439	580	793	1108	923	663
35.6	262	261	384	505	767	1028	807	590
17.8	220	216	315	397	433	859	718	480
0	93	93	279	180	274	450	304	226

TABLE 5-O1 END FIN FOR S=11 mm

Heat transfer through each sub section (W)

SECTION No.	MID SECTION	END SECTION
1	1.894	2.071
2	3.341	3.561
3	3.337	3.531
4	3.353	3.531
5	3.381	3.541
6	3.410	3.583
7	3.522	3.713
8	3.685	3.842
9	3.950	4.266
10	3.097	3.006

TABLE 5-R1 COMPUTED SUB SECTION HEAT FLOWS FOR S=11 mm

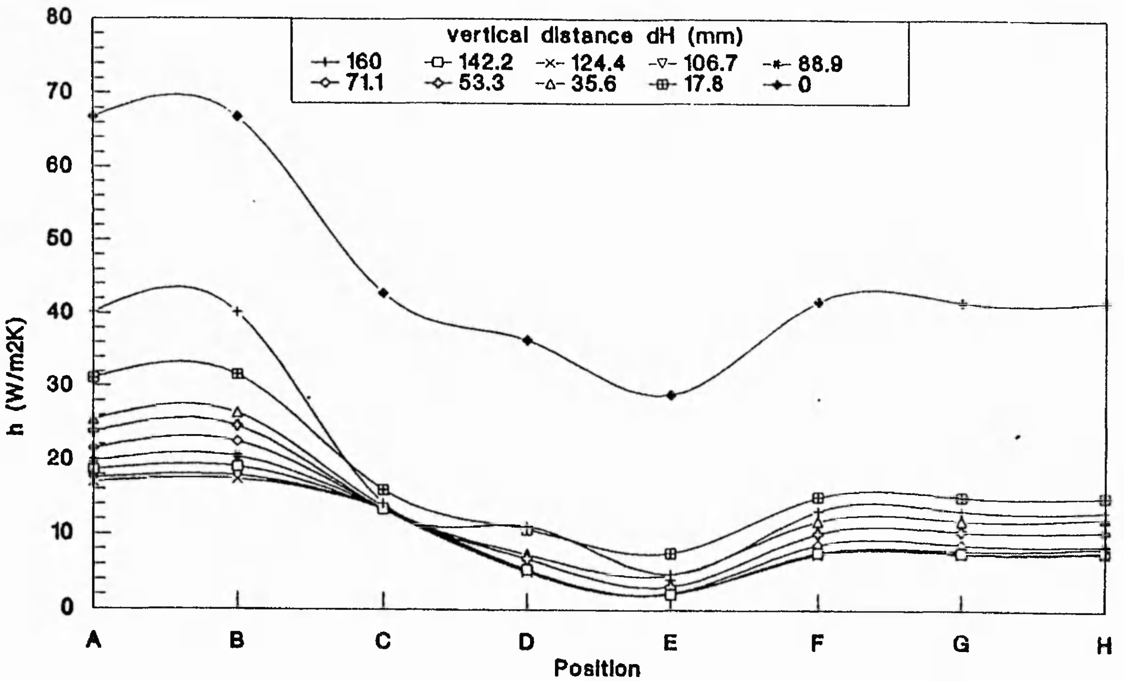

FIGURE 5-42 Mid section horizontal heat transfer coefficient map for S=11mm

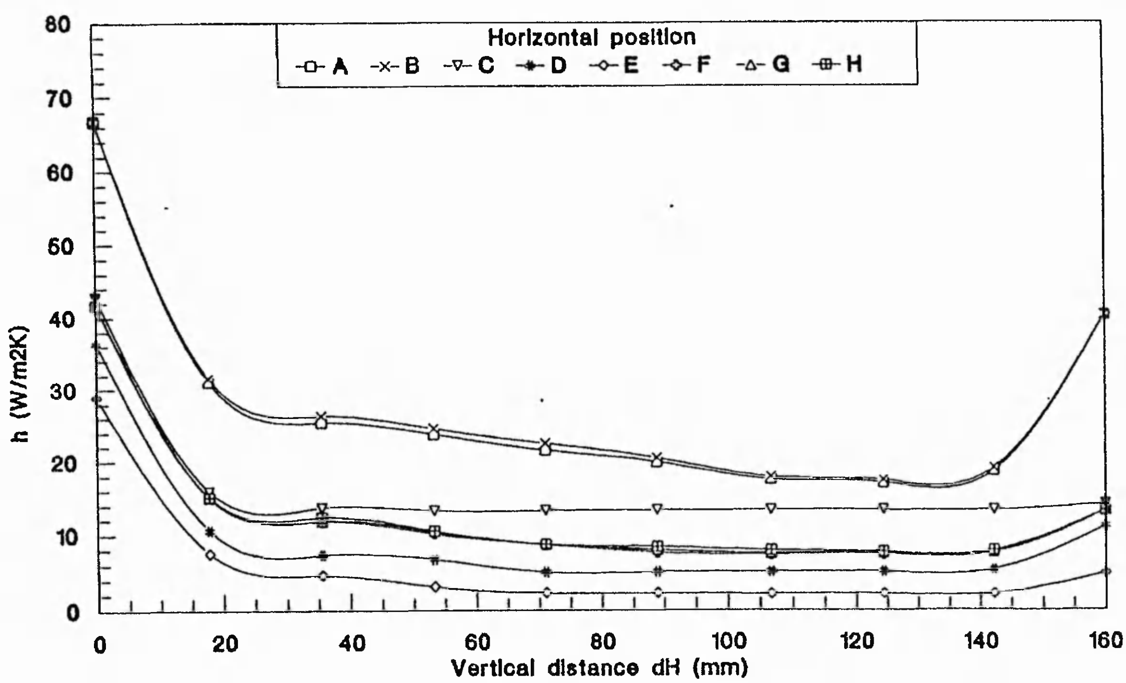

FIGURE 5-43 Mid section vertical heat transfer coefficient map for S=11mm

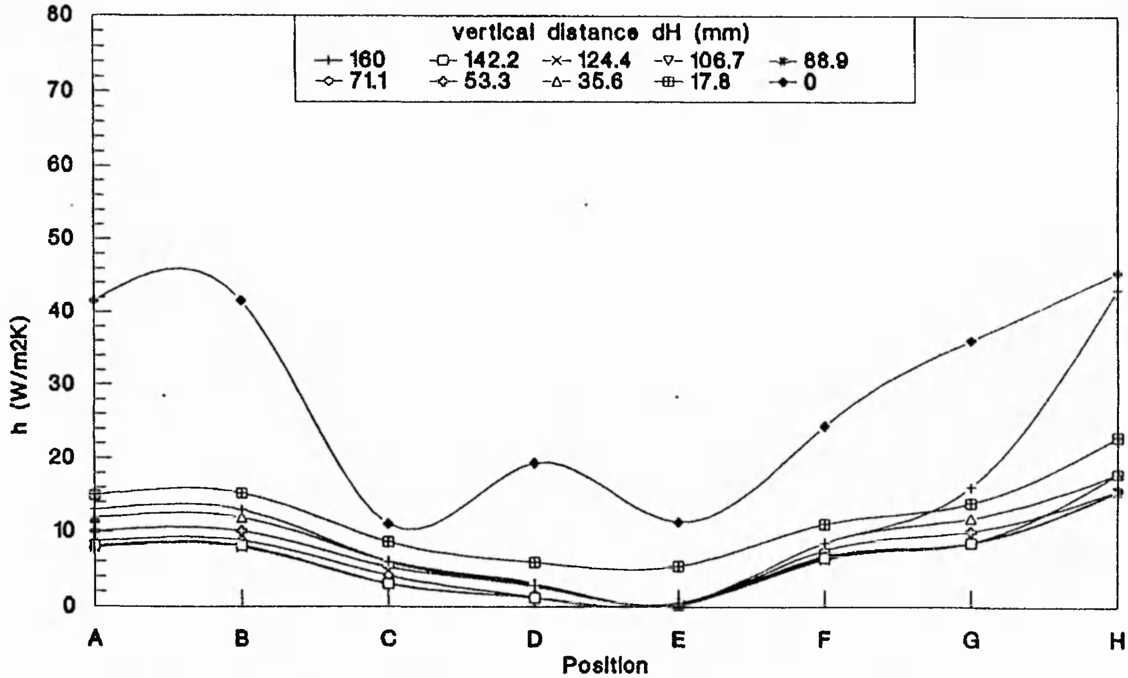

FIGURE 5-44 End section horizontal heat transfer coefficient map for S=11mm

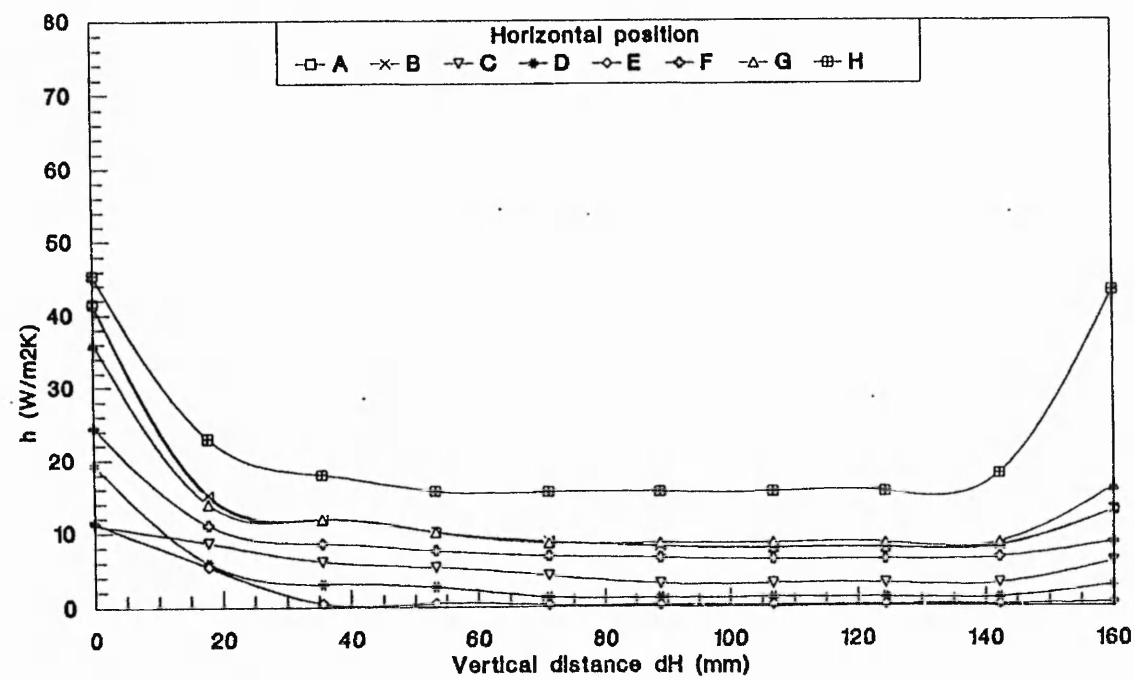

FIGURE 5-45 End section vertical heat transfer coefficient map for S=11mm

The total heat transfer through the heat exchanger is,

$$\mathbf{Q_{TOT} = 855 \pm 3 \quad W} \tag{5.3.28}$$

The heat exchange area and volume are,

$$\mathbf{A = 0.136 \quad m^2} \tag{5.3.29}$$

$$\mathbf{V = 4.76 \times 10^{-4} \quad m^3} \tag{5.3.30}$$

5.3.11 Summary

The total amount of heat transferred, from the heat exchange sections tested, increases as the fin separation decreases. This is shown in Figure (5-46). The increase in heat transfer is due to an increase in surface area, following the form of the general equation for convection, *(3.2.1)*. As there is an increase in surface area, due to the addition of fins, there is also an increase in material volume. It is the material volume to heat transfer ratio that is of interest, and plotting the increase in heat transferred against increase in material volume (above that of the vertical flat plate), a curve is given, Figure (5-47), that shows a maxima relating to a spatial separation of 14 mm.

The Brazilia Slimline 5 has a total heat output of 1.5 kW, and in comparison the representing model, with the fins at 20 mm separation, has a heat output of 0.687 Kw. The estimated value is approximately 50% lower than the actual value, however this is in the correct order of magnitude as the 1.5 kW output takes into consideration losses from the un-finned part of the heat exchanger and losses through the back wall of the appliance.

Taking the maximised separation of 14 mm, based upon volumetric considerations, an increase in heat transfer, for the appliance, is estimated at 9% for a 5% volumetric rise. If the 11 mm separation is taken, then a rise of 11% in heat transfer would be given, although this is in respect to a volumetric increase of 10%. This indicates a law of diminishing returns.

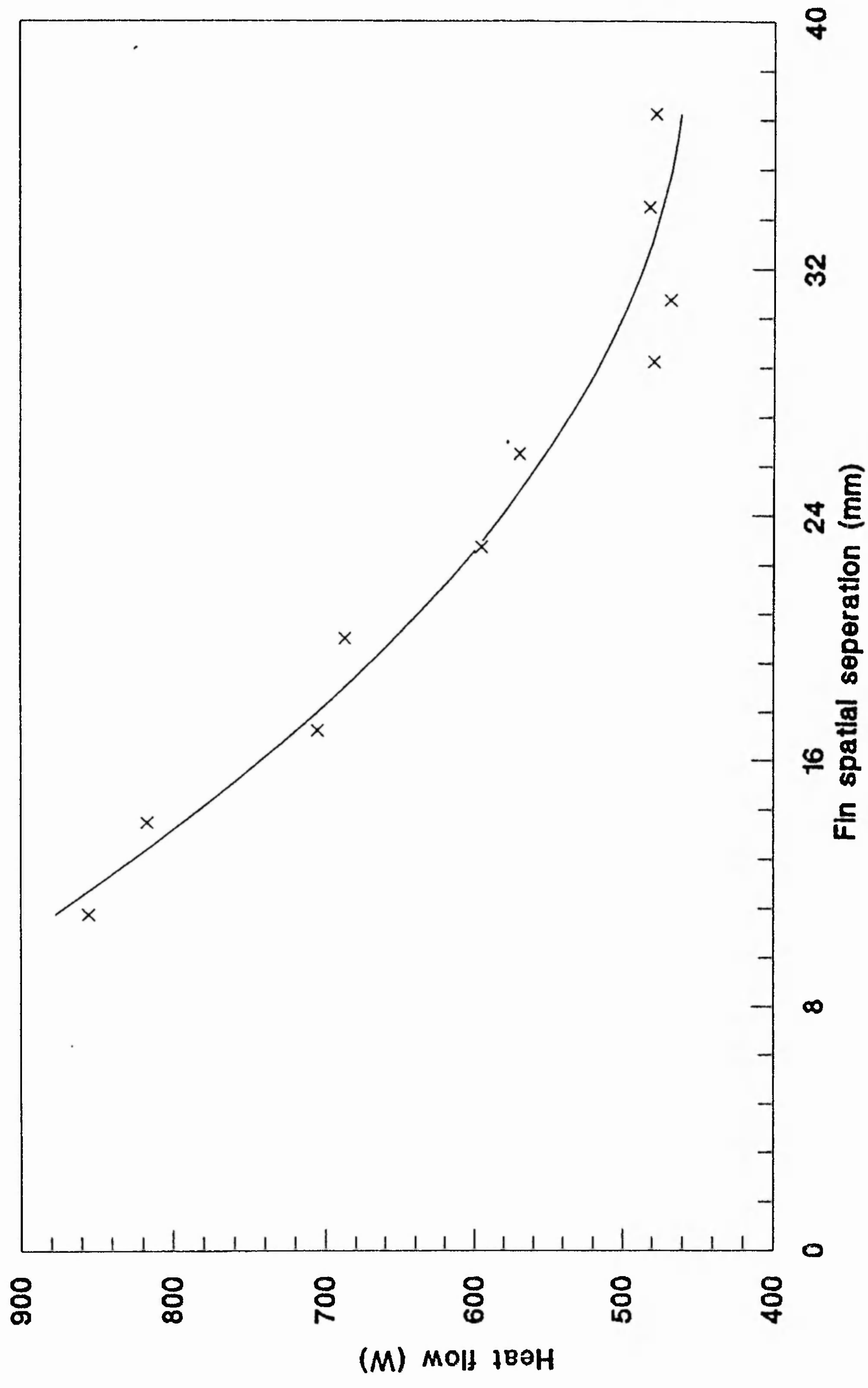

FIGURE 5-46 Heat flow for varying fin spacing

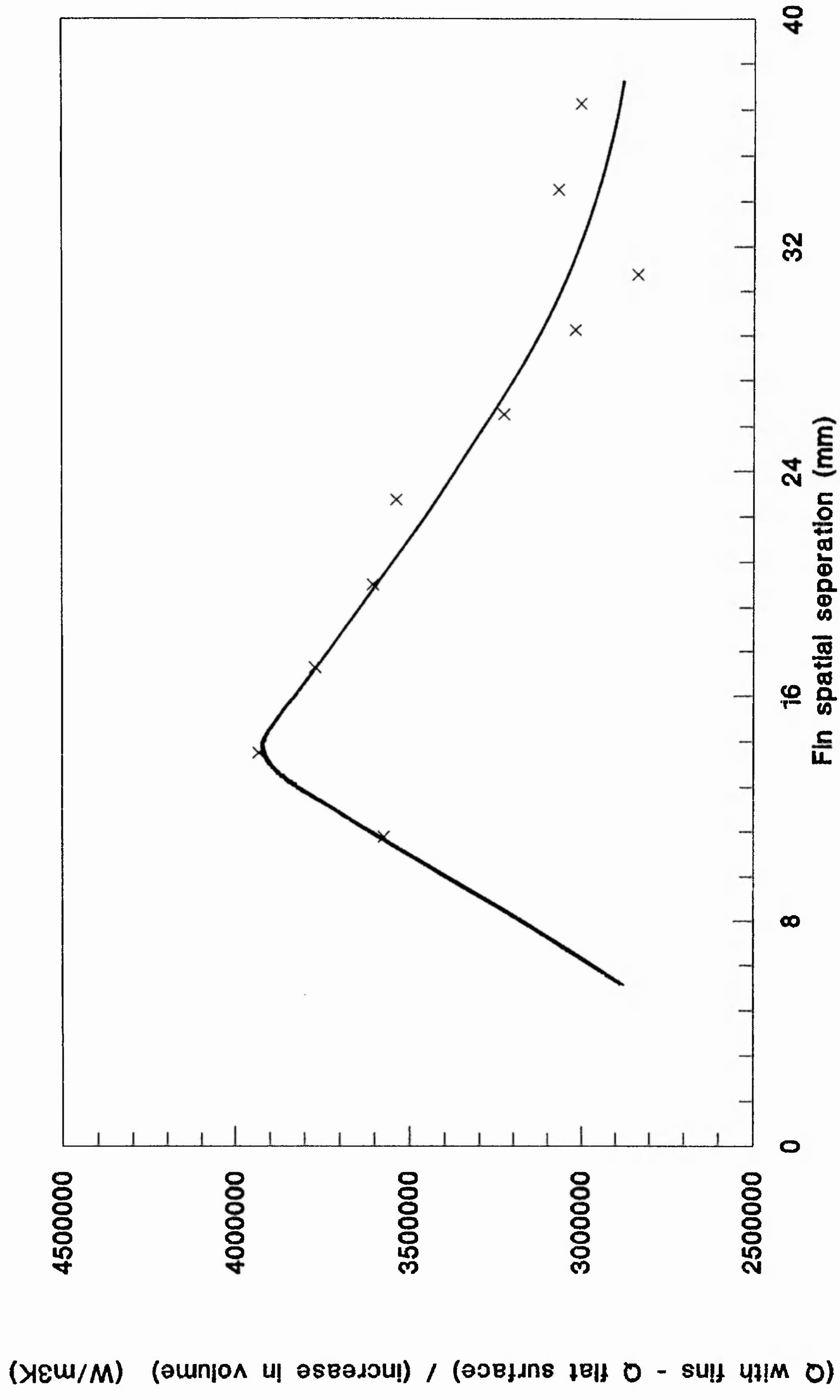

FIGURE 5-47 Increase in heat per increase in volume

5.4 Finned section of varying length

The investigation into varying the fin length is based upon the maximised spatial separation of 14 mm. From the previous investigation it can also be shown that the end fins have only a marginal difference, in heat transfer, to the mid fins, hence only the effects upon a mid fin need to be considered. The length of the fins are altered between 15 mm and 30 mm in 5 mm steps. The test conditions and timing data are given in tabular form, and both types of graphical representation are used to display the local heat transfer coefficients.

5.4.1 15 mm long fin

Test conditions

VARIABLE	CONDITION
T_I	59.3
T_b	24.2

TABLE 5-S1 INITIAL CONDITIONS FOR L=15 mm

Timing data (s)

dH(mm)	A	B	C	D	E	F	G	H
160	167	167	400	419	615	1317	1317	1317
142.2	398	397	410	487	675	1665	1665	1665
124.4	408	406	410	471	625	1702	1680	1680
106.7	409	407	410	471	585	1705	1700	1688
88.9	357	356	410	471	585	1665	1665	1640
71.1	326	325	410	471	585	1600	1600	1578
53.3	279	278	393	471	585	1414	1412	1400
35.6	243	241	375	464	585	1297	1277	1277
17.8	180	180	263	419	559	1042	1042	1042
0	71	71	121	160	180	501	501	501

TABLE 5-T1 TIMING DATA FOR L=15 mm

$$Q_{TOT} = 562 \pm 1 \quad W \tag{5.4.1}$$

$$A = 0.0848^2 \ m^2 \tag{5.4.2}$$

$$V = 3.992 \times 10^{-4} \ m^3 \tag{5.4.3}$$

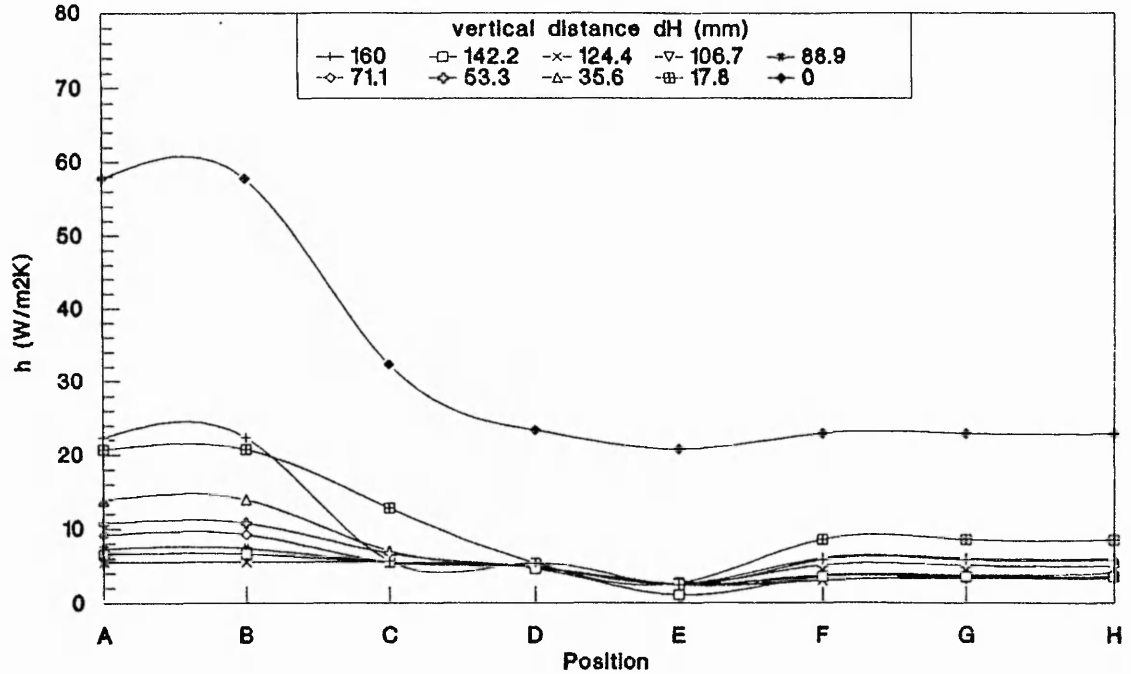

FIGURE 5-48 Horizontal heat transfer coefficient map for L=15mm

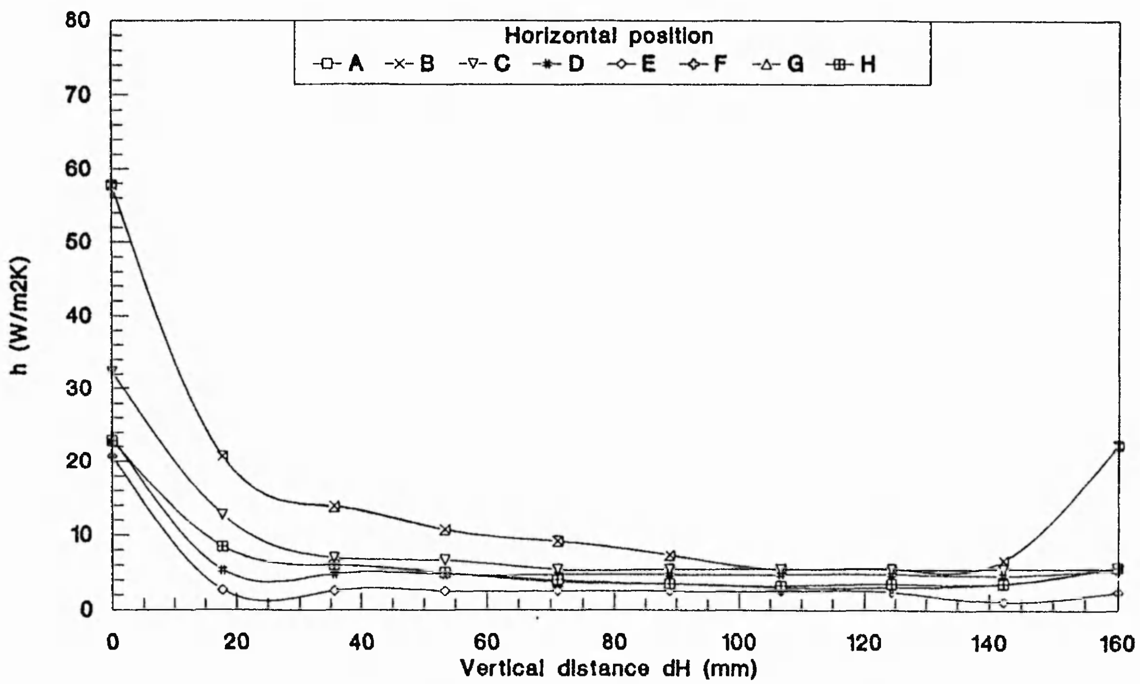

FIGURE 5-49 Vertical heat transfer coefficient map for L=15mm

5.4.2 20 mm long fin

Test conditions

VARIABLE	CONDITION
T_I	63.2
T_b	22.8

TABLE 5-U1 INITIAL CONDITIONS FOR L=20 mm

Timing data (s)

dH(mm)	A	B	C	D	E	F	G	H
160	158	158	371	453	744	1378	1378	1378
142.2	298	296	432	755	863	1667	1665	1665
124.4	313	313	441	501	863	1525	1525	1525
106.7	313	313	441	501	862	1688	1680	1568
88.9	313	313	441	501	862	1665	1665	1665
71.1	283	280	441	501	755	1550	1550	1550
53.3	263	260	353	434	755	1409	1409	1409
35.6	258	256	352	441	684	1224	1224	1224
17.8	198	195	345	400	549	1029	1029	1029
0	69	69	134	170	198	283	283	283

TABLE 5-V1 TIMING DATA FOR L=20 mm

$$Q_{TOT} = 676 \pm 4 \quad W \tag{5.4.4}$$

$$A = 0.1024 \ m^2 \tag{5.4.5}$$

$$V = 4.256 \times 10^{-4} \ m^3 \tag{5.4.6}$$

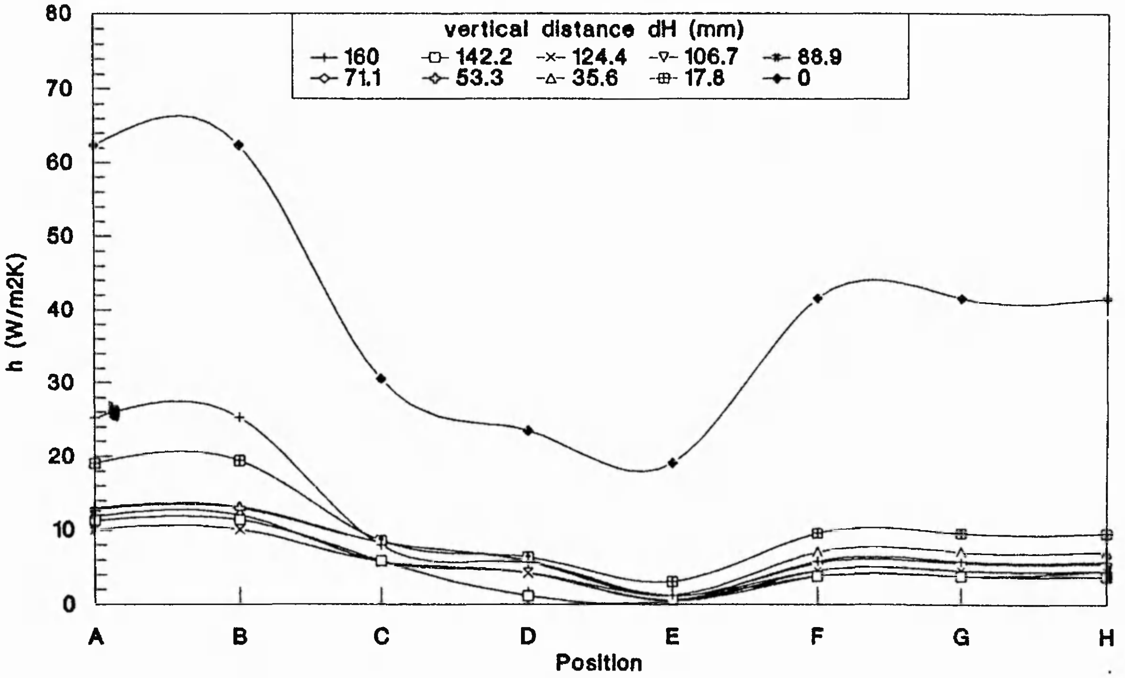

FIGURE 5-50 Horizontal heat transfer coefficient map for L=20mm

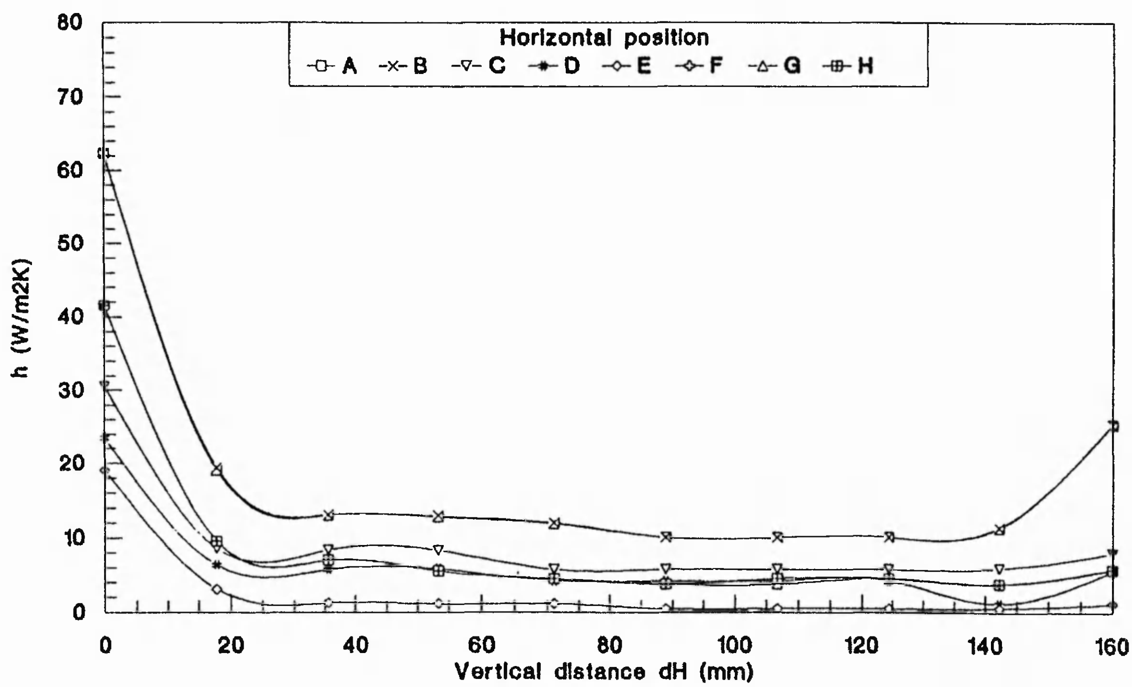

FIGURE 5-51 Vertical heat transfer coefficient map for L=20mm

5.4.3 25 mm long fin

Test conditions

VARIABLE	CONDITION
T_I	53
T_b	22

TABLE 5-W1 INITIAL CONDITIONS FOR L=25 mm

Timing data (s)

dH(mm)	A	B	C	D	E	F	G	H
160	70	68	230	286	450	1005	1005	1005
142.2	135	133	281	407	480	1149	1145	1141
124.4	143	140	281	407	480	1150	1130	1123
106.7	135	133	281	407	480	1130	1121	1108
88.9	131	130	276	392	480	1100	1090	1080
71.1	123	122	270	380	480	1080	1070	1059
53.3	113	112	237	348	435	1040	1015	1005
35.6	92	91	219	323	447	930	925	920
17.8	79	79	190	281	407	739	739	739
0	39	39	70	100	133	304	304	304

TABLE 5-X1 TIMING DATA FOR L=25 mm

$$Q_{TOT} = 817 \pm 5 \quad W \tag{5.4.7}$$

$$A = 0.12 \ m^2 \tag{5.4.8}$$

$$V = 4.52 \times 10^{-4} \ m^3 \tag{5.4.9}$$

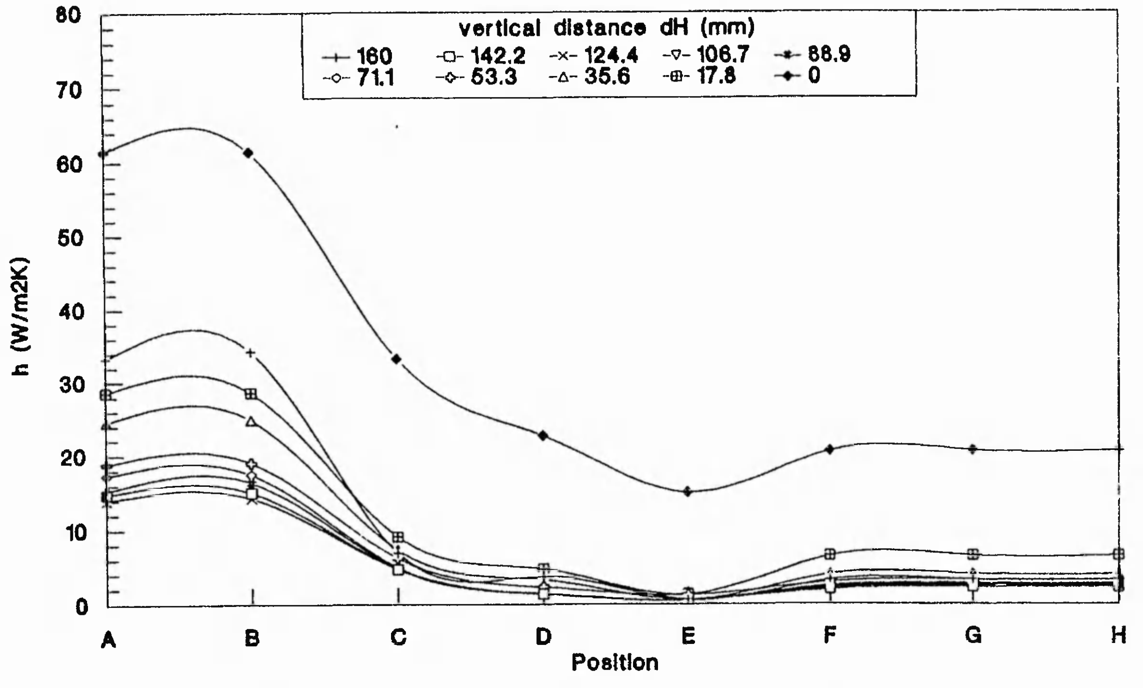

FIGURE 5-52 Horizontal heat transfer coefficient map for L=25mm

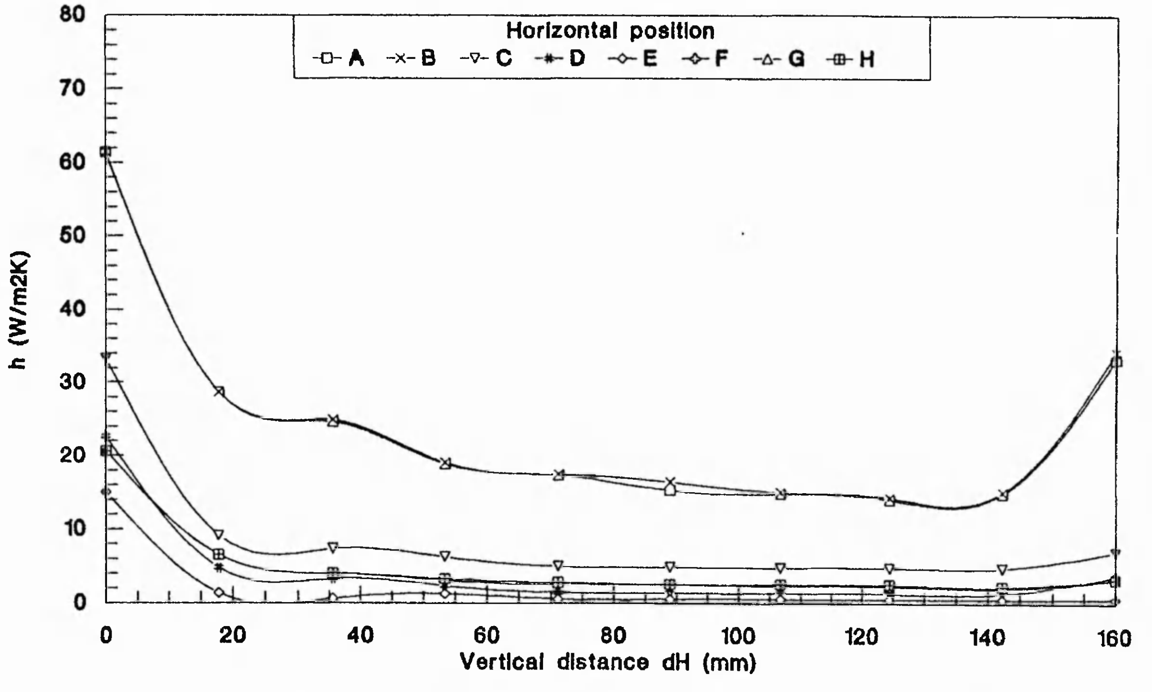

FIGURE 5-53 Vertical heat transfer coefficient map for L=25mm

5.4.4 30 mm long fin

Test conditions

VARIABLE	CONDITION
T_I	62.8
T_b	22.3

TABLE 5-S1 INITIAL CONDITIONS FOR L=30 mm

Timing data (s)

dH(mm)	A	B	C	D	E	F	G	H
160	167	167	369	494	699	1440	1440	1440
142.2	229	229	429	627	850	1695	1695	1680
124.4	249	249	404	570	850	1740	1735	1730
106.7	249	249	394	570	850	1740	1735	1730
88.9	249	249	389	562	840	1651	1651	1620
71.1	237	237	380	559	795	1546	1546	1532
53.3	221	220	358	541	779	1395	1395	1380
35.6	214	213	351	494	686	1236	1236	1236
17.8	184	183	306	394	541	953	953	943
0	92	92	149	191	199	387	387	387

TABLE 5-T1 TIMING DATA FOR L=30 mm

$$Q_{TOT} = 797 \pm 5 \quad W \qquad (5.4.10)$$

$$A = 0.1376 \ m^2 \qquad (5.4.11)$$

$$V = 4.784 \times 10^{-4} \ m^3 \qquad (5.4.12)$$

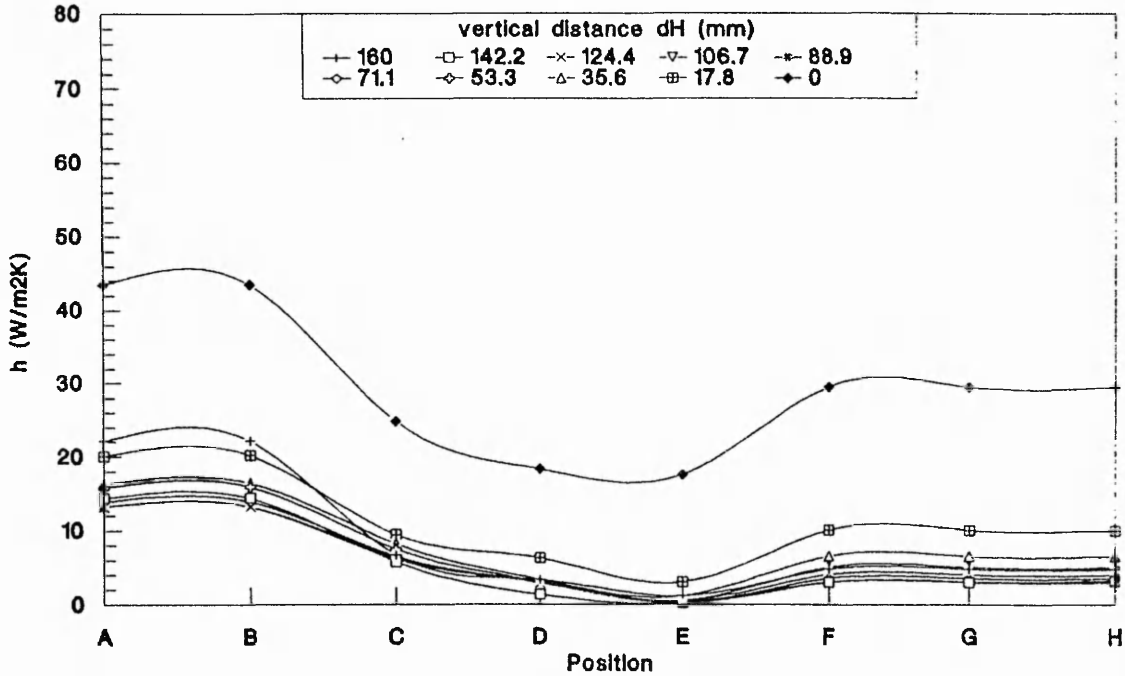

FIGURE 5-54 Horizontal heat transfer coefficient map for L=30mm

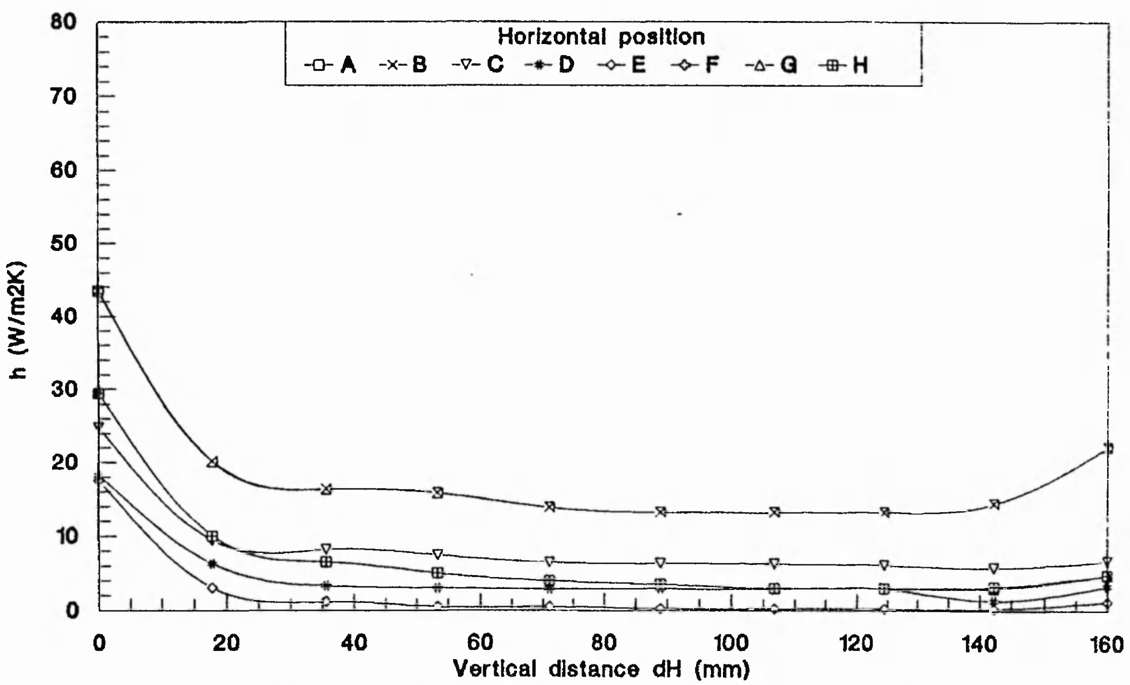

FIGURE 5-55 Vertical heat transfer coefficient map for L=30mm

5.4.5 Summary

Figure (5-56) shows the heat transfer, for the model heat exchangers, at different fin lengths. Comparing the heat transfer value from the model representing the Brazilia Slimline 5, to the given curve, the comparative fin length is 20 mm. Comparison of the volumes, Table 5-U1, shows there is virtually no volumetric saving by the addition of the two extra fins at a reduced length. Advantages however can be assessed as to the strength of the fins , and spatial saving in the total heat exchanger width. The strength of the fins, with regard to shear stress, is of importance when the casting is placed onto the shaking machine, to remove the casting sand. Undergoing this process tends to break the thinner and longer, weaker fins. Figure (5-52) also shows that as the length increases the gain in heat transfer decreases, again indicating a law of diminishing returns.

Fin Spacing (mm)	Fin length (mm)	No. of fins	**Volume (m^3) × 10^{-4}**
20	25	9	**4.28**
14	20	11	**4.256**

TABLE 5-U1 Volumetric comparison

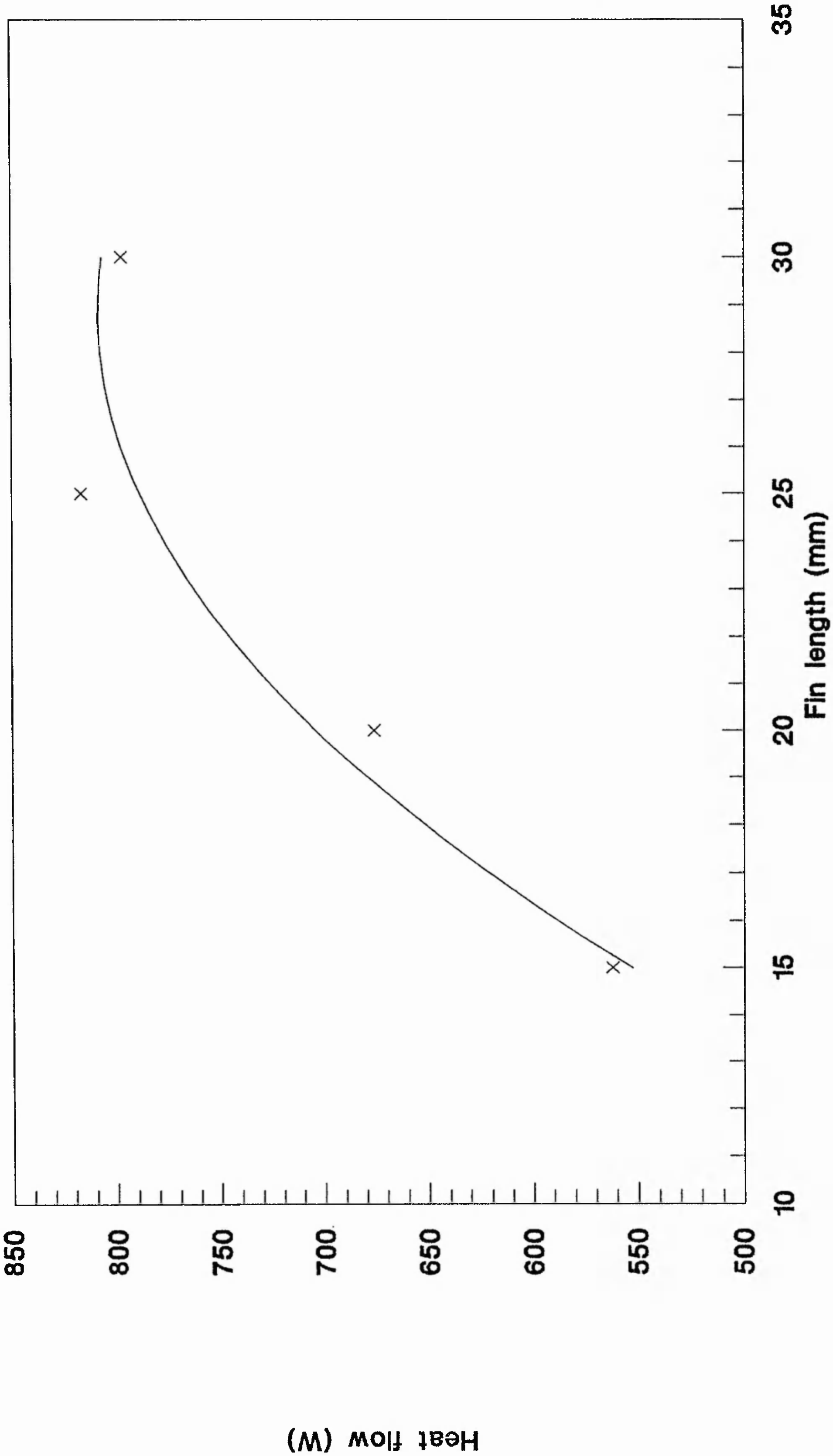

FIGURE 5-56 Heat flow for varying fin length

5.5 Conclusion of results

The optimal design for the Brazilia Slimline 5 heat exchanger has not been attained, based upon maximum heat transfer available from the base area, Figure (5-46), and physical size considerations, Figure (5-56). In spite of this, the existing design, based upon a 1.5 kW output, has good material usage and no volumetric saving is proposed. If higher heat transfer is required, then a cost increase will occur, due to additional material volume. Figure (5-57) indicates the casting manufacturing and retail costs, from Baxi Partnership Ltd in November 1991, associated with material volume changes.

Considering heat transfer with regard to volumetric constraints, an optimal spatial separation of 14 mm is proposed. This is shown in Figure (5-47). Using this separation, Figure (5-56) shows the effect of varying the fin length. Plotting the increase in heat transfer (above that of the vertical flat plate *(5.2.12)*) against the material volume of the fins, shows a similar trend to both the variable separation and the variable fin length. This plot, Figure (5-58), shows a correlation relating to a cast iron heat exchanger with vertical fins, of 3 mm sectional width, on a vertical base of dimensions 200 mm wide and 160 mm high. For the fin sizes investigated the correlation equation is represented by,

$$\mathbf{Q_{inc} = -25367\,(V_{f,TOT}\times 10^3)^2 + 9.313\,V_{f,TOT}\times 10^6 - 300.293} \qquad (5.5.1)$$

Given that the volume of the fins ($V_{f,TOT}$) relates to a fin thickness of 3 mm,

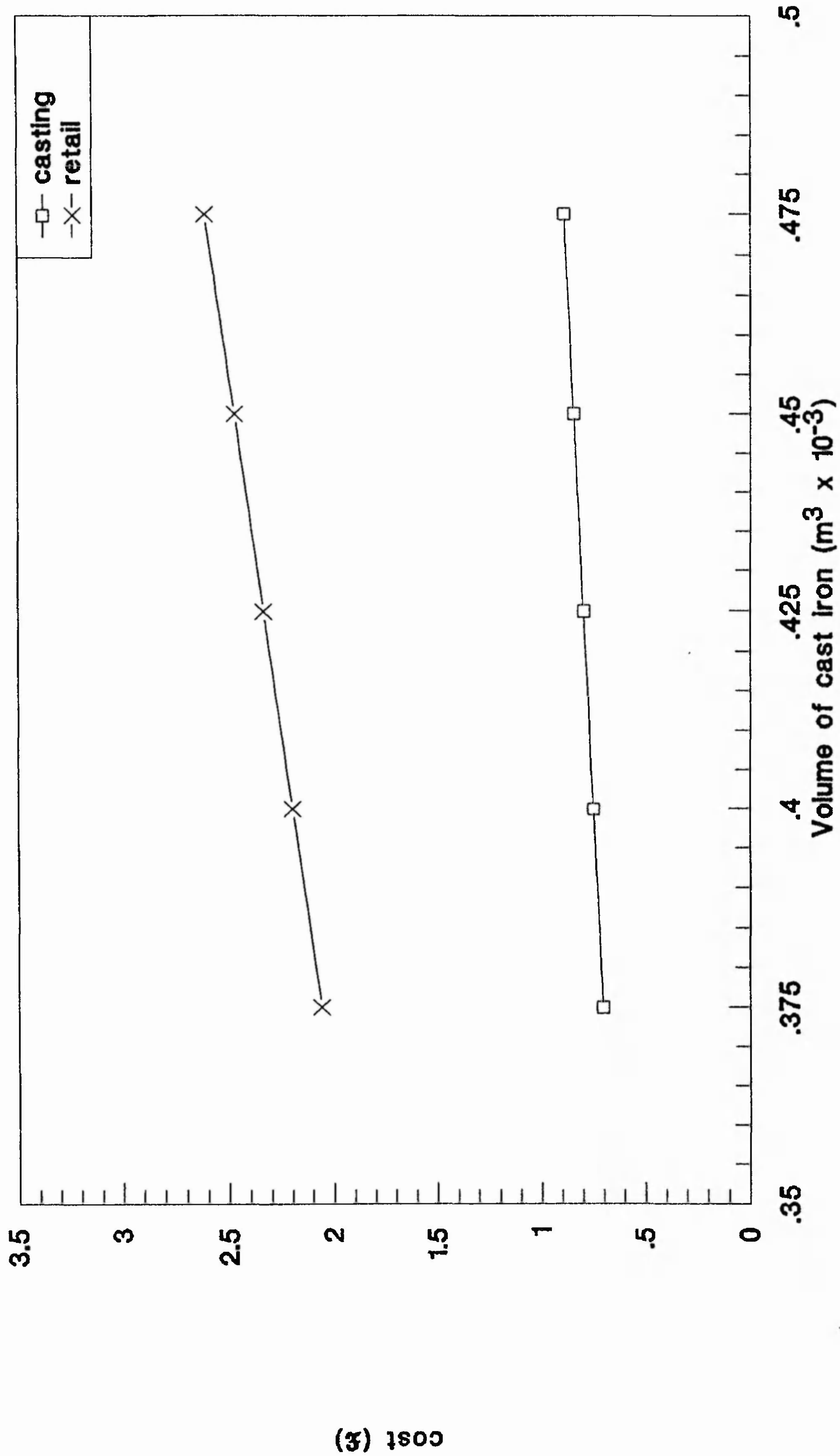

FIGURE 5-57 Manufacturing and retail cost for a cast iron heat exchanger

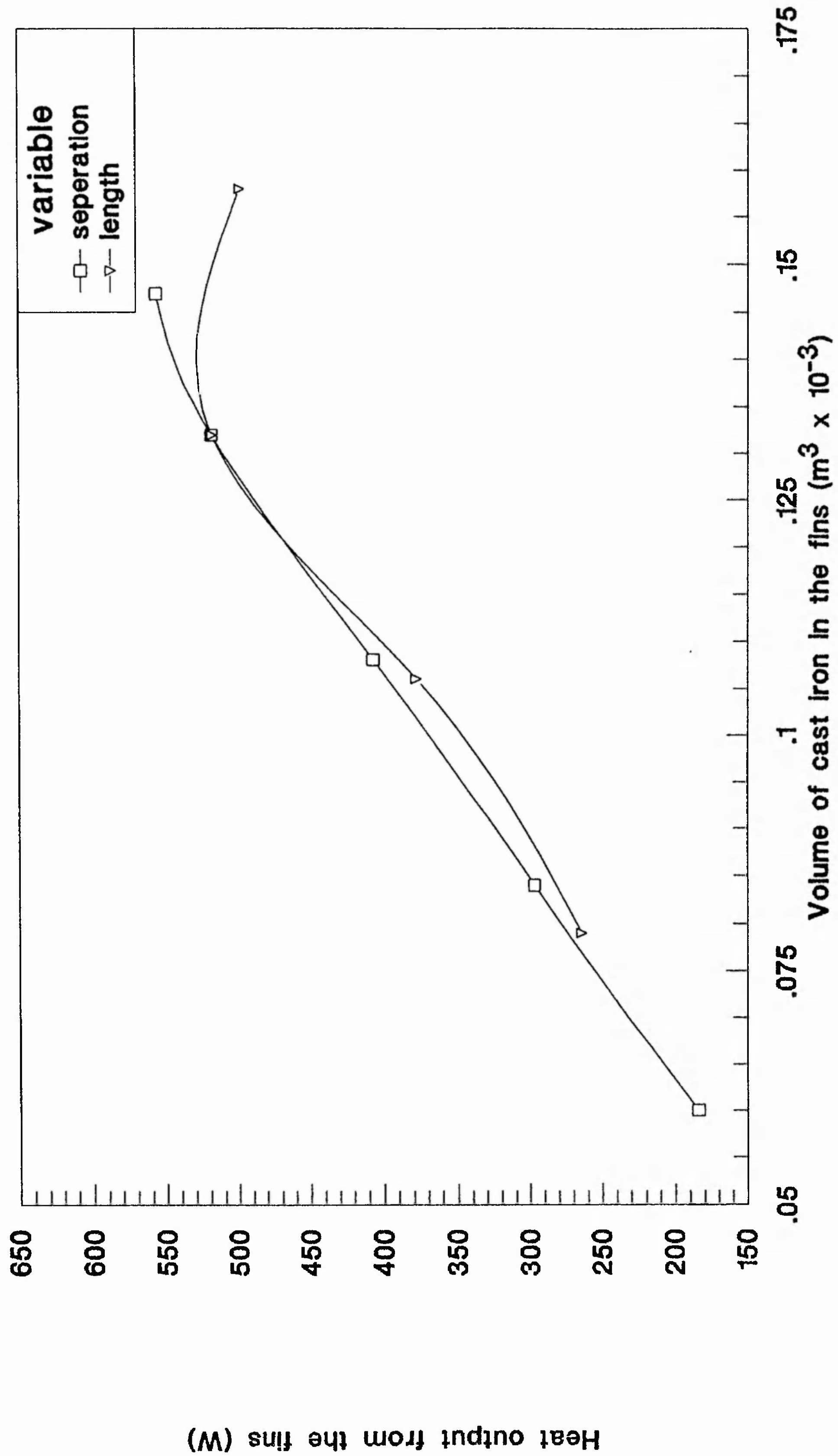

FIGURE 5-58 Comparison of varying fin spacial separation and length

then the equation can be written in terms of fin height (H), fin length (L) and number of fins (N), this being

$$\mathbf{V_{f,TOT} = 0.003\ H\ L\ N} \tag{5.5.2}$$

Equation *(5.5.1)* hence becomes,

$$\mathbf{Q_{inc} = -228303\ H^2\ L^2\ N^2 + 27939\ H\ L\ N - 300.293} \tag{5.5.3}$$

The maximum number of fins (N_{max}), that can be placed on the base area, can be calculated from the relationship of the base width (Bw) and fin spatial separation (S). This is given in equation *(5.5.4)*, noting that the resultant maximum number of fins is the nearest integer value.

$$\mathbf{N_{max} = \frac{Bw}{0.003 + S}} \tag{5.5.4}$$

The correlations given require the total fin volume to be in the limits of,

$$\mathbf{60 \times 10^{-6} < V_{f,TOT} < 165 \times 10^{-6}} \tag{5.5.5}$$

CHAPTER 6

CONCLUSIONS AND RECOMMENDATIONS

6.1 Conclusions

This investigation is concerned with the design of free convection extended surface heat transfer from finned vertical plates, with particular reference to volumetric constraints. The investigation also considered a method which gives the design engineer a relatively low cost development aid, for extended surface heat transfer. This method allows the study, and mapping, of the local convective heat transfer coefficients.

Chapter 3 gives a discussion on available methods for experimental heat transfer investigations, and outlines the liquid crystal method which is considered the most suitable for this application. A review of the liquid crystal technique is given, along with its theory, and a description of the methodology used and the experimental procedure.

The numerical investigation of Chapter 4, outlines the mathematical method for the transient and steady state techniques used, and the steps developed for the implementation of the computer programs. Flow diagrams for the computer programs are given, with reference to the actual program listings. The validity of the developed programs is outlined in Chapter 5, this showing good agreement with published correlation for vertical plates in free convection.

Chapter 5 outlines the results of the investigation of a vertical flat plate, offering a non-dimensional correlation for the local Nusselt number, equation *(5.2.11)* and Figure (5-5). In Figure (5-3) the effects, upon the vertical plate, by a finite thickness can be seen, leading to an increase in the measured local convective heat transfer coefficient. Also given is the recorded timing data and computed contour plots, of the local convective heat transfer coefficient, for the finned heat transfer surfaces tested. These are outlined in Chapters 5.3 and 5.4. The results are referenced to the model representing the Baxi Brazilia Slimline 5, which is a production heat exchanger for use with domestic wall convector heaters.

The Baxi Brazilia Slimline 5, discussed in Chapter 1, has design constraints imposed, namely maximum heat output and fin length. The conclusion drawn, from this investigation, indicates that the original design has good material usage, and no volumetric enhancement, using vertical fins, is proposed. However, by consideration of Figure (5-47), the optimal spatial separation, based upon volumetric consideration, is 14 mm, and by considering Figure (5-56), either the same heat output can be achieved at a smaller height (20 mm opposed to 25 mm), or achieved at a lower heat input. The former change in design allows space between the fin and outer case heat shield, which will result in reduced heat shield and outer case temperatures. The latter design change gives improved efficiency, hence running costs, and also reduces the possibility of poor combustion when run in an overload condition. Another effect of increasing the efficiency, of the appliance, is the beneficial effect to environmental issues. An increase in efficiency allows the same heat output to be obtained at a lower heat input, hence reducing the amount of fuel burned. This reduces the total amount of emissions, with regard to Carbon monoxide (CO), Carbon dioxide (CO_2) and Nitrogen oxides (NO_x), which may be causing adverse effects on the ozone layer (Green House Effect). With an increase in efficiency it may be possible to reduce the combustion chamber temperature, hence flame temperature. By reducing these temperatures a greater reduction in the NO_x levels will be achieved, above that due to the reduction in gas consumption. This method of NO_x reduction takes place in two stages, known as the Zeldovich mechanism and the fast prompt mechanism. Both of these mechanisms are explained by Jones [53]. This improvement to the design is however at a unit cost increase, due to the additional fin volume.

Comparison of the results, obtained for the finned heat exchangers, with the papers reviewed in Chapter 2, shows that the optimal separation is 3 mm higher than the recommended value of 11 mm, given by Leung and Probert [5]. However, the investigation by Leung and Probert considered the maximum heat transfer from a surface, and not volumetric optimisation. As shown by Figure (5-46) and (5-47), the optimal separation based on maximum heat transfer does not yield the same value as that based on volumetric optimisation, hence a direct comparison is not possible.

The method used in this investigation is not confined to the heat exchanger discussed, but is a generalised heat transfer measurement technique. The programs developed use three modes of heat transfer, namely conduction, convection and radiation, and can be used to develop any vertical or horizontal straight finned section. The 1-D transient technique developed is for use directly with the liquid crystal technique, however it can be used with any other method where the initial temperature, final temperature, ambient temperature and time differential is known. The equation used to give the initial estimation for the local heat transfer coefficient, equation *(4.2.33)*, returns a value that is close to the finalised computed value, and is usable as a first approximation correlation without the need for the time consuming iteration technique. This investigation also presents a relationship between extended surface material volume and increase in heat transfer, above that of a vertical flat surface in free convection. Given that the extended surface is a vertical fin of 3 mm width, the relationship is given by the equation,

$$\mathbf{Q_{inc} = -25367\,(V_{f,TOT} \times 10^{3})^{2} + 9.313\,V_{f,TOT} \times 10^{6} - 300.293}$$

This equation is applicable within the limits of $60 \times 10^{-6} < V_{f,TOT} < 165 \times 10^{-6}$. The equation is expanded to provide a correlation between the fin length (L) and the increase in heat transfer, this being given by,

$$\mathbf{Q_{inc} = -228303\,H^{2}\,L^{2}\,N^{2} + 27939\,H\,L\,N - 300.293}$$

By taking the maximum number of fins (N_{max}) to be an integer value, the spatial separation of the fins can be included in the above correlation, by replacing the number of fins (N) by,

$$N_{max} = \frac{Bw}{0.003 + S}$$

The investigation renders a design approach, for vertical heat exchangers in free convection, that is simplistic in its method, low in cost, of both material and design time, and which imparts localised information in the form of heat transfer coefficients. The method employed is the use of liquid crystals sprayed onto an acrylic model of the heat transfer surface. This model is heated to a pre-determined temperature, then cooled under the influence of free convection, whilst recording the isothermal data. The approach is to determine the heat transfer from differing geometric configurations, comparing them with each other to ascertain the most appropriate design to fit the given constraints.

For this investigation a thermal wind tunnel was used for the heating of the model. Such elaborate apparatus, with free convection measurements, is not essential (unlike the case with forced convection where the Reynolds number needs to be known), and a heated oven will suffice. The main constraint for this type of method is a known uniform model temperature. The time taken, for a model of the size investigated, to cool to a point where all the surface temperature is lower than the crystal melt temperature, is in the order of 20 minutes. Due to this long time period a cooling of the centre temperature occurs, and although compensated for, does introduce experimental uncertainties in the computed value. The extent of the uncertainty will vary with cooling times, heat exchanger size and type of convection process, due to the differing amounts of cooling of the centre temperature. Further uncertainties relating to the calibration of the liquid crystals, the non-uniformity of the liquid crystal layer, and thermal conductivity of the substrate must be acknowledged. It is also important to have a suitable temperature differential between the liquid crystal melt temperature and the initial temperature, with temperature differentials in the order of 20 °C to 30 °C being successfully used in this investigation. Other factors causing uncertainty can be associated to the recording of the isotherms. Due to the response of the camera, loss of quality on play back and human colour sensation, the exact location of the isotherm may be difficult to derive. The intensity of the displayed isotherm may also alter due to the unevenness of the incident light, onto the model. This investigation used a halogen light for illumination, and was of extreme importance to bounce the light onto the model, eliminating the effects of thermal radiation, from the light, heating the liquid crystals, hence altering the cooling times. Although the accumulation effects of these uncertainties may seem large, it is reported, by Ashforth-Frost et al [54], that the total uncertainty in the computed heat transfer coefficient can be kept in the region of 10%. For this investigation the validity of the method is proven by the comparison of the experimental Nusselt number to that calculated from published correlations.

The uncertainty introduced by the manual recording of the timing data, due to human colour sensation, and also the speed of recording the timing data, can be improved by the use of video imaging techniques, onto a micro computer. Video imaging techniques have been employed, for the capture of isotherms onto a micro computer, by Akino et al [55]. By combining this method with the 1-D transient analysis technique, a powerful engineering tool can be produced. A system of this type requires video frame store techniques. This can be achieved by video imaging boards, available from Data Translation [56], or from personalised systems using transputers, available from SGS-Thomson micro electronic group [57]. The former video data capture system is limited to capturing complete frames, which are then stored, and analysed later. The latter video data capture technique ensures fast data capture, with computational analysis to store only the timing data and grid reference points of interest. Transputers work in parallel, and are programmed in a special assembly language called OCCAM, Pountain and May [58]. Using this feature, it is feasible to perform the transient analysis parallel to the data capture. This will enhance the speed of the data analysis, and obviate the human error. Video imaging, using transputers, is extensively published, for example Reijns et al [59] and Yagi et al [60], however the cost considerations are high and beyond the scope of this investigation.

6.2 Recommendations

The following recommendations are aimed at providing possible directions for future work, based upon the presented investigation.

1. The model, when removed from the thermal tunnel, has a decay in its internal temperature. The finite difference program compensates for this decay,

however this is still a source of uncertainty. A technique that would allow free convection cooling, under transient conditions, whilst keeping the rear base temperature constant could be investigated.

2. Uncertainty associated with human colour sensation can be removed by video imaging techniques. Investigations have been undertaken in this field, however these techniques use frame stores, of the video image, to which post processing is undertaken later. A suggested direction would be the use of transputer technology to undertake near real time data acquisition and processing. The methodology could consist of capturing the model image, into the computer, and fitting a computer wire mesh around it. The associated dimensions can be added, with nodal points where the localised heat transfer coefficients are required, for computational analysis. Using this method the transient analysis, video data capture and computation of the local heat transfer coefficients can be undertaken in parallel. The use of this type of approach will greatly improve the response time, from the test to the final solution, and also the accuracy of the resultant value.

3. The equation presented for the increase in heat transfer for increase in material volume, due to the addition of fins, *(5.5.1)*, has imposed volumetric limitations. Further investigation could be undertaken to increase the range of these limits.

4. From the study of the heat transfer coefficient maps, a trend appears giving a minima, for the local heat transfer coefficient, of approximately 30 mm from both the top and bottom edge of the fins. Fin enhancement using interruptions, in the form of a slot across the fin, can be investigated, placing the interruption at the depicted minima.

5. It is suggested that the increase in efficiency of the heat exchanger can give rise to reduced combustion and flame temperatures. This has a beneficial effect for environmental issues, due to the reduction in emissions of Nitrogen oxides. Investigations into the effects of heat exchanger efficiency, especially on the forced convection side of the heat exchanger, can be undertaken, along with the effects of flow distribution, to determine the effects of both combustion and heat transfer upon the emissions of Nitrogen oxides.

REFERENCES

1 **Naik S, Probert S.D, Shilston M.J** Maximising the performances of flat-plate heat exchangers experiencing free or forced convection: Applied Energy, 22, 1986, 225-239

2 **Jambunathan K, Probert S.D, Shilston M.J** Enhancing heat transfer rates from closed-sided, open-topped heat exchangers, each having vertical rectangular fins extending upwards from a horizontal base: Applied Energy, 17, 1984, 47-75

3 **Leung C.W, Probert S.D, Shilston M.J** Heat exchanger: optimal separation for vertical rectangular fins protruding from a vertical rectangular base: Applied Energy, 19, 1985, 77-85

4 **Leung C.W, Probert S.D, Shilston M.J** Heat transfer performances of vertical rectangular fins protruding from rectangular bases: effect of fin length: Applied Energy, 22, 1986, 313-318

5 **Leung C.W, Probert S.D** Natural-convective heat exchanger with vertical rectangular fins and base: IMechE, 1987, 103-187

6 **Leung C.W, Probert S.D** Thermal effectiveness of short-protrusion rectangular heat exchanger fins: Applied Energy, 34, 1989, 1-8

7 **Van De Pol D.W, Tierney J.K** Free convection heat transfer from vertical fin arrays: IEEE Transactions on Parts, Hybrids and Packing, Vol PHP-10, No.4, 1974

8 **Sukhatme S.P** heat transfer from rectangular vertical arrays: 1988, 247-60, ISBN 0-89116-578-9

9 **Sukhatme S.P, Saikhedkar N.H** Natural convection heat transfer from rectangular cross sectioned vertical fin arrays: Journal of Thermal Engineering, 1, pt.3, 1980, 125-32

10 **Tanaka S, Kunitomo T** Optimum fin geometries for simultaneous convective and radiative heat transfer: Heat Transfer Japan res, 12, pt.3, 1983, 60-77

11 **Tanaka S, Yoshida T, Kunitomo T** Optimization and heat transfer fora vertical fin array on isothermal and non-isothermal plane surfaces with combined natural convection and radiation: Heat Transfer Japan res, 16, pt.1, 1987, 91-112

12 **Leung C.W, Probert S.D, Rapley C.W** Natural convection and radiation from vertically based arrays of vertical rectangular fins: a numerical model: Applied Energy, 35, 1990, 253-266

13 **Kraus A.D, Snider A.D** Choking and optimization of extended surface arrays: Journal of Heat Transfer Nov.85, 107, 746-749

14 **Kraus A.D** Analysis of extended surfaces: Journal of Heat Transfer Nov.88, 110, 1071-80

15 **Hrymak A.N, McRae G.J, Westerberg A.W** Combined analysis and optimisation of extended heat transfer surfaces: Journal of Heat Transfer Aug.85, 107, 527-32

16 **BS 5258** Specification for safety of domestic gas appliances: part 13. convector heaters, 1985

17 **Roberts C.C Jr.** Analysis of heat pipe performance using infra-red thermography: Proc BIENN infra-red INF EXCH, 1977, 127-135

18 **Kreider K.G, Sheahen, T.P** Use of infra-red thermography for industrial heat balance calculations: Heat and mass transfer in metal syst int cent heat mass trans seminar prep, Dubrovnic, 1979

19 **Jambunathan K, Edwards R.J, Button B.L** Convective heat transfer coefficients the colour change paint technique: Applied Energy, 28, 1987, 137-152

20 **Ouden C, Hoogendoorn C.J** local convective heat transfer coefficients for jets impinging on a plate; experiments using a liquid crystal technique:

MA2.5, 1974, 293-297

21 **Galaud A** Application of holographic interferometry to air jet impingement for mass transfer measurement: BEng Project report, Trent Polytechnic, 1988

22 **Gates J.W.C** Holographic methods of visualization and measurement in engineering: Journal of Photographic Science, 19, 1971

23 **Saluja C.L, Button B.L, Dobbins B.N** Full field in situ measurement of local mass transfer coefficient using ESPI with swollen polymer technique: Int J. Heat and Mass Transfer, 31, No.7, 1988, 1375-84

24 **Pirodda L** Shadow projection moiré techniques for absolute or relative mapping of surface shapes: Optical Engineering, 21, 1882, 640-49

25 **Flanagan M, Wilcock D, Wykes C** Measurement of surface profile changes by the use of moiré fringes with particular application to mass transfer: Optical Components and Systems, 805, 1987

26 **Reid G.T, Rixon R.C, Messer H.I** Absolute and comparative measurements of three dimensional shape by phase measuring moiré topography: Optics and Laser Technology, 1984, 315-319

27 **Simonich J.C, Moffat R.J** New technique for mapping heat transfer coefficient contours: Review of scientific instruments, 53, 5, 1982, 678-683

28 **Law H, Masliyah J.H** Coherent optical measurement techniques in profilometric determination of local mass transfer coefficients: Optics and Lasers in Engineering, 5, 1984, 211-19

29 **Button B.L, Mohamad T.T** Experimental techniques to determine the convective heat transfer coefficients for flat and curved surfaces: High Temperature Technology, 1983, 163-69

30 **Jambunathan K, Moor G, Button B.L** Review of experimental techniques for heat transfer measurements: Nottingham Polytechnic, Submitted to Applied Energy, 1991

31 **Fitzjarrald D.E** An experimental investigation of convection in a fluid that exhibits phase change: J. Fluid Mech, 102, 1981, 85-100

32 **Hodson D.A, Barratt P.J, Sloan D.M** A nonlinear analysis of thermal instabilities in nematic liquid crystals: J. Non-Equilib. Thermodynamics, 9, 1984, 107-130

33 **Ireland P.T, Jones T.V** The measurement of local heat transfer coefficients

in blade cooling geometries: AGARD CONF, 390, 1985, paper 28

34 **Ireland P.T, Jones T.V** Detailed measurements of heat transfer on and around a pedestal in fully developed passage flow: Int Heat Transfer Conf. 8th San Francisco, 1986, 975-80

35 **Simonich J.C, Moffat R.J** Liquid crystal visualization of surface heat transfer on a concavely curved turbulent boundary layer: J. Eng. for Gas Turbines and Power, 106, 1984, 619-27

36 **Jones T.V, Hippensteele S.A** High resolution heat transfer coefficient maps applicable to compound curve surfaces using liquid crystals in a transient wind tunnel: Developments in EXp. Heat Transfer and Combustion ASME HTD, 71, 1987, 1-9

37 **Edwards R.J, Jambunathan K, Button B.L** Experimental investigation of turbulent heat transfer in simultaneously developing flow in finned annuli: First world conference on Experimental Heat Transfer, Fluid mechanics and Thermodynamics, Dubrovnik, Yugoslavia, 1988

38 **Yianneskis M** Thermal monitoring by liquid crystals: Int. Conf. on Condition Monitoring, May 1986, paper E2

39 **BDH** Licritherm thermonic liquid crystals: Advanced materials division, Poole (personal communication)

40 **Hallcrest** An introduction to thermonic liquid crystals: Illinois, 1987 (personal communication)

41 **Edwards R.J** Enhancement of heat transfer in smooth annular ducts using longitudinal fins or swirling flow: PhD thesis, Nottingham Polytechnic, 1987

42 **Mulholland H, Jones C.R** Fundamentals of statistics: Butterworths, ISBN 0408492007

43 **The Open University** The handling of experimental data: Science foundation course Unit E, S100 E

44 **Perry R.H, Chilton C.H** Chemical engineers handbook: M^c^Graw Hill, 5^TH^ Edition, ISBN 0 07 049478 9

45 **Croft D.R, Stone J.A.R** Heat transfer calculations using finite difference equations: Pavic publications, ISBN 0 86 339120 6

46 **Simonson J.R** Engineering heat transfer: Macmillan Education Ltd, 2^ND^ Edition, 1988, ISBN 0 37 74599 7

47 **Chapman A.J** Heat transfer: Collier Macmillan, 4^{TH} Edition, 1984, ISBN 0 02 946080 8

48 **Kreith F, Bohn M.S** Principles of heat transfer: Harper International, 4^{TH} Edition, 1986, ISBN 0 06 043785 5

49 **Kays W.M, Crawford M** Convective heat and mass transfer: M^{c}Graw Hill, 2^{ND} Edition, 1980

50 **Chen T.S, Armaly B.F, Ramachandran N** Correlations for laminar mixed flows on vertical, inclined and horizontal flat plates: Journal of Heat Transfer, Nov 86, 108, 835-840

51 **Cranfield** Short course on heat transfer: Cranfield Institute of Technology, 1991

52 **Eckert E.R.G, Robert M.D Jr.** Analysis of heat and mass transfer: Hemisphere publishing corporation, 1987, ISBN 3 54 0177086

53 **Jones H.R.H** The application of combustion principles to domestic gas burner design: British Gas, ISBN 0-419-14800-0

54 **Ashforth-Frost S, Wang L.A, Jambunathan K** Application of image

processing to liquid crystal thermography: I Mech E CONF on Optical methods and data processing in heat and fluid flow, April 92, 121-6

55 **Akino N, Kunugi T, Ichimiya K** Improved liquid crystal thermometry excluding human color sensation: Transactions of the ASME, Vol 111, May 89, 558-565

56 **Data Translation** Image processing handbook: Data Translation INC, Marlboro USA, 1990

57 **SGS-Thomson** The transputer databook: Inmos, 2nd edition, 1989

58 **Pountain D, May D** A tutorial introduction to OCCAM programming: BBP professional books, 1988, ISBN 0-632-01847-X

59 **Reijns G.L, Kraus U.E, Kirana G** Parallel processing of video images: Highly Parallel Computers, Elsevier Science Publishers B.V. , 1987

60 **Yagi N, Yajima R, Sasaki N** Real time video signal processing system for dynamic images: SPIE, Vol 1199, 1989

APPENDIX A

DIMENSIONAL DRAWINGS

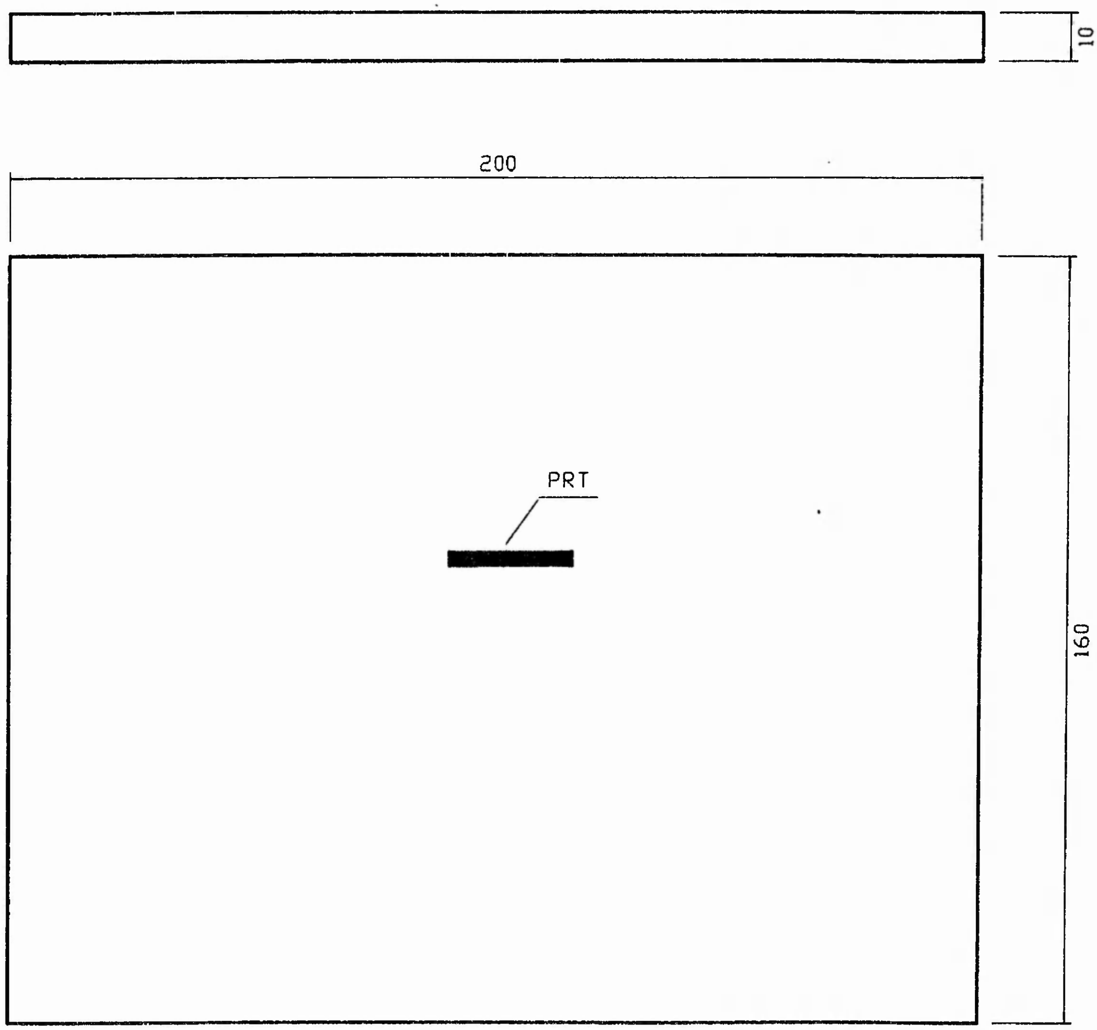

FIGURE A-1 CALIBRATION PLATE

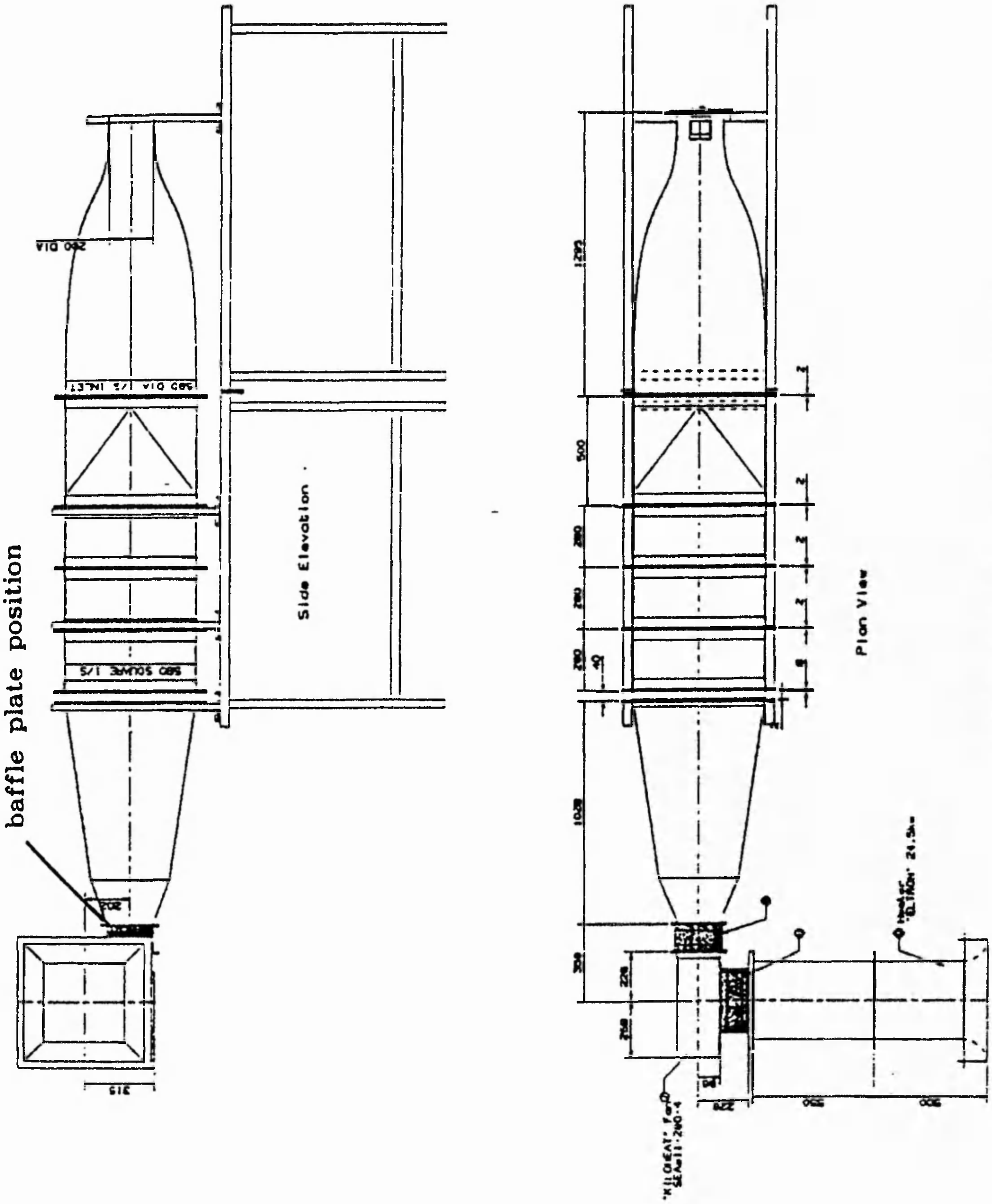

FIGURE A-2 Thermal tunnel

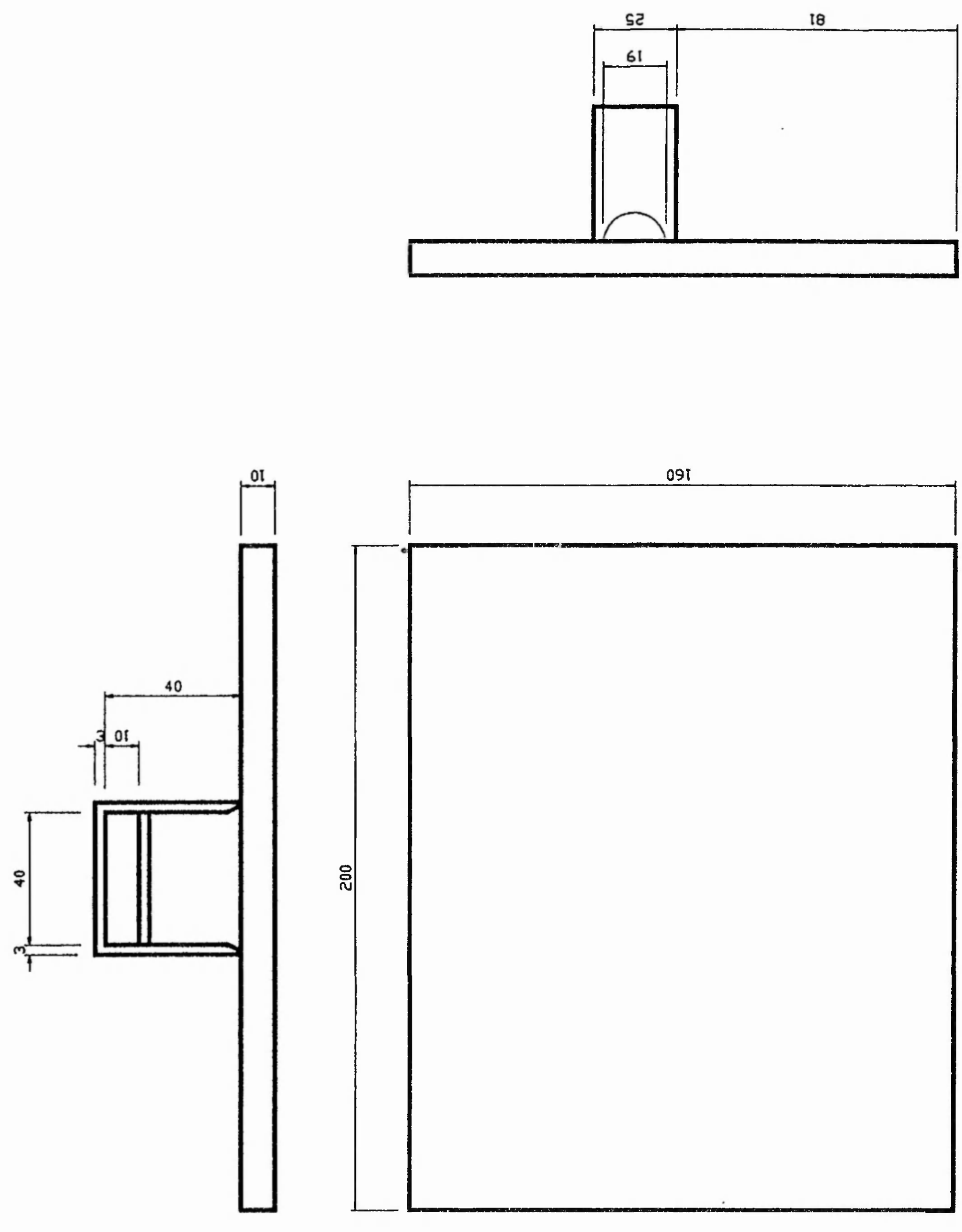

FIGURE A-3 MODEL BASE PLATE

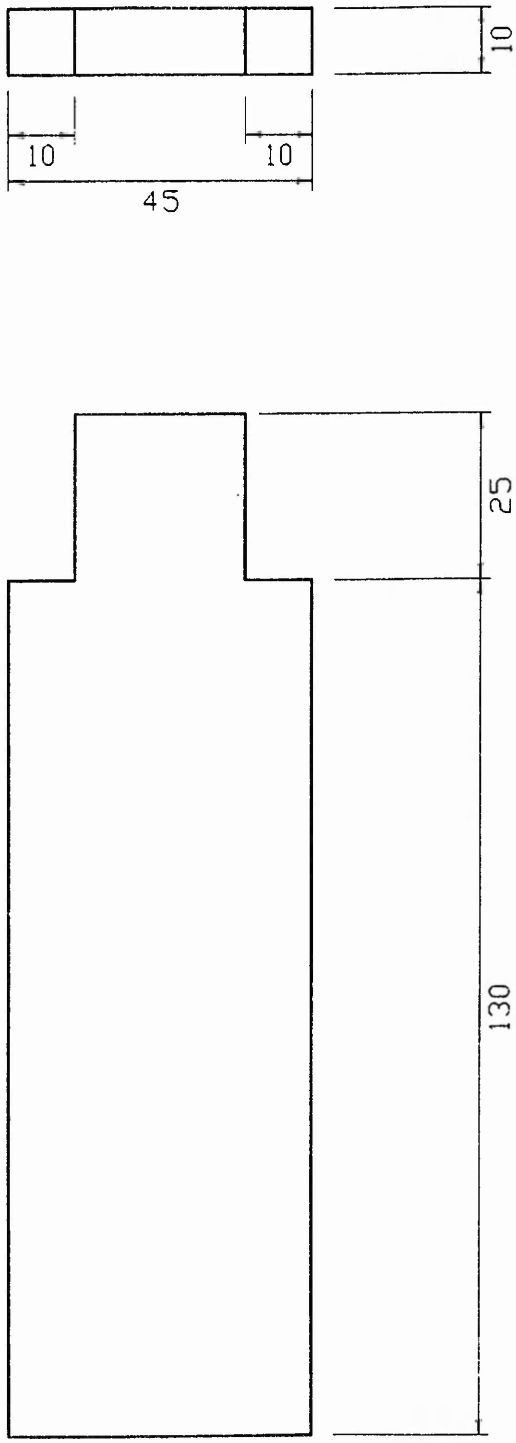

FIGURE A-4 MODEL STAND

APPENDIX B

STATISTICAL FORMULAE

B.1 Linear regression

From Mulholland and Jones [42], page 207-211 for linear regression,

Y = estimated value of dependent variable

y = dependent variable

x = independent variable

n = number of records

$$\beta = \frac{n\,\Sigma xy - \Sigma x\,\Sigma y}{n\,\Sigma x^2 - (\Sigma x)^2}$$

$$y^* = \frac{\Sigma y}{n} \qquad x^* = \frac{\Sigma x}{n}$$

hence

$$Y = y^* - \beta\,(x - x^*)$$

B.2 Error estimation

Estimation of the standard deviation, mean and standard error from the Open University [43], page 7-11, given

x = sample reading

d = residuals $(x_n - x^*)$

n = number of readings

s = standard deviation

s_m = standard error on mean

$$x^* = \frac{\Sigma x}{n}$$

$$s = \left(\frac{\Sigma_{1,n} dn}{n} \right)^{1/2}$$

$$s_m = \frac{s}{(n-1)^{1/2}}$$

giving an answer of: $x^* \pm s_m$

B.3 Rectangular hyperbola curve fit

Y = estimated value of dependent variable

y = dependent variable

x = independent variable

n = number of records

C = constant

$$C = \frac{\sum_{1,n} \frac{y}{x}}{\sum_{1,n} \frac{1}{x^2}}$$

and:

$$Y = \frac{C}{x}$$

APPENDIX C

FORTRAN PROGRAMS

(1) 1-D transient

```
100    FORMAT (///' DETERMINATION OF LOCAL CONVECTIVE'/
     1 ' HEAT TRANSFER COEFFICIENTS USING THE LIQUID'/
     2 ' CRYSTAL TECHNIQUE, EXPLICIT FINITE DIFFERENCE'/
     3 ' ANALYSIS AND A SUCCESSIVE APPROXIMATION'/
     4 ' APPROACH.(G.MOOR MARCH 90)'/)

C    ********************************************
C    * TI=initial temp          Tg= melt temp           *
C    * T=node temp              T_est=estimated temp    *
C    * dt=time increment        tc=time const           *
C    * Bi=Biot                  Fo=Fourier              *
C    * SB=Stefan Boltzmann      A=diffusivity           *
C    * R=radiation term         k=conduction coeff      *
C    * dx=node spacing          h=heat transfer coeff   *
C    * W=width                  E=emissivity            *
C    * t=time                   Tb=ambient              *
C    *      NB radiation shape factor of 1 used         *
C    ********************************************

      REAL k,E,SB,A
      INTEGER n,Y,M
      DOUBLE PRECISION T(20),T_est(20)
      DIMENSION h(500),t(500)
      OPEN(UNIT=27,STATUS='UNKNOWN',FILE='HVALUE.DATA')

      WRITE (6,100)
      WRITE (6,110)
      READ (5,*) Tb,TI,Tg,W,n
      DO 5 Y=1,n
       WRITE(6,120) Y
5      READ (5,*)t(Y)

C------ SET VARIABLES FOR PROGRAM CONSTRAINTS ------
      W=W*0.001/2
      Tb=Tb+273.15
      TI=TI+273.15
      Tg=Tg+273.15
      dx=W/9
```

1-D transient continued

```
C------ SETTING CONSTANTS ------
        A=1.0692E-7
        k=0.1884
        E=.96
        SB=5.67E-8


C****** MAIN LOOP   CALCULATE H COEFFICIENTS n TIMES ******
        WRITE (6,130)
        DO 50 Y=1,n

C------ INITIAL SETTINGS ------
        Fo=0.4
        Hi=0
        Lo=0
        h(Y)=(-850-115*TI-284*Tg+290*Tb+307*W)/t(Y)
10       DO 15 I=1,14
          T(I)=TI
15         T_est(I)=TI

C------ CALCULATE Bi, dt ,TEST FOR INSTABILITY ------
        R=E*SB*dx/k
        Bi=dx*h(Y)/k
        dt=Fo*(dx**2)/A
        DO WHILE(Fo.GT.(.5/(Bi+1+R*TI**3)) .OR. dt.GT.t(Y))
           Fo=Fo*0.8
        END DO
        dt=Fo*(dx**2)/A
        M=(t(Y)/dt)+1
        dt=t(Y)/M
        Fo=dt*A/(dx**2)
        tc=-t(Y)/ALOG(TI/Tg)
        D=1/Fo-2

C------ EVALUATING THE EXPLICIT NODAL EQUATIONS ------
        DO 30 I=1,M
        T(11)=2*Fo*(T(2)+Bi*Tb+R*Tb**4+T(1)*
     +                     (1/(2*Fo)-Bi-R*T(1)**3-1))
        T_est(11)=TI/EXP(-I*dt/tc)
        DO 25 J=2,9
          T(10+J)=Fo*(T(J+1)+T(J-1)+D*T(J))
25         T_est(J+10)=Fo*(T_est(J+1)+T_est(J-1)+D*T_est(J))
        T_est(20)=Fo*(2*T_est(9)+T_est(10)*D)
```

1-D transient continued

```
      T(20)=T_est(20)
      DO 30 J=1,10
       T(J)=T(J+10)
30      T_est(J)=T_est(J+10)

C------ TEST FOR CONVERGENCE ------
      IF(T(1).LT.(Tg+.05).AND.T(1).GT.(Tg-.05)) GOTO 45

C------ NEW ESTIMATION FOR h ------
      IF (T(1).LT.Tg ) THEN
         Hi=h(Y)
       ELSE
         Lo=h(Y)
      ENDIF
      IF (Hi.GT.0) THEN
         h(Y)=((Hi-Lo)/2)+Lo
       ELSE
         h(Y)=h(Y)*2
      ENDIF
      GOTO 10

C------ OUTPUT h TO SCREEN AND FILE ------
45     WRITE (6,140) Y,t(Y),h(Y)
      WRITE (27,140) Y,t(Y),h(Y)

50     CONTINUE


      WRITE (6,*) ( '  DATA STORED IN...  HVALUE.DATA')
      STOP

C****** FORMAT STATEMENTS  ******

110    FORMAT (/' ENTER: THE ROOM AIR TEMP (C),'/
    1 '       THE INITIAL SPECIMEN TEMPERATURE (C),'/
    2 '       COLOUR CHANGES TEMP (C),'/
    3 '       THICKNESS (MM),'/
    4 '       NUMBER OF READINGS TAKEN,'/
120    FORMAT ( '  TIME OF READING ',I4,' (s)...  ')
130    FORMAT ( '    READING    TIME(s)    H(W/m2K)')
140    FORMAT (  2I10,F13.2)
       END
```

(2) 2-D steady state

```
100    FORMAT (///' DETERMINATION OF HEAT FLOW THROUGH'/
     1 ' A CAST IRON HEAT EXCHANGER BY USE OF LIQUID'/
     2 ' CRYSTALS ON A PERSPEX MODEL OF BASE THICKNESS'/
     3 ' 10 mm AND FIN WIDTH 3 mm (G.MOOR JAN 91)'/)

C     ********************************************
C     * TI=initial temp          Tg= melt temp             *
C     * T=node temp              T_est=estimated temp      *
C     * dt=time increment        tc=time const             *
C     * Bi=Biot                  Fo=Fourier                *
C     * SB=Stefan Boltzmann      A=diffusivity             *
C     * shape factor=1           k=conduction coeff        *
C     * R=radiation term         r=residual value          *
C     * dx=node spacing          h=heat transfer coeff     *
C     * W=width                  E=emissivity              *
C     * t=time                   Tb=ambient                *
C     * hs=h around surface      dH=sectional fin height   *
C     * S=fin spacing            L=Fin length              *
C     ********************************************

      CHARACTER*15 NAME
      REAL k,L,E,SB,A
      INTEGER n,Y,M
      DOUBLE PRECISION T(20),T_est(20)
      DIMENSION h(500),t(500)
      WRITE (6,100)
      WRITE (6,*) 'OUTPUT FILE NAME?...   ********.DATA'
      READ (6,*) NAME
      OPEN(UNIT=27,STATUS='UNKNOWN',FILE=NAME)

      WRITE (6,110)
      READ (5,*) Tb,TI,Tg,dH,S,L
      DO 5 Y=1,8
        WRITE(6,120) Y
5       READ (5,*)t(Y)

C------ SET VARIABLES FOR PROGRAM CONSTRAINTS ------
      dH=dH*0.001
      S=S*.001/24
      L=L*.001/24
```

2-D steady state continued

```
      Tb=Tb+273.15
      TI=TI+273.15
      Tg=Tg+273.15

C------ SETTING CONSTANTS ------
      A=1.0692E-7
      k=0.1884
      E=.96
      SB=5.67E-8


C****** SETTING NODE SPACING FOR EACH TIME VALUE ******
      DO 50 Y=1,8

      W=.003/2
      IF(Y.GT.5) W=.01/2
      dx=W/9

C------ INITIAL SETTINGS ------
      Fo=0.4
      Hi=0
      Lo=0
      h(Y)=(-850-115*TI-284*Tg+290*Tb+307*W)/t(Y)
10     DO 15 I=1,14
        T(I)=TI
15       T_est(I)=TI

C------ CALCULATE Bi, dt ,TEST FOR INSTABILITY ------
      R=E*SB*dx/k
      Bi=dx*h(Y)/k
      dt=Fo*(dx**2)/A
      DO WHILE(Fo.GT.(.5/(Bi+1+R*TI**3)) .OR. dt.GT.t(Y))
         Fo=Fo*0.8
      END DO
      dt=Fo*(dx**2)/A
      M=(t(Y)/dt)+1
      dt=t(Y)/M
      Fo=dt*A/(dx**2)
      tc=-t(Y)/ALOG(TI/Tg)
      D=1/Fo-2

C------ EVALUATING THE EXPLICIT NODAL EQUATIONS ------
      DO 30 I=1,M
```

2-D steady state continued

```
      T(11)=2*Fo*(T(2)+Bi*Tb+R*Tb**4+T(1)*
     +                    (1/(2*Fo)-Bi-R*T(1)**3-1))
      T_est(11)=TI/EXP(-I*dt/tc)
      DO 25 J=2,9
        T(10+J)=Fo*(T(J+1)+T(J-1)+D*T(J))
25      T_est(J+10)=Fo*(T_est(J+1)+T_est(J-1)+D*T_est(J))
      T_est(20)=Fo*(2*T_est(9)+T_est(10)*D)
      T(20)=T_est(20)
      DO 30 J=1,10
        T(J)=T(J+10)
30      T_est(J)=T_est(J+10)

C------ TEST FOR CONVERGENCE ------
      IF(T(1).LT.(Tg+.05).AND.T(1).GT.(Tg-.05)) GOTO 45

C------ NEW ESTIMATION FOR h ------
      IF (T(1).LT.Tg ) THEN
          Hi=h(Y)
        ELSE
          Lo=h(Y)
      ENDIF
      IF (Hi.GT.0) THEN
          h(Y)=((Hi-Lo)/2)+Lo
        ELSE
          h(Y)=h(Y)*2
      ENDIF
      GOTO 10

C------ OUTPUT h TO FILE ------
45      WRITE (27,140) Y,t(Y),h(Y)

50     CONTINUE


C****** STEADY STATE ANALYSIS OF NODAL TEMPS ******
       WRITE (6,*) ( '  COMPUTING NODAL TEMPS ')

C------ SETTING h VALUES AROUND SURFACE PROFILE ------
      hs(1,23)=h(1)
      DO 60 X=2,6
60      hs(4,23-(X-2)*3)=h(X)
        hs(7,11)=h(7)
        hs(10,11)=h(8)
        DO 70 X=1,2
```

2-D steady state continued

```
          hs(X+1,23)=hs(1,23)-(hs(1,23)-hs(4,23))*X/3
          hs(X+4,11)=hs(4,11)-(hs(4,11)-hs(7,11))*X/3
70        hs(X+7,11)=hs(7,11)-(hs(7,11)-hs(10,11))*X/3
        DO 80 Y=14,20,3
        DO 80 X=1,2
80          hs(4,Y+X)=hs(4,Y)-(hs(4,Y)-hs(4,Y+3))*X/3
        DO 81 Y=1,2
81          hs(4,14-Y)=hs(4,14)+(hs(4,14)-hs(4,15))*Y

C------ SET CONSTANTS AND NODAL TEMPS ------
      k=44.7
      Tb=20+273.15
      DO 90 X=1,10
      DO 90 Y=1,23
90        T(X,Y)=(300-(Y-1)*9)+273.15

C------ CALCULATING NODAL TEMPS ------
      rmax=1
      DO WHILE(rmax.GT.0.001)
        rmax=0
      DO 91 X=1,10
      DO 91 Y=23,2,-1
      IF (X.GT.4 .AND. Y.GT.11)THEN
          SKIP=1
      ELSEIF (X.EQ.1 .AND. Y.EQ.23) THEN
          CALL PERAMS2(X,Y,hs,k,DX1,DY1,DH,S,L,R,E,SB)
          P=2*DX1+DY1+DH+R*T(X,Y)**3
          r=2*T(X+1,Y)*DX1+T(X,Y-1)*DY1+Tb*DH+
     +              R*Tb**4-T(X,Y)*P
      ELSEIF (X.EQ.1) THEN
          CALL PERAMS1(X,Y,DX1,DX2,DY1,DY2,S,L)
          P=2*DX2+DY1+DY2
          r=T(X+1,Y)*DX2*2+T(X,Y+1)*DY1+T(X,Y-1)*DY2-
     +              T(X,Y)*P
      ELSEIF (X.EQ.10 .AND. Y.EQ.11) THEN
          CALL PERAMS2(X,Y,hs,k,DX1,DY1,DH,S,L,R,E,SB)
          P=2*DX1+DY1+DH+R*T(X,Y)**3
          r=2*T(X-1,Y)*DX1+T(X,Y-1)*DY1+Tb*DH+
     +              R*Tb**4-T(X,Y)*P
      ELSEIF (X.EQ.10) THEN
          CALL PERAMS1(X,Y,DX1,DX2,DY1,DY2,S,L)
          P=2*DX1+DY1+DY2
          r=T(X-1,Y)*DX1*2+T(X,Y+1)*DY1+T(X,Y-1)*DY2-
     +              T(X,Y)*P
```

2-D steady state continued

```
      ELSEIF ((X.LT.4 .AND. Y.EQ.23) .OR.
     +                (X.GT.4 .AND. Y.EQ.11))THEN
        CALL PERAMS2(X,Y,hs,k,DX1,DY1,DH,S,L,R,E,SB)
        P=2*DX1+DY1+DH+R*T(X,Y)**3
        r=(T(X+1,Y)+T(X-1,Y))*DX1+T(X,Y-1)*DY1+Tb*DH+
     +              R*Tb**4-T(X,Y)*P
      ELSEIF (X.EQ.4 .AND. Y.EQ.11) THEN
        CALL PERAMS3(X,Y,hs,k,DX1,DX2,DY1,DY2,
     +                DH,S,L,R,E,SB)
        P=DX1+DX2+DY1+DY2+DH+R*T(X,Y)**3
        r=T(X-1,Y)*DX1+T(X+1,Y)*DX2+T(X,Y-1)*DY1+
     +            T(X,Y+1)*DY2+Tb*DH+R*Tb**4-T(X,Y)*P
      ELSEIF (X.EQ.4 .AND. Y.EQ.23) THEN
        DX1=L/0.5E-3
        DY1=.25E-3/2/L
        DH=hs(X,Y)*(.25E-3+L,R)/k
        R=E*SB*(.25E-3+L)/k
        P=DX1+DY1+DH+R*T(X,Y)**3
        r=T(X-1,Y)*DX1+T(X,Y-1)*DY1+Tb*DH+R*Tb**4-T(X,Y)*P
      ELSEIF (X.EQ.4 .AND. Y.GT.11) THEN
        DX1=L/.25E-3
        DY1=.25E-3/2/L
        DH=2*L*hs(X,Y)/k
        R=E*SB*2*L/k
        P=DX1+2*DY1+DH+R*T(X,Y)**3
        r=T(X-1,Y)*DX1+(T(X,Y-1)+T(X,Y+1))*DY1+
     +               Tb*DH+R*Tb**4-T(X,Y)*P
      ELSE
        CALL PERAMS1(X,Y,DX1,DX2,DY1,DY2,S,L)
        P=DX1+DX2+DY1+DY2
        r=T(X-1,Y)*DX1+T(X+1,Y)*DX2+T(X,Y+1)*DY1+
     +                   T(X,Y-1)*DY2-T(X,Y)*P
      ENDIF

C------ DETERMINE MAXIMUM RESIDUAL ------
      IF (X.GT.4 .AND. Y.GT.11) THEN
       SKIP=1
      ELSE
       T(X,Y)=T(X,Y)+r/P
       IF (r.LT.0) r=-r
       IF (r.GT.rmax) rmax=r
      ENDIF
91     CONTINUE
```

2-D steady state continued

```
      END DO

C------ COMPUTING HEAT LOSS AND HEAT INPUT ------
      Qout=(T(1,23)-Tb)*dH*.75E-3*h(1)
      Qout=(T(4,23)-Tb)*dH*(.75E-3+L*3)*h(2)+Qout
      Qout=(T(4,20)-Tb)*dH*L*6*h(3)+Qout
      Qout=(T(4,17)-Tb)*dH*L*6*h(4)+Qout
      Qout=(T(4,14)-Tb)*dH*L*6*h(5)+Qout
      Qout=(T(4,11)-Tb)*dH*3*(L+S)*h(6)+Qout
      Qout=(T(7,11)-Tb)*dH*S*6*h(7)+Qout
      Qout=(T(10,11)-Tb)*dH*S*3*h(8)+Qout
      Qout=(T(1,23)**4-Tb**4)*dH*.75E-3*E*SB+Qout
      Qout=(T(4,23)**4-Tb**4)*dH*(.75E-3+L*3)*E*SB+Qout
      Qout=(T(4,20)**4-Tb**4)*dH*L*6*E*SB+Qout
      Qout=(T(4,17)**4-Tb**4)*dH*L*6*E*SB+Qout
      Qout=(T(4,14)**4-Tb**4)*dH*L*6*E*SB+Qout
      Qout=(T(4,11)**4-Tb**4)*dH*3*(L+S)*E*SB+Qout
      Qout=(T(7,11)**4-Tb**4)*dH*S*6*E*SB+Qout
      Qout=(T(10,11)**4-Tb**4)*dH*S*3*E*SB+Qout

      Qin=(T(1,1)-T(1,2))*dH*.25E-3/.001*k
      Qin=(T(2,1)-T(2,2))*dH*.5E-3/.001*k + Qin
      Qin=(T(3,1)-T(3,2))*dH*.5E-3/.001*k + Qin
      Qin=(T(4,1)-T(4,2))*dH*(.25E-3+ S)/.001*k + Qin
      DO 66 X=5,9
66       Qin=(T(X,1)-T(X,2))*dH*2*S/.001*54 + Qin
      Qin=(T(10,1)-T(10,2))*dH*S/.001*54 + Qin

      ERROR=100-Qout/Qin*100

C------ OUTPUT TO FILE ------
      WRITE(27,145)
      WRITE(27,150) (((T(X,Y)-273.15),X=1,10),Y=1,11)
      WRITE(27,155) (((T(X,Y)-273.15),X=1,4),Y=12,23)
      WRITE(27,160) Qin,Qout,ERROR

      STOP


C****** FORMAT STATEMENTS ******

110   FORMAT (/' ENTER: THE ROOM AIR TEMP (C),'/
     1 ' THE INITIAL SPECIMEN TEMPERATURE (C),'/
     2 ' COLOUR CHANGES TEMP (C),'/
```

2-D steady state continued

```
     3 ' FIN HEIGHT (mm),'/
     4 '  IN SPACING (mm),'/)
120    FORMAT ( '    TIME OF READING ',I4,' (s)...  ')
140    FORMAT (  '     ',2I10,F13.2)
145    FORMAT (///'        TEMPERATURE PROFILE ...'//)
150    FORMAT (  '        ',10F7.2)
155    FORMAT (  '        ',4F7.2)
160    FORMAT (////'        HEAT OUTPUT DATA ...'/
     1 '              Qin  IS    (W)   ... ',F11.3,/
     2 '              Qout  IS   (W)   ... ',F11.3,/
     3 '              % ERROR          ... ',F10.2)

      END


C****** SUBROUTINES (A,B,C,D = NODE SEPARATION VARIABLES)
      SUBROUTINE PERAMS1(X,Y,DX1,DX2,DY1,DY2,S,L)
      REAL A,B,C,D,DX1,DX2,DY1,DY2,S,L
      INTEGER X,Y
      A=.25E-3
      C=.5E-3
      D=C
      IF (X.GT.4) A=S
      B=A
      IF (X.EQ.4) B=S
      IF (X.LT.4) THEN
        IF (Y.GT.10) C=L
        IF (Y.GT.11) D=C
      ENDIF
      DX1=(C+D)/2/A
      DX2=(C+D)/2/B
      DY1=(A+B)/2/C
      DY2=(A+B)/2/D
      RETURN
      END

      SUBROUTINE PERAMS2(X,Y,H,k,DX1,DY1,DH,S,L,R,E,SB)
      DIMENSION H(10,23)
      REAL A,D,DX1,DY1,DH,S,L,k,R,E,SB
      INTEGER X,Y
      A=.25E-3
      D=.5E-3
      IF (X.GT.4) A=S
```

2-D steady state continued

```
      IF (Y.EQ.23) D=L
      DX1=D/2/A
      DY1=A/D
      DH=2*A*H(X,Y )/k
      R=2*A*E*SB/k
      RETURN
      END

      SUBROUTINE PERAMS3(X,Y,H,k,DX1,DX2,DY1,DY2,
     +            DH,S,L,R,E,SB)
      DIMENSION H(10,23)
      REAL A,B,C,D,DX1,DX2,DY1,DY2,DH,S,L,k,R,E,SB
      INTEGER X,Y
      A=.25E-3
      B=S
      D=.5E-3
      C=L
      DX1=(D+C)/2/A
      DX2=D/2/B
      DY1=(A+B)/2/D
      DY2=A/2/C
      DH=(C+B)*H(X,Y)/k
      R=(C+B)*E*SB/k
      RETURN
      END
```

(3) Sample program output

```
SECTION NUMBER   1

  1      120      26.93
  2      115      29.07
  3      250      10.70
  4      319       6.99
  5      570       1.56
  6     1109       6.00
  7      961       7.75
  8      960       7.75

TEMPERATURE PROFILE ...

300.00 300.00 300.00 300.00 300.00 300.00 300.00 300.00 300.00 300.00
299.47 299.47 299.47 299.48 299.53 299.60 299.66 299.70 299.72 299.73
298.93 298.93 298.94 298.95 299.06 299.20 299.32 299.40 299.45 299.46
298.37 298.37 298.38 298.40 298.59 298.80 298.98 299.11 299.18 299.20
297.78 297.79 297.80 297.83 298.11 298.41 298.66 298.82 298.92 298.94
297.16 297.16 297.19 297.22 297.62 298.03 298.35 298.55 298.66 298.70
296.47 296.48 296.51 296.56 297.13 297.67 298.05 298.29 298.42 298.46
295.69 295.70 295.75 295.83 296.65 297.33 297.77 298.05 298.19 298.24
294.77 294.80 294.88 295.00 296.20 297.02 297.52 297.82 297.98 298.03
293.64 293.69 293.82 294.02 295.79 296.75 297.30 297.62 297.78 297.83
292.16 292.24 292.46 292.87 295.52 296.55 297.12 297.44 297.61 297.65
287.26 287.25 287.25 287.22
282.40 282.39 282.37 282.32
277.84 277.83 277.80 277.75
273.60 273.59 273.56 273.51
269.70 269.69 269.66 269.61
266.17 266.16 266.12 266.07
263.02 263.01 262.97 262.92
260.27 260.25 260.22 260.16
257.92 257.91 257.87 257.81
256.00 255.98 255.94 255.87
254.59 254.57 254.52 254.43
253.77 253.75 253.69 253.59

HEAT OUTPUT DATA ...
     Q IN IS    (W)  ...      2.560
     Q OUT IS   (W)  ...      2.599
     % ERROR         ...     -1.52
```

APPENDIX D

TABLES

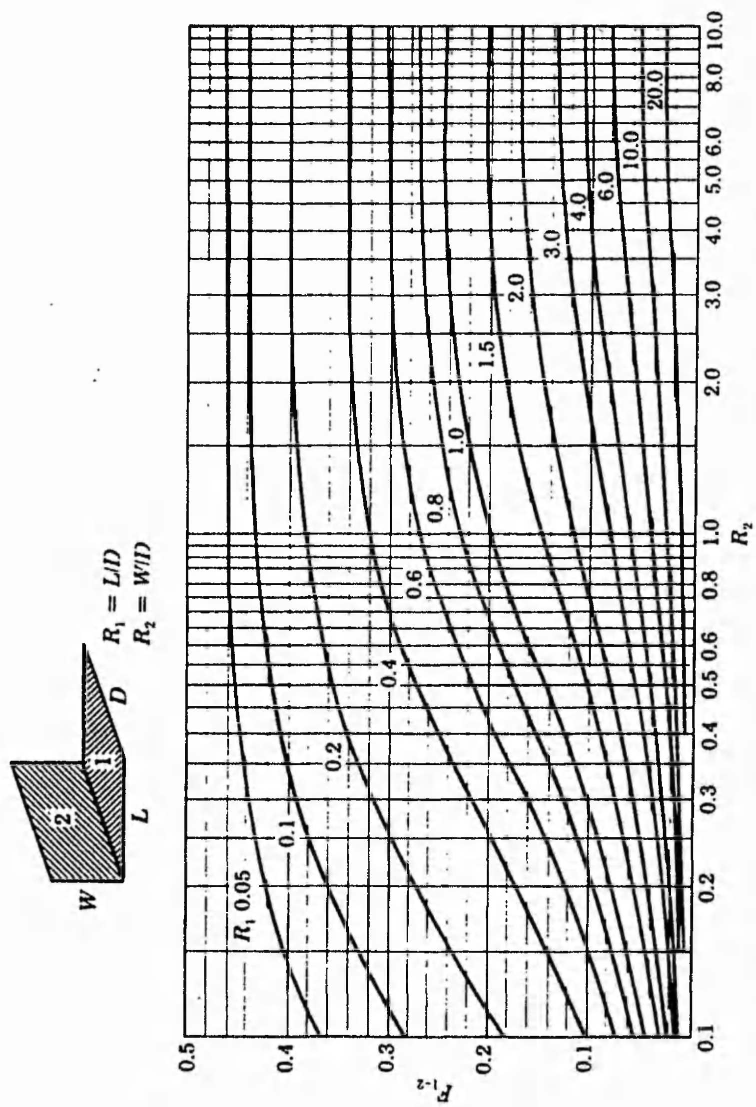

FIGURE D-1 Shape factor for perpendicular rectangles with a common edge.

t °C	c_p kJ/kg-°C	ρ kg/m^3	$\mu \times 10^6$ kg/m-s	$\nu \times 10^6$ m^2/s	$k \times 10^3$ W/m-°C
−50	1.0064	1.5819	14.63	9.25	20.04
−40	1.0060	1.5141	15.17	10.02	20.86
−30	1.0058	1.4518	15.69	10.81	21.68
−20	1.0057	1.3944	16.20	11.62	22.49
−10	1.0056	1.3414	16.71	12.46	23.29
0	1.0057	1.2923	17.20	13.31	24.08
10	1.0058	1.2467	17.69	14.19	24.87
20	1.0061	1.2042	18.17	15.09	25.64
30	1.0064	1.1644	18.65	16.01	26.38
40	1.0068	1.1273	19.11	16.96	27.10
50	1.0074	1.0924	19.57	17.92	27.81
60	1.0080	1.0596	20.03	18.90	28.52
70	1.0087	1.0287	20.47	19.90	29.22
80	1.0095	0.9996	20.92	20.92	29.91
90	1.0103	0.9721	21.35	21.96	30.59
100	1.0113	0.9460	21.78	23.02	31.27
110	1.0123	0.9213	22.20	24.10	31.94
120	1.0134	0.8979	22.62	25.19	32.61
130	1.0146	0.8756	23.03	26.31	33.28
140	1.0159	0.8544	23.44	27.44	33.94
150	1.0172	0.8342	23.84	28.58	34.59
160	1.0186	0.8150	24.24	29.75	35.25
170	1.0201	0.7966	24.63	30.93	35.89
180	1.0217	0.7790	25.03	32.13	36.54
190	1.0233	0.7622	25.41	33.34	37.18
200	1.0250	0.7461	25.79	34.57	37.81
210	1.0268	0.7306	26.17	35.82	38.45
220	1.0286	0.7158	26.54	37.08	39.08
230	1.0305	0.7016	26.91	38.36	39.71
240	1.0324	0.6879	27.27	39.65	40.33
250	1.0344	0.6748	27.64	40.96	40.95
260	1.0365	0.6621	27.99	42.28	41.57
270	1.0386	0.6499	28.35	43.62	42.18
280	1.0407	0.6382	28.70	44.97	42.79
290	1.0429	0.6268	29.05	46.34	43.40
300	1.0452	0.6159	29.39	47.72	44.01
310	1.0475	0.6053	29.73	49.12	44.61
320	1.0499	0.5951	30.07	50.53	45.21
330	1.0523	0.5853	30.41	51.95	45.84
340	1.0544	0.5757	30.74	53.39	46.38

FIGURE D-2 PROPERTIES OF DRY AIR